# Synthesis, characterization and development of aluminium hydroxide–based adsorbents for defluoridation of drinking water


**Prepared by: Eyobel Mulugeta**

**Supervisors: Dr. Feleke Zewge**

**Dr. C. Annette Johnson**

**Prof. Bhagwan Singh Chandravanshi**

**June 5, 2014**

**Synthesis, characterization and development of aluminium hydroxide–based adsorbents for defluoridation of drinking water**

**A Thesis Submitted to**

**The Department of Chemistry**

**Presented in Partial Fulfilment of the Requirements for the Degree of**

**Doctor of Philosophy (Chemistry)**

**Addis Ababa University**

**Addis Ababa, Ethiopia**

**June 5, 2014**

## Addis Ababa University

## School of Graduate Studies

This is to certify that the thesis prepared by Eyobel Mulugeta Damte entitled: ***Synthesis, characterization and development of aluminium hydroxide–based adsorbents for defluoridation of drinking water*** and submitted in partial fulfilment of the requirements for the Degree of Doctor of Philosophy (Analytical Chemistry) complies with the regulations of the university and meets the accepted standards with respect to originality and quality.

Signed by the Examining Committee:

| Name | Signature | Date |
|---|---|---|
| _____ | _____ | 5 June 2014 |
| External Examiner | | |
| _____ | _____ | 5 June 2014 |
| Examiner | | |
| _____ | _____ | 5 June 2014 |
| Examiner | | |
| Dr. Feleke Zewge | _____ | 5 June 2014 |
| Advisor | | |
| Dr. C. Annette Johnson | _____ | 5 June 2014 |
| Advisor | | |
| Prof. Bhagwan S. Chandravanshi | _____ | 5 June 2014 |
| Advisor | | |

_____

Chair of Department

# ABSTRACT

**Synthesis, characterization and development of aluminium hydroxide–based adsorbents for defluoridation of drinking water**

Eyobel Mulugeta

Addis Ababa University, 2014

In this study, the fluoride removal potential of aluminium hydroxide–based adsorbents; aluminium hydro(oxide) (AO), aluminium oxide–manganese oxide (AOMO) composite material and nanoscale aluminium oxide hydroxide (nano–AlOOH) have been investigated. The adsorbents were synthesised and characterized. A series of batch adsorption experiments were carried out to assess parameters that influence the adsorption process. The parameters considered were contact time and adsorbent dose, initial fluoride concentration, and raw water pH. The adsorption isotherms and kinetics models were used to determine adsorption parameters.

AOMO was prepared from manganese(II) chloride and aluminium hydroxide. The surface area of AOMO was found to be 30.7 $m^2/g$ and its specific density was determined as 2.78 $g/cm^3$. Detailed investigation of the adsorbent by inductively coupled plasma–optical emission spectrometry (ICP–OES), inductively coupled plasma–mass spectrometry (ICP–MS) and ion chromatography (IC) (for sulfate only) showed that it contains Al, Mn, $SO_4$, and Na as major components and Fe, Si, Ca and Mg, as minor components. Thermogravimetric analysis (TGA) was used to study the thermal behaviour of AOMO. X–ray diffraction (XRD) analysis showed that the adsorbent is poorly crystalline. The point of zero charge was determined as 9.54.

Batch experiments (by varying the proportion of MnO) showed that fluoride removal efficiency of AOMO varied significantly with % of MnO with an optimum value of about 11% of manganese oxide in the adsorbent. The pH for optimum fluoride removal was found to be in the range 5 to 7. The adsorption data was analyzed using linear and non–linear Freundlich, Langmuir, and D–R models. The minimum adsorption capacity obtained from non–linear Freundlich isotherm model was 4.94 mg/g and the maximum capacity from Langmuir was 19.2 mg/g. Non–linear methods were found to best represent the adsorption characteristics, than their linearized counter–parts. The non–linear Freundlich isotherm most closely represented fluoride adsorption on AOMO. Kinetic studies showed that the adsorption is well described by a non–linear pseudo–second order reaction model with an average rate constant of $3.1 \times 10^{-2}$ g/min·mg.

Results from experiments with nano–AlOOH showed that most of the adsorption took place during the first 30 min; and equilibrium was reached at one hour contact time with an adsorbent dose of 1.6 g/L and an initial fluoride concentration of 20 mg/L. Maximum adsorption occurred at around pH 7 at an initial fluoride concentration of 20 mg/L. The adsorption data were well fitted to the Langmuir isotherm model with a maximum adsorption capacity of 62.5 mg/g. The kinetic studies showed that the adsorption of fluoride by nano–AlOOH obeys a pseudo–second order rate equation with an average rate constant of $2.22 \times 10^{-3}$ g/min·mg.

The AO adsorbent was synthesized at different OH:Al ratios to optimize the material, characterized and tested in batch and column experiments. The maximum fluoride uptake was achieved for the AO adsorbent synthesized at OH:Al ratio between 2.5 and 2.7. The surface area of the AO (OH:Al = 2.7) was found to be 37.7 $m^2$/g. The composition was determined to be 90% $Al(OH)_{2.7}(SO_4)_{0.1}$ (*or* 78.3% $Al(OH)_3$ plus 10.7% $Al_2(SO_4)_3$) with 10% $Na_2SO_4$ (as an impurity).

The material is X–ray amorphous and scanning electron microscopic (SEM) studies show AO to be a network of fibers with a size range of 200 to 300 nm. The FTIR spectrum of AO indicated the presence of Al–OH and Al–O bonds, sulfate and water, but could not shed light on the nature of aluminium hydro(oxide). However, it is possible to postulate the presence of basaluminite, because spectral comparison of AO with basaluminite has very similar features in many aspects.

At an OH:Al ratio of 2.7, the surface site concentration of AO determined by acid–base titrations is 0.5 meq/g (equivalent to a surface site concentration of 8 sites/$nm^2$) and an acidic component of 1.4 meq/g. At an OH:Al ratio of 3, the acidic component is no longer present and the uptake capacity of AO significantly reduced. The role of the acidic component may be the control of pH, but may also be the exchange of sulfate with fluoride.

In experiments to test the competitive adsorption of fluoride with ions typically found in natural waters, uptake was found to be unaffected by sodium salts of chloride and sulfate in concentrations up to 500 mg/L. A reduction of fluoride uptake with increasing concentrations of hydroxide and bicarbonate was ascribed to the pH dependence of fluoride sorption (as the addition of these ions caused an increase in pH), while phosphate appeared to compete with fluoride for sorption sites.

Continuous packed column experiments with AO (OH:Al = 2.7) showed that at a flow rate of 100 empty bed volumes (eBV) per day using deionized water, the fluoride adsorption capacity was 26.2 mg/g. The pH of treated water ranged between 4.4 and 7.0. In solutions representing buffering conditions of Ethiopian groundwaters (pH 8 ± 0.2, 10 mM $NaHCO_3$, 3000 ppm $CO_2$) uptake capacities at 100 and 10 eBV/day were 4.65 and 9.0 mg/g respectively. Aluminium was

initially released in concentrations ranging from 0.6–2.0 mg/L in the experiments using deionized waters when the pH was less than 5. With the introduction of calcite post–column treatment, the pH was maintained in the range of 7.5–8.5, which significantly reduced sulfate concentrations due to gypsum precipitation and the prevention of early aluminium release were achieved.

The comparative performance of AO with activated alumina (AA) and pseudoboehmite (PB) was evaluated in terms of surface acidity and surface site concentrations, fluoride adsorption capacity, and potential for repetitive regeneration. The fluoride removal capacity of the adsorbents determined from mini–column studies was found to be 10.6, 1.9, and 2.4 mg/g for AO, AA, and PB, respectively. This significant difference in fluoride adsorption capacity is strongly related to the surface acidity and surface site concentration. Regeneration experiments showed, however, that AA and PB can be regenerated for more than 3 cycles; whereas the potential of regeneration of AO for more than 3 cycles is limited. This is due to the loss of the acidic component during regeneration with NaOH.

The AO was pilot tested in a rural community in the Ethiopian Rift Valley where groundwaters are heavily enriched with fluoride. The capital and operation cost of AO defluoridation plant were estimated based on information collected from field experience. The result from community the defluoridation plant showed that fluoride in the feed water (8–10 mg/L) is removed below 0.1 mg/L. The average adsorption capacity was determined to be 2.11 mg/g based on continuous field monitoring results obtained until the fluoride content in the treated water exceeds the breakthrough value of 1.5 mg/L. The capital and operational costs of the 1200 L/day defluoridation plant was estimated at approximately Birr 161,987 (9700 USD) and Birr

220 (13 USD) per $m^3$ of treated water, respectively. No major operational problems and complaints from the beneficiaries were experienced during operation.

Due to its high adsorption capacity compared to all commercially available aluminium hydroxide–based adsorbents for fluoride removal, AO is a highly promising material for defluoridation of drinking water both at household and community levels.

**Acknowledgments**

First and foremost, I would like to express my sincere appreciation for my supervisors Dr. Feleke Zewge, Dr. C. Annette Johnson and Prof. Bhagwan Singh Chandravanshi; for their guidance, contribution and encouragements. Particularly, Dr. Feleke who was also my supervisor during my M.Sc. study has special place in my educational journey. My appreciation is also goes to Prof. Chandravanshi for his continuous support and frank advices in my personal life and to Dr. Annette Johnson for her enormous contributions in my scientific work and supporting my project in multiple ways.

Special thanks go to Eawag staff Ralf Kaegi, Hermann Moench, and Lars Osterwalder; and EMPA staff Barbara Lothenbach, Belaye Zeleke, and Hans Jourg for supporting my work in their laboratories and for their valuable discussions, and deep engagements in the project.

This acknowledgment is also extended to Dr. Hofius Henning from Albemarle, Germany for offering the aluminium hydroxide–based adsorbents and Dr. Daniel Rentsch from Swiss Federal Laboratories for Material Sciences and Technology (EMPA) for undertaking the $^{27}$Al NMR analysis. Special thanks go to Eawag staff, Mr. Michael Simmler and Mr. Marcel Mathis for assisting me while I was doing experimental work.

I am obliged to thank the following institutions that played a major role in my project work. These are Swiss National Science Foundation (SNSF) for financial support and the Swiss Federal Institute of Aquatic Science and Technology (Eawag) for technical support. I also like to thank the Swiss Federal Laboratories for Material Sciences and Technology (EMPA) for undertaking material characterization.

I would also like to express my utmost gratitude to Addis Ababa University, Department of Chemistry and its staff members for their uninterrupted cooperation and contribution for my study. I also want to thank Ambo University for giving this opportunity to do my PhD and financial support.

Some part of this study was also supported by the International Foundation for Science (IFS), Stockholm, Sweden and Organization for the Prohibition of Chemical Weapons (OPCW), The Hague, Netherlands, through a grant to Dr. Feleke Zewge.

Ethiopian Ministry of Water and Energy (MoWE) and a local non–governmental organization, Oromo Self Help Organization (OSHO) are also appreciated for their technical support during my field work.

## Table of contents

Pages

List of Figures ..... xvi

List of Tables ..... xx

List of Abbreviations ..... xxi

Chapter 1

1. Introduction and motivation ..... 1

1.1. Occurrence of fluoride in groundwater ..... 1

1.2. Global distribution of fluoride ..... 2

1.3. Health effects of fluoride ..... 4

1.4. Guidelines for fluoride in drinking water ..... 5

1.5. Fluorosis mitigation options ..... 6

1.5.1. Search for alternative sources ..... 6

1.5.2. Defluoridation of water ..... 7

1.6. Technologies for fluoride removal from water ..... 8

1.7. Rationale of the study ..... 12

1.8. The aim of this study ..... 14

1.8.1. Significance of the study ..... 16

Chapter 2

2. Literature review ..... 18

2.1. Adsorbents for defluoridation of water ..... 18

2.1.1. Alumina and aluminium–based adsorbents ..... 18

2.1.1.1. Activated alumina ..... 18

2.1.1.2. Modified aluminium based adsorbents ..... 22

2.1.2. Calcium–based adsorbents ..... 25
2.1.3. Carbon–based adsorbents ..... 27
2.1.4. Natural materials as adsorbent ..... 28
2.1.5. Industrial wastes as adsorbent ..... 31
2.1.6. Nano–adsorbents ..... 33
2.2. Field experiences of aluminium hydroxide–based adsorbents ..... 36
2.2.1. Global scenario ..... 37
2.2.2. Ethiopian scenario ..... 39
Chapter 3
3. Materials and methods ..... 41
3.1. Synthesis and characterization of aluminium hydroxide–based adsorbents ..... 41
3.1.1. Synthesis of AO, AOMO and nano–AlOOH ..... 41
3.1.1.1. Synthesis of aluminium hydro(oxide) (AO) ..... 41
3.1.1.2. Synthesis of aluminium oxide–manganese oxide (AOMO) composite material ..... 41
3.1.1.3. Synthesis of nanoscale aluminium oxide hydroxide (nano–AlOOH) ..... 42
3.1.2. Characterization of AO, AOMO and nano–AlOOH ..... 42
3.2. Batch adsorption studies of AO, AOMO and nano–AlOOH ..... 44
3.2.1. Effect of process parameters on fluoride removal efficiency of AOMO ..... 45
3.2.2. Effect of process parameters on fluoride removal efficiency of nano–AlOOH ..... 45
3.2.3. Adsorption isotherms and kinetics of fluoride adsorption onto AOMO ..... 46
3.2.4. Adsorption isotherms and kinetics of fluoride adsorption onto nano–AlOOH ..... 47
3.3. Optimization of aluminium hydro(oxide) (AO) ..... 47

3.3.1. Optimization of AO produced at different OH:Al ..... 47
3.3.2. Characterization and acid–base titration of AO produced at different ratios ..... 47
3.3.2.1. Characterization ..... 47
3.3.2.2. Acid–base titration ..... 48
3.3.3. Effect of co–existing anions on fluoride adsorption capacity of AO ..... 48
3.3.4. Mini–column experiments with AO ..... 49
3.3.5. Granulation of AO ..... 49
3.4. Comparison of AO with aluminium hydroxide–based adsorbents ..... 50
3.4.1. Adsorbents ..... 50
3.4.2. Surface acidity of the adsorbents ..... 51
3.4.3. Investigation of AO instability in batch experiments ..... 51
3.4.4. Coordination geometry of Al species by $^{27}$Al MAS NMR ..... 52
3.4.5. FTIR spectroscopy ..... 52
3.4.6. Comparison of fluoride breakthrough in continuous column experiments ..... 52
3.4.7. Comparison of repetitive regeneration potential ..... 53
3.5. Field implementation of AO in a pilot community defluoridation plant in rural Ethiopia ..... 53
3.5.1. Study area ..... 53
3.5.2. Pilot scale production of AO adsorbent ..... 54
3.5.3. Design and construction of AO community defluoridation plant ..... 57
Chapter 4
4. Results and discussions ..... 61
4.1. Characterization results of AO, AOMO, and nano–AlOOH ..... 61
4.1.1. Physical and chemical characteristics of AO ..... 61

4.1.2. Physical and chemical characteristics of AOMO ..... 64

4.1.3. Physical and chemical characteristics of nano–AlOOH ..... 67

4.2. Batch adsorption studies of AOMO and nano–AlOOH ..... 70

4.2.1. Factors affecting fluoride adsorption onto AOMO ..... 70

4.2.1.1. Effect of manganese oxide proportion ..... 70

4.2.1.2. Effect of solution pH ..... 71

4.2.2. Factors affecting fluoride adsorption onto nano–AlOOH ..... 73

4.2.2.1. Effect of adsorbent dose and contact time ..... 73

4.2.2.2. Effect of initial fluoride concentration ..... 76

4.2.2.3. Effect of solution pH ..... 77

4.2.3. Adsorption isotherms and kinetics of fluoride adsorption onto AOMO and nano–AlOOH ..... 78

4.2.3.1. Adsorption isotherms and kinetics of fluoride adsorption onto AOMO ..... 78

4.2.3.2. Adsorption isotherms and kinetics of fluoride adsorption onto nano–AlOOH ..... 84

4.3. Fluoride adsorption performance of aluminium hydro(oxide) (AO) ..... 86

4.3.1. Fluoride uptake capacity of AO synthesised at different OH:Al ratios ..... 87

4.3.2. Effect of co–existing ions on fluoride uptake ..... 88

4.3.3. Fluoride removal performance of AO in packed bed column ..... 90

4.3.4. Performance of granulated AO powder ..... 94

4.4. Comparison surface properties, elemental composition, and geometry of AO with aluminium hydroxide–based adsorbents ..... 95

4.4.1. Surface acidity and elemental composition ..... 95

4.4.2. Solubility of aluminium hydroxide–based adsorbents ..... 95

4.4.3. Coordinate geometry of Al in aluminium hydroxide–based adsorbents ..... 97
4.4.4. Surface characterization of AO and AA based on FTIR spectroscopic technique ..... 99
4.4.5. Fluoride breakthough in packed bed columns ..... 101
4.4.6. Regeneration potential of Al–hydroxide–based adsorbents ..... 103
4.5. Proposed structure of AO ..... 104
4.5.1. Basaluminite ..... 104
4.5.2. Occurrence of basaluminite ..... 104
4.5.3. Comparision of AO with basaluminite ..... 105
4.5.4. Proposed chemical structure of AO adsorbent ..... 108
4.6. Pilot community defluoridation plant using AO in rural Ethiopia ..... 110
4.6.1. Performance evaluation of AO community scale defluoridation system ..... 110
4.6.2. Evaluation of the potential of AO for uptake of other contaminant ions ..... 113
4.6.3. Estimated capital and operational cost for AO community defluoridation pilot plant ..... 114
Chapter 5
5. Conclusions ..... 116
References ..... 120
Appendices ..... 140

**List of Figures**

Page

Figure 1: Predicted probability of fluoride concentration in the groundwater exceeding the WHO guideline for drinking water of 1.5 mg/L ..... 3

Figure 2: Fluoride concentrations (mg/L) in deep and shallow wells in and outside Ethiopian Rift Valley ..... 4

Figure 3: Applied temperature ranges for alumina production ..... 19

Figure 4: Thermal production of granular activated alumina (Compalox$^{R}$ AN/V–812) from boehmite ..... 51

Figure 5: Areal map of the study area (Tsuchigragona) ..... 54

Figure 6: Raw materials for the production of AO ..... 55

Figure 7: Simple AO production process ..... 56

Figure 8: Calcite obtained after crushing the marble leftover ..... 57

Figure 9: The design of AO community defluoridation pilot plant implemented in Tuchigragona, Oromya Regional State, Ethiopia ..... 58

Figure 10: AO community defluoridation pilot plant implemented in Tuchigragona ..... 59

Figure 11: X–ray diffractogram of AO ..... 63

Figure 12: SEM photographs of AO (magnification; a) 16,000X and b) 30,000X), showing $Na_2SO_4$ on the left and amorphous Al hydroxide on the right ..... 63

Figure 13: Thermogravimetric analysis of AOMO ..... 64

Figure 14: a) X–ray diffractogram of AOMO and b) SEM images of AOMO ..... 66

Figure 15: The X–ray diffraction pattern of nano–AlOOH ..... 67

Figure 16: Thermogravimetric analysis of nano–AlOOH ..... 69

Figure 17: Effect of thermal treatment and percentage of manganese oxide on fluoride

removal efficiency of AOMO (adsorbent dose = 4 g/L, initial fluoride concentration = 20 mg/L, contact time = 180 min, pH = 7.0 ± 0.20) ..... 70

Figure 18: Effect of initial solution pH on fluoride removal efficiency (initial $F^-$ concentration = 20 mg/L, adsorbent dose = 4 g/L, contact time = 120 min) ..... 72

Figure 19: Residual $F^-$ concentration as a function of time for different dose of nano–AlOOH ($C_o$ = 20 mg/L) ..... 74

Figure 20: Capacity and efficiency (%) as a function of adsorbent dose ($C_o$ = 20 mg/L, contact time = 60 min) ..... 75

Figure 21: Effect of initial fluoride concentration on fluoride removal efficiency as a function of contact time (dose = 1.6 g $L^{-1}$) ..... 76

Figure 22: Effect of initial solution pH on fluoride removal efficiency of the media (dose = 1.6 g/L, $C_o$ = 20 mg/L, and contact time = 60 min) ..... 78

Figure 23: Linear and non–linear isotherm models for the adsorption of fluoride by AOMO (a) linearized Langmuir, (b) linearized Freundlich, (c) linearized Dubinin–Radushkevich (d) non–linear isotherms (adsorbent dose = 4 g/L, contact time = 4 h, pH = 7.0 ± 0.2) ..... 81

Figure 24: a) linear and c) non–linear pseudo–first order and b) linear and d) non–linear pseudo–second order kinetics for the adsorption of fluoride on AOMO with initial fluoride concentrations of 10 mg/L, 20 mg/L and 40 mg/L, to adsorbent doses of 1.0, 2.0 and 4 g/L respectively (pH = 7.0 ± 0.2, contact time = 10 h) ..... 82

Figure 25: Linearized Langmuir isotherm of the adsorption process ($C_o$ = 50 mg/L, contact time = 24 h, and pH = 7) ..... 84

Figure 26: Average pseudo–second order plot of fluoride adsorption kinetics on adsorbents each with the same initial load (pH = 7.01–7.18, contact time, 10 h) ..... 86

Figure 27: Fluoride uptake and binding sites as a function of OH:Al synthesis ratios ..... 88

Figure 28: Effect of co–existing anions on fluoride removal efficiency of AO ..... 89

Figure 29: Fluoride removal from deionized water with influent fluoride concentration of a) 0, and b) 20 mg/L at flow rate of 100 empty bed volume/day ..... 91

Figure 30: Fluoride removal from raw water with influent fluoride concentration of 20 mg/L at flow rate: (a) 100, (b) 10, (c) 10 empty bed volume/day ..... 93

Figure 31: Breakthrough curve for granulated AO with influent fluoride concentration of 20 mg/L and at flow rate of 10 eBV/day ..... 94

Figure 32: Solubility profiles. Concentration of [Al(III)] in solution (log scale) as a function of pH for AO (♦), crystalline $Al(OH)_3$ (dotted line), and amorphous $Al(OH)_3$ (dashed line) ..... 97

Figure 33: $^{27}Al$ MAS NMR spectra recorded at room temperature for AO, psuedoboehmite (PB) and activated alumina (AA); before and after (10 mg/g) fluoride adsorption ..... 98

Figure 34: FTIR spectra of AO and AA before and after adsorption of 10 mg/g of fluoride .. 101

Figure 35: Fluoride breakthrough curves for AO (♦), AA (■) and (▲) at influent fluoride concentration (20 mg/L) and flow rate (10 eBV/day) ..... 102

Figure 36: Repetitive performance of AO, AA and PB with regeneration between cycles ..... 103

Figure 37: [a] XRD spectra of AO and basaluminite (Kim *et al*., 2002), [b] TGA of AO and basaluminite (Kim J.J. and Kim S.J., 2003), and [c] FTIR spectra of AO, basaluminite and hydrobasaluminite (Tien, 1968) ..... 105–107

Figure 38: The crystal structure of basaluminite; grey (Al), red (O bonded with Al), yellow (S), blue (O bonded with S), pink ($H_2O$ molecule) (Farkas and Pertlik, 1997) ..... 110

Figure 39: Breakthrough curve for field tests conducted in 2011 and 2012 ..... 111

Figure 40: Potential of AO for uptake of other contaminants (As, U and Se) ..... 114

**List of Tables**

**Page**

Table 1: Comparison of difference technologies for fluoride removal ..... 11

Table 2: Elemental composition, surface area (SA), density and point of zero charge (PZC) of AO, AOMO and nano–AlOOH ..... 62

Table 3: Linear and non–linear isotherm equations and parameters ..... 79

Table 4: Linear and non–linear kinetic equations and parameters ..... 80

Table 5: Comparison of linear and non–linear models using error functions ..... 83

Table 6: Langmuir, Freundlich, Dubinin–Radushkevich (D–R), and Temkin model constants at pH = 7 and 25 $^{o}$C ..... 85

Table 7: Composition of AO synthesised at different OH:Al ratios ..... 87

Table 8: Acidity and surface site concentration, surface area, and elemental composition of AO, AA and PB ..... 95

Table 9: Average water quality characteristics of groundwater and treated water before the fluoride concentration reaches 2.0 mg/L ..... 113

Table 10: Capital and operational costs for AO community defluoridation systems ..... 115

**List of Abbreviations**

| | |
|---|---|
| AA | Activated Alumina |
| AAU | Addis Ababa University |
| ACFs | Activated carbon fibers |
| AFM | Atomic force microscopy |
| AlLS | Aluminium hydroxide impregnated limestone |
| $^{27}$Al MAS NMR | $^{27}$Al magic angle spinning nuclear magnetic resonance |
| AO | Aluminium hydro(oxide) |
| AOMO | Aluminium oxide–manganese oxide composite material |
| CIP | Common intersection point |
| CNFs | Carbon nano–fibers |
| CNTs | Carbon nano–tubes |
| CRS | Catholic Relief Service |
| DIW | Deionized water |
| D–R | Dubinin–Radushkevitch |
| Eawag | Swiss Federal Institute of Aquatic Science and Technology |
| eBV | empty bed volume |
| EC | Electrical conductivity |
| ED | Electrodialysis |
| FTIR | Fourier transform infrared |
| GAC | Granular activated carbon |
| GZLB | Granular Zr–loaded bentonite |
| HMOCA | Hydrous–manganese–oxide–coated alumina |
| IC | Ion chromatography |

| | |
|---|---|
| ICP–MS | Inductively coupled plasma–mass spectrometry |
| ICP–OES | Inductively coupled plasma–optical emission spectrometry |
| IPCL | Indian PetroChemicals Limited |
| ISE | Ion selective electrode |
| MAAA | Magnesia–amended activated alumina |
| meq | milli equivalent |
| MOCA | Manganese oxide–coated alumina |
| nano–AlOOH | Nano aluminium oxy hydroxide |
| NEERI | National Environmental Engineering Research Institute of India |
| NF | Nano–filtration |
| NGOs | Non–governmental organizations |
| NSF | National Science Foundation |
| OSHO | Oromo Self Help Organisation |
| PB | Pseudoboehmite |
| PZC | Point of zero charge |
| RO | Reverse osmosis |
| SA | Surface area |
| SD | Standard deviation |
| SEM | Scanning electron microscope |
| TDS | Total dissolved solids |
| TGA | Thermo gravimetric analysis |
| THA | Treated hydrated alumina |
| UHA | Untreated hydrated alumina |
| UNICEF | United Nations International Children's Emergency Fund |

| | |
|---|---|
| USD | United States Dollar |
| USEPA | United States Environmental Protection Agency |
| WHO | World Health Organization |
| XPS | X–ray photoelectron spectroscopy |
| XRD | X–ray diffraction |
| ZICFC | Zirconium ion–impregnated coconut fiber charcoal |

# Chapter 1

# 1. Introduction and motivation

## 1.1. Occurrence of fluoride in groundwater

Fluorine is the most reactive and the most electronegative non–metal and therefore almost never occurs in nature in its elemental state. It is the 13$^{th}$ most abundant element in the earth's crust (Koritnig, 1951). It occurs in a combined form as fluorides in rocks and soil in a wide variety of minerals such as fluorspar (fluorite) ($CaF_2$), cryolite ($Na_3AlF_6$), apatite ($Ca_5(PO_4)_3F$), and topaz $Al_2SiO_4(F,OH)_2$ (Buxton and Shernoff, 1999; WHO, 1994; Hamilton *et al*., 1982).

Traces of fluoride are present in many natural waters, and higher concentrations often associated with groundwaters. The release of fluoride to groundwater is dependent on chemical and physical processes that take place between the groundwater and its geological environment. Fluorite ($CaF_2$) is the predominant mineral that controls the dissolved fluoride concentration in the groundwater (Edmunds and Smedley, 2005; Saxena and Ahmed, 2003; Handa, 1975). Thus fluoride–rich groundwaters are often associated with low calcium concentrations associated with rocks with low calcium content, or high pH conditions where sodium bicarbonate dominates the groundwater composition and calcium precipitates as calcite ($CaCO_3$). Apart from the groundwater chemistry, hydrological properties (e.g., residence time) as well as climatic conditions (e.g., evapotranspiration, precipitation) and soil conditions (e.g., pH, soil type) have an influence on fluoride concentration (Edmunds and Smedley, 2005; Ayoob and Gupta, 2006; Saxena and Ahmed, 2003; Hudak, 1999; Valenzuela–Vasquez *et al*., 2006). The links between high fluoride and both high alkalinity ($HCO_3^-$) and increased temperature are quite strong in the Ethiopian groundwaters. These parameters can therefore be used as potential indicators of groundwater–fluoride problems in areas of exploration for new groundwater sources.

Drinking water is often the main source of fluoride intake by humans, especially in areas where fluoride concentrations in groundwater and/or surface water are high (Jaffery *et al*., 1998; Edmunds and Smedley, 2005; Tekle–Haimanot *et al*., 2006). In some areas, foodstuffs (tea in particular can contain high fluoride concentrations, and levels in dry tea are on average 0.1 mg/g) (Zerabruk *et al.*, 2010) and/or indoor air pollution due to the burning of coal may make significant contributions to the daily intake of fluoride (Nielsen and Dahi, 2002; Ando *et al*., 2001). On a local scale anthropogenic activities, such as the application of phosphate–containing fertilizers or aluminium smelting, may introduce considerable amounts of fluoride into the environment (Saxena and Ahmed, 2003).

### 1.2. Global distribution of fluoride

High fluoride concentrations can be found in many parts of the world, particularly in some parts of India, China, Central and East Africa and South America (Figure 1, Amini *et al.*, 2008). The most well–known and documented area associated with volcanic activity follows the East African Rift system from the Jordan valley down through Eritrea, Ethiopia, Uganda, Kenya and Tanzania. Many of the lakes of the Rift Valley system, especially the soda lakes, have extremely high fluoride concentrations; 1,640 mg/L and 2,800 mg/L, respectively, in the Kenyan Lakes Elmentaita and Nakuru (Nair *et al*., 1984), and up to 690 mg/L in the Tanzanian Momella soda lakes.

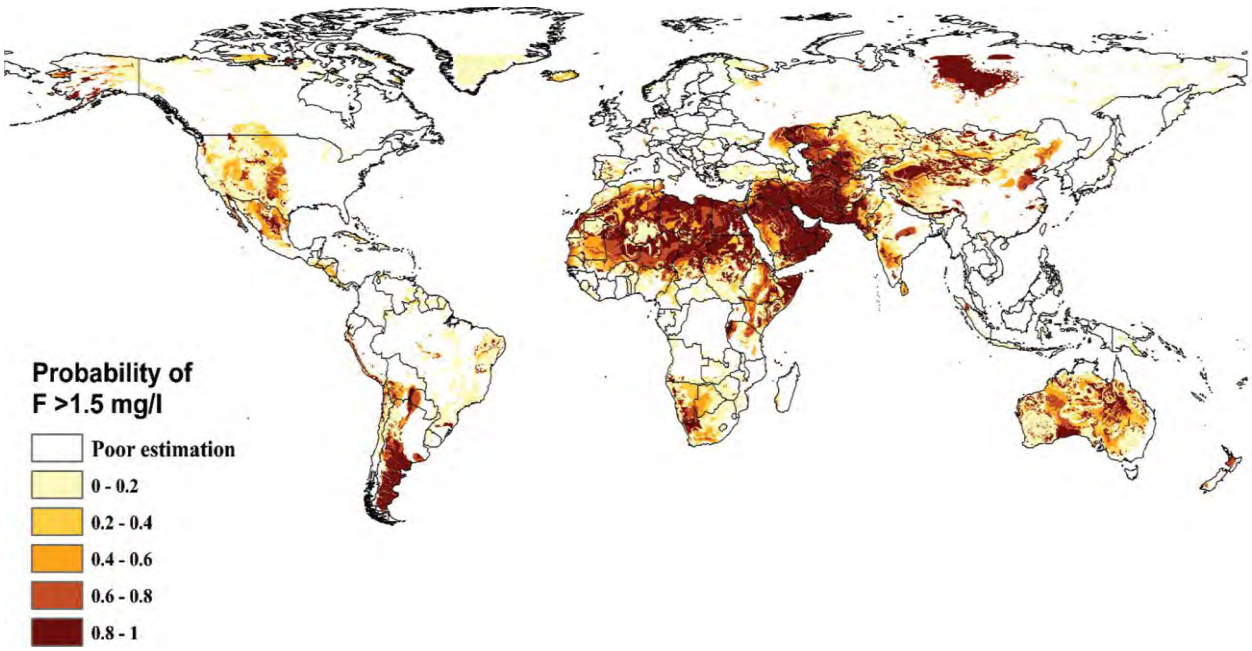


Figure 1. Predicted probability of fluoride concentration in the groundwater exceeding the WHO guideline for drinking water of 1.5 mg/L (Amini *et al.*, 2008).

Of the total 1438 water samples tested in Ethiopia, 24.2% had fluoride concentrations above the 1.5 mg/L. Regionally, by far the highest fluoride levels were recorded in the Ethiopian Rift Valley, where 41.2% of all samples exceeded the 1.5 mg/L level. The highest fluoride concentrations were recorded for Ethiopian Rift Valley lakes Shala (264.0 mg/L) and Abijata (202.4 mg/L) and the lowest in Lake Tana (1.0 mg/L), and rivers, wells and springs in the highlands (Figure 2, Tekele–Haimanot *et al*., 2006).

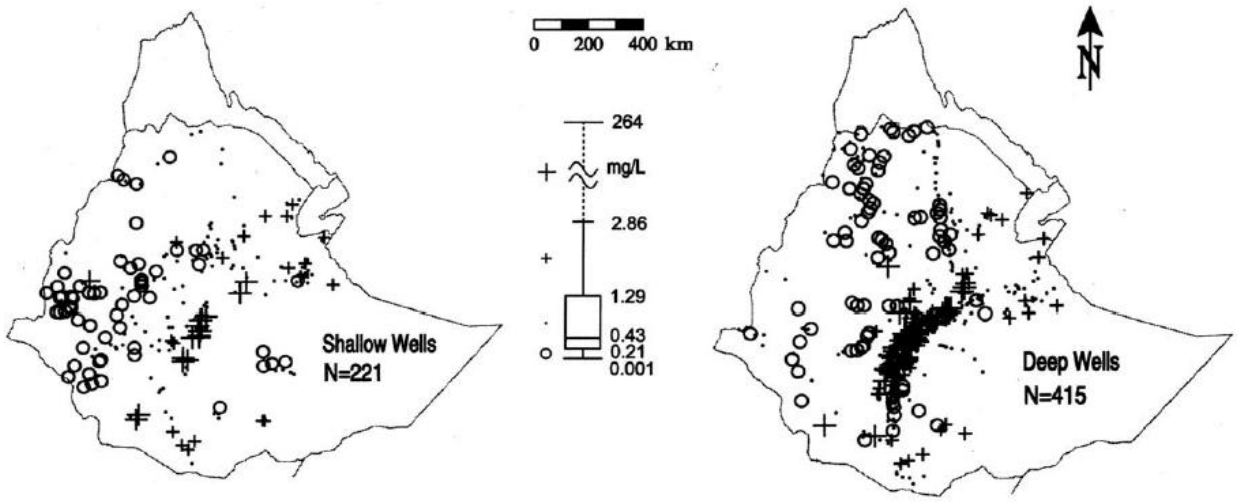


| F (mg/L) | Outside Rift Valley | | | | Within Rift Valley | | | |
|---|---|---|---|---|---|---|---|---|
| | Deep wells | | Shallow wells | | Deep wells | | Shallow wells | |
| | No. of samples | % | No. of samples | % | No. of samples | % | No. of samples | % |
| < 1.0 | 225 | 86.5 | 169 | 92.3 | 192 | 37.9 | 90 | 55.6 |
| 1.0 –1.5 | 25 | 9.6 | 4 | 2.2 | 61 | 12.1 | 28 | 17.3 |
| 1.51–3.0 | 9 | 3.5 | 10 | 5.5 | 93 | 18.4 | 19 | 11.7 |
| 3.1–7.0 | 1 | 0.4 | – | – | 102 | 20.2 | 15 | 9.3 |
| 7.1–13.0 | – | – | – | – | 53 | 10.5 | 7 | 4.3 |
| >13.0 | – | – | – | – | 5 | 1.0 | 3 | 1.9 |
| Total | 260 | 100 | 183 | 100 | 506 | 100 | 162 | 100 |

Figure 2. Fluoride concentrations (mg/L) in deep and shallow wells in and outside Ethiopian Rift Valley (Tekele–Haimanot *et al*., 2006).

### 1.3. Health effects of fluoride

The effects of fluoride upon human health have been studied since the early 20$^{th}$ century. Both the benefits of minimal exposure and the risks of high fluoride doses have been established

(Hichour *et al*., 2000). A higher daily dose has been linked to permanent dental and skeletal fluorosis (Mahramanlioglu *et al*., 2002). It is estimated that more than 200 million people worldwide (UNESCO, 2012) rely on drinking water with fluoride concentrations exceeding the present WHO guideline of 1.5 mg/L (WHO, 2004). The incidence of fluorosis has been reported in some parts of Ethiopia, where fluoride concentrations in drinking water exceed the WHO guideline value of 1.5 mg/L (Tekle–Haimanot *et al*., 1987; Zeng and Hong, 1988; Dissanayake, 1991; Reimann and Banks, 2004; Zewge, 2005; Tekele–Haimanot *et al*., 2006; WHO, 2011). Many water sources in Ethiopia contain fluoride in elevated concentrations up to 26 mg/L (Kloos and Tekle–Haimanot, 1999). According to estimates of the Ethiopian Ministry of Water Resources, more than 11 million people in the Ethiopian Rift Valley rely on drinking water contaminated by fluoride (Tekle–Haimanot, 2005). Tekele–Haimanot *et al.* (2006) reported that over 40% of deep and shallow wells are contaminated and over 80% of children suffer from different degrees of dental fluorosis and skeletal fluorosis is increasing, mainly among older people.

### 1.4. Guidelines for fluoride in drinking water

Taking health effects into consideration, the WHO (1996) has set a guideline value of 1.5 mg/L as the maximum permissible level of fluoride in drinking waters. However, it is important to consider climatic conditions, volume of water intake, diet and other factors in setting national standards for fluoride. As the fluoride intake determines health effects, standards are bound to be different for countries with temperate climates and for tropical countries, where significantly more water is consumed. Although water is generally the major route of fluoride intake, exposure from diet and air may become important in some situations. However, in many cases, the required data on different routes of exposure may be lacking. Data obtained by monitoring

fluoride levels in local water supplies and the incidence of fluorosis in the local population can be used to arrive at the appropriate standards.

### 1.5. Fluorosis mitigation options

#### 1.5.1. Search for alternative sources

If the fluoride concentration in a community's water supply is significantly and consistently beyond the permissible level, it is essential to consider remedial measures to combat fluorosis. The first choice should be to search for water with a lower fluoride level (Lyengar, 1996).

***a) Provision of a new and alternate source of water with acceptable fluoride levels***

It may be possible to get a safe water source in the vicinity by drilling a new well and/or drawing the water from different depths, as leaching of fluoride into groundwater is a localised phenomenon. Periodic monitoring is needed though, as mixing of water from different aquifers with different fluoride concentrations can occur.

***b) Transporting water from a distant source***

This may lead to lasting benefits, but initial cost will be high. Such an approach has been implemented in endemic fluorosis areas in few countries. For example in Ethiopia, Wonji/Shoa sugar state was connected to the Adama treated surface water supply system dependent on the Awash River (Tekle–Haimanot, 2005).

***c) Blending high fluoride with low fluoride water***

Mixing high and low fluoride waters so as to bring the concentration within permissible levels could be an appropriate long–term solution provided the low fluoride source is available within

reasonable distance and is of acceptable quality with respect to other health standards. This has been successfully implemented in the USA. Recently it has been tried in some parts of India.

***d) Rainwater harvesting***

There are two ways in which rainwater harvesting can be used as a solution for the fluoride problem. Individual household–roof rainwater harvesting and container storage can provide potable water for families. Harvested surface water run–off can be used to recharge high–fluoride groundwater sources.

### 1.5.2. Defluoridation of water

When none of the above options is feasible or if the only solution would take a long time for planning and implementation, defluoridation of drinking water has to be implemented. Defluoridation of drinking water is then available for the community in two options: (i) the central treatment of water at the source and (ii) the treatment of water at the point of use that is, at the household level. Defluoridation practiced at community scale is considered to be advantageous over defluoridation at the household level because of several factors listed below:

i) total cost per liter of the treated water is lower
ii) all dweller has equal access to the treated water
iii) monitoring and intervention activities are easier
iv) measures could also be taken to reduce microbial contamination
v) regeneration is cost–effective

### 1.6. Technologies for fluoride removal from water

Defluoridation technologies can be broadly divided into four categories based on the fluoride removal mechanism. These include precipitation, membrane separation, ion–exchange, and adsorption methods. The precipitation and coagulation processes with iron(III) (Tressaud, 2006), alum sludge (Sujana *et al*., 1998) and calcium (Huang and Liu, 1999) have been widely investigated. In addition, ion–exchange (Popat *et al*., 1994; Luo and Inoue, 2004; Solangi *et al*., 2009; Meenakshi and Viswanathan, 2007; Viswanathan and Meenakshi, 2009), reverse osmosis (Simons, 1993; Sehn, 2008) and electrodialysis (Adhikary *et al*., 1989) have also been studied for the removal of excess fluoride from drinking water. Many materials have been examined for their fluoride removal capacity (Bhatnagar *et al.*, 2011).

Precipitation methods have been found generally effective in the defluoridation of drinking water; however, they are unsuccessful in bringing fluoride down to desired concentration levels (Ayoob *et al*., 2008). The Nalgonda process developed by National Environmental Engineering Research Institute (NEERI) is one of the most widely used defluoridation method in India, particularly at the community level (Nawlakhe and Rao, 1990; Nawlakhe *et al*., 1975; Bulusu *et al*., 1979). It has been used for defluoridation of water in developing countries (e.g. India, Kenya, Senegal and Tanzania) (Ayoob *et al*., 2008). The possibility of using aluminium sulfate and lime combination to precipitate fluoride has also been tested in Ethiopia (Feleke and Bekele, 2000). The process comprises the addition of prescribed quantities of alum, lime, and bleaching powder to raw water, followed by rapid mixing, flocculation, sedimentation, filtration, and disinfection. After adding alum and lime to the raw water, insoluble aluminium hydroxide flocs are formed; which sink to the bottom and co–precipitate the fluoride ions. The bleaching powder ensures disinfection during the process. The entire operation of a commonly used “fill and draw type”

defluoridation unit for small community (around 200 people) can be completed within 2–3 h, with a number of batch performances in a day (Ayoob *et al*., 2008). However, some disadvantages of this technique have also been reported by few researchers, e.g. high residual aluminium concentration (2–7 mg/L) in the treated water, high dose and sludge disposal, low treatment efficiency and requirement of skilled man power (Jagtap *et al*., 2012; Ayoob *et al*., 2008; WHO, 2004; Meenakshi and Maheshwari, 2006).

Membrane processes such as reverse osmosis (RO), nano–filtration (NF), and electrodialysis have also been used for fluoride removal from water (Schoeman and Steyn, 2000; Lhassani *et al*., 2001; Garmes *et al*., 2002). RO is a physical process in which the contaminants are removed by applying pressure on the feed water to direct it through a semi–permeable membrane. RO membrane rejects ions based on size and electrical charge. Reverse osmosis produces water of extremely high purity. Ndiaye *et al*. (2005) studied fluoride removal from effluents using RO technique. It was observed that the rejection of fluoride ion was typically higher than 98%, considering that the RO membrane was fully regenerated after each set of experiments. Nano–filtration makes use of the same overall phenomenon as reverse osmosis except that the membranes have slightly larger pores than those used for reverse osmosis and offer less resistance to passage of both the solvent and the solutes. As a consequence, pressures required are much lower, energy requirements are less, removal of solutes is much less exhaustive, and flows are faster. Conversely, RO operates at higher pressures with greater rejection of all dissolved solids. The factors influencing the membrane selection are cost, recovery, rejection, raw water characteristics, and pre–treatment. The efficiency of the process is governed by various factors such as raw water characteristics, pressure, temperature, and regular monitoring and maintenance. However, RO membranes are subject to fouling and can also act as media for

microbiological growth (Ndiaye *et al*., 2005). Moreover, RO systems produce concentrated brine discharges that must be disposed of safely. Reverse osmosis systems also result in significant water loss and are not suitable for arid regions where water scarcity is a serious problem. The capital cost implications are not in favour of RO systems. Electrodialysis (ED) is a membrane process similar to RO, except that it uses an applied dc (direct current), instead of pressure, to separate ionic contaminants from water. Lounici *et al*. (2001) have also studied fluoride removal using electrodialysis. However, the ED process, besides having disadvantages associated with RO processes, is energy–intensive and hence is not suitable for rural applications.

Ion–exchange resins have also been evaluated for fluoride removal from drinking water. Fluoride can be removed from water with a strongly basic anion–exchange resin containing quaternary ammonium functional groups. The removal takes place according to the following reaction:

$$\text{Matrix}–NR_3^+Cl^- + F^- \rightarrow \text{Matrix}–NR_3^+F^- + Cl^-$$

The fluoride ions replace the chloride ions of the resin. This process continues until all the sites on the resin are occupied. The resin is then backwashed with water that is supersaturated with dissolved sodium chloride salt. New chloride ions then replace the fluoride ions, leading to recharge of the resin and starting the process again. The driving force for the replacement of chloride ions from the resin is the stronger electronegativity of the fluoride ions. Chikuma and Nishimura (1990) studied the fluoride removals by a chloride–loaded anion exchanger, Amberlite IRA–400. The chloride ions held on the surface of this resin were exchanged for fluoride ions in aqueous solution. However, Ku *et al*. (2002) noted that anion exchange resins are more vulnerable to interference than cation exchange resins. Lopez *et al*. (1992) had made

similar observations, finding that for Amberlite IRA–410 anionic resin the order of selectivity was sulfate > chloride > bicarbonate > hydroxide > fluoride. Mohan Rao and Bhaskaran (1988) reported the removal of fluoride using ion–exchange materials and their regeneration using aluminium sulfate solution (2–4%). Haron *et al*. (1995) also studied the fluoride removal using yttrium–loaded poly–(hydroxamic acid) resin.

Table 1 summarizes the advantages and limitations of different technologies for fluoride removal. Among various methods used for defluoridation of water, the adsorption process is widely used and offers satisfactory results and seems to be a more attractive method for the removal of fluoride in terms of cost, simplicity of design and operation (Jagtap *et al*., 2012).

Table 1. Comparison of difference technologies for fluoride removal.

| Methods | Advantage | Disadvantage |
|---|---|---|
| <u>Precipitation</u><br>Lime + Alum (Nalgonda technique) | – Can be used on household and community level<br>– Raw materials are locally available | – High chemical dose<br>– Disposal of sludge<br>– Risk of residual Al<br>– Not effective technique<br>– Skilled labour required<br>– Not cost effective |
| <u>Membrane</u><br>– Reverse osmosis (RO)<br>– Nano–filtration (NF)<br>– Electrodialysis | – Highly effective technique<br>– No chemicals are required<br>– No interference by anions<br>– Works under a wide pH range | – Skilled labour required<br>– Not cost effective<br>– May not be suitable for water with high salinity and TDS |
| <u>Ion exchange</u> | – Highly effective technique<br>– Retains the taste and colour of water intact | – Presence of $SO_4^{2-}$, $PO_4^{3-}$, $HCO_3^-$, etc. results in ionic competition<br>– Not cost effective<br>– Regeneration is required<br>– Treated water sometimes has low pH and high levels of $Cl^-$ |
| <u>Adsorption</u> | – Can be used on household and community level<br>– Raw materials are locally available<br>– Highly effective technique<br>– Cost effective | – Presence of $SO_4^{2-}$, $PO_4^{3-}$, $HCO_3^-$, etc. results in ionic competition<br>– Regeneration is required<br>– Disposal of saturated material<br>– Process is dependent on pH |

### 1.7. Rationale of the study

The commercially available defluoridation methods used by industrialized countries, such adsorption by activated alumina, reverse osmosis, electrodialysis and ion–exchange require more technical support for operation and maintenance and/or the capital investment cost is very high.

The Nalgonda technique in which fluoride is co–precipitated from the mixing of Al–sulphate and Ca–hydroxide, has been studied on a pilot scale in various countries such as Kenya, Ethiopia, Tanzania and Senegal (Dahi *et al.*, 1996). In early studies the Nalgonda technique was field–tested in Ethiopia and preferred at the time because of the local availability of chemicals. The community defluoridation units were piloted and implemented at full scale in collaboration with the Catholic Relief Service (CRS) (Moges *et al.*, 1996; Zewge, 2005). The ministry of water and energy of Ethiopia is implementing the Nalgonda technique in several villages, but the method is not suitable for treating water with high TDS and raw water fluoride concentration exceeding 10 mg/L. The required chemical dose is about 170 mg to remove 1 mg of fluoride with an additional lime dose 50% of alum which result in large amount of sludge. The treatment efficiency is limited to about 70% removal. There is a chance of residual aluminum and excess sulfate in treated water which may lead to health problems. Bone char as an adsorbent media has been implemented on a local scale in different countries such as Kenya (Jacobsen and Dahi, 1997), Tanzania (Mjengera and Mkongo, 2003), and Thailand (Phantumvanit *et al.*, 1988) but its acceptability is limited in some countries because of religious beliefs. Recently, a local NGO called Oromo Self Help Organization (OSHO) field tested bone char technology both at household and community scale in rural villages of Ethiopia. Although, charring of bones removes organic matter and greatly increases the specific surface area and fluoride adsorption

capacity on the bone hydroxyapatite (Christoffersen *et al.,* 1991; Larsen *et al.,* 1994), religious and cultural beliefs may render cow bone char undesirable in certain regions including Ethiopia. Dr. David Sabatini, who is our principal collaborator at the University of Oklahoma and his research group, evaluated fish bone char as an alternative and found that it performed similar to cow bone char (Brunson and Sabatini, 2009). In their current National Science Foundation (NSF) project, they are working on how to enhance the fluoride uptake capacity of fish bone char by coating with aluminium oxyhydroxide and other materials to prolong its life span during actual field implementation.

In addition, as the Ethiopian Rift Valley groundwater is highly enriched with fluoride, the commercially available adsorption technologies such as activated alumina and bone char are not cost effective due to their limited fluoride uptake capacity.

Hence, there is a need to find locally–available defluoridation media with high fluoride adsorption capacity as an alternative method for safe and easy use both at household and small community levels.

A fluoride removal method using aluminium hydro(oxide) (AO) as an adsorbent has been under development in the Chemistry Department of Addis Ababa University (AAU) since 2004. The AO can easily be produced from locally manufactured aluminium sulfate, $Al_2(SO_4)_3 \cdot 14H_2O$, which is purchased from Awash Melkasa Aluminium Sulfate and Sulfuric Acid Factory, Ethiopia. Laboratory tests have demonstrated a very high removal capacity of about 23.7 mg/g (Shimelis *et al*., 2006). Studies so far have indicated that the adsorbent has better performance

than activated alumina (AA), which is well known commercially available material for fluoride removal.

However, this highly promising adsorbent needs detailed physical and chemical characterization in order to understand the sorption process and the manufacturing method should be refined to make it suitable for field application. Further investigations are needed to understand the relationship between bulk and surface acid–base properties and fluoride adsorption capacity in comparison to aluminium hydroxide–based adsorbents. Another important issue is related to the health aspects in using AO filters, namely aluminium solubility. The potential for regeneration and the effect of regeneration on adsorption capacity also needs to be studied. Finally, the adsorbent should be tested in a pilot community filter plant in Ethiopian Rift Valley to evaluate its performance under real condition.

### 1.8. The aim of this study

**General objective**

- The main aim of this study is to develop fluoride removal adsorbent based on the experience with AO (aluminium hydro(oxide), to understand the fluoride adsorption mechanism, to evaluate and compare its performance and to demonstrate the performance of this technology at pilot scale in rural community. In addition to AO, aluminium oxide–manganese oxide (AOMO) composite material and nanoscale aluminium oxide hydroxide (nano–AlOOH) will be tested.

**Specific objectives**

- Synthesis of AO, AOMO and nano–AlOOH.
- Characterization of aluminium hydroxide–based adsorbents using different instrumental techniques:
  - ✓ Determination of elemental composition by ICP–MS, ICP–OES, and IC
  - ✓ Determination of density and surface area of AO, AOMO and nano–AlOOH
  - ✓ Investigation of AO, AOMO and nano–AlOOH by XRD, SEM, and TGA
  - ✓ To analyze the coordination geometry of Al in AO, AA and PB using $^{27}$Al MAS NMR
  - ✓ Investigation of AO and AA using FTIR
  - ✓ Determination of PZC of AO, AOMO, and nano–AlOOH.
- To study the batch adsorption process parameters for AOMO and nano-AlOOH.
- To optimize the synthesis of AO adsorbent by using different OH:Al ratios.
- To carry out acid–base titration for the determination of surface acidity and surface site concentration of AO.
- To investigate the effect of co–existing anions on fluoride adsorption onto AO.
- To carry out column experiments to demonstrate AO adsorbent performance under various operation conditions.
- To compare the performance of different aluminium hydroxide–based adsorbents (AO, AA, PB), in terms of surface acidity and surface site concentrations, fluoride adsorption capacity, and potential for repetitive regeneration.
- To test AO in a pilot community scale defluoridation system in Tuchigragona, Oromya Regional State, Ethiopia.

### 1.8.1. Significance of the study

In the Ethiopian Rift Valley Regions, excessive fluoride in groundwater is a serious water safety problem, mainly affecting areas in Afar, Oromia, and the Southern Nations, Nationalities and Peoples Regional States. Yet, groundwater provides drinking water is the sole source of drinking water for many rural communities and urban centers in the Rift Valley. The use of groundwater is increasing sharply due to increasing population density and scarcity of surface waters. Furthermore, it is often assumed that natural, uncontaminated waters from deep wells are clean and healthy. After many years of use of drinking water from drilled wells in the Rift Valley, Ethiopia, dental and skeletal fluorosis has become a serious medical problem (Tekle–Haimanot *et al.*, 1987; Kloos and Tekle–Haimanot, 1999).

Over 80% of children suffer from varying degrees of dental fluorosis, and skeletal fluorosis is increasing, mainly among adults and older people. The mitigation of this health problem has been hampered mainly by the lack of an efficient, inexpensive, acceptable removal method. A switch to treated surface waters for drinking is being assessed, but it is well recognized that fluoride removal systems are required for communities without any alternative drinking water supply sources. To date there have been only a few field trials of fluoride mitigation systems in Ethiopia. The tested methods have low acceptability by the local community due to complexity in operation and maintenance, cost, and socio–cultural reasons which seriously affect sustainability.

Thus, there is a pressing need for high performance, and sustainable water treatment technologies for fluoride removal–the subject of this research. Sustainability requires technical efficiency, local availability, economic and social viability, and simplicity of operation and

maintenance. While motivated by challenges in rural villages of Ethiopia, research results will also benefit those living in rural communities of other East African countries impacted by fluoride.

# Chapter 2

# 2. Literature review

## 2.1. Adsorbents for defluoridation of water

### 2.1. 1. Alumina and aluminium–based adsorbents

#### 2.1.1.1. Activated alumina

Activated alumina (AA) has been an adsorbent of interest and extensively studied for years for fluoride removal from drinking water. It has a high affinity and selectivity for fluoride. Defluoridation processes based on AA have been used at both community and domestic levels.

The term ‘‘activation’’ is used to indicate a change in properties resulting from heating. In general, as a hydrous alumina precursor is heated, water is driven off leaving a porous solid structure of activated alumina. Figure 3 shows the decomposition sequence for several hydrous precursors and indicates approximate temperatures at which the activated forms occur.

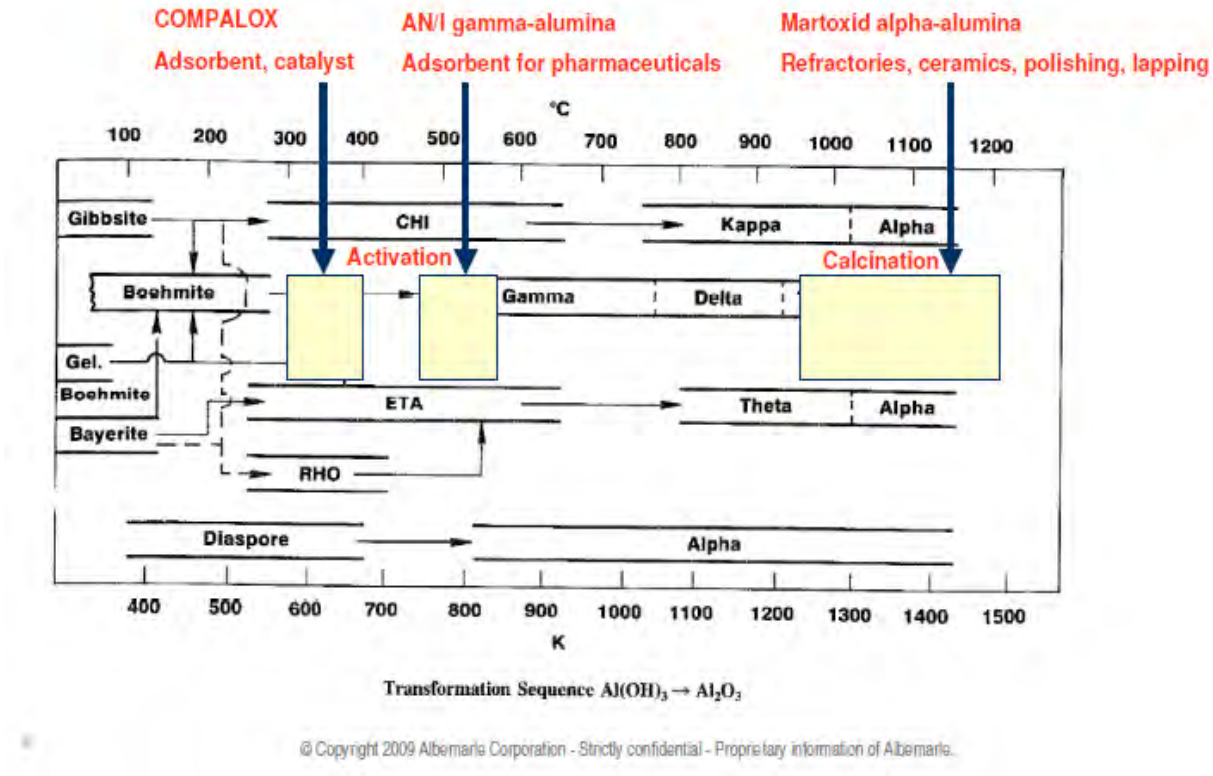


Figure 3. Applied temperature ranges for alumina production.

Farrah *et al*. (1987) studied the interaction of fluoride ion with amorphous $Al(OH)_3$, gibbsite and alumina ($Al_2O_3$) over a wide pH range (3–8) and $F^-$ concentrations (0.1–1.0 mM). It was found that at pH < 6 and total F:Al ratios > 2.5, most of the amorphous $Al(OH)_3$ gel dissolved through the formation of $AlF_x$ complexes. At lower F:Al ratios, some solid persisted in the pH 4–7 region and strongly adsorbed $F^-$ from solution. It was also observed that maximum uptake of $F^-$ occurs in the pH range of 5.5–6.5 (up to 9 mol/kg). At lower pH, fluoride uptake decreased due to the preferential formation of $AlF_x$ soluble species; at higher pH, $OH^-$ displaced $F^-$ from the solid and the amount of $F^-$ adsorbed or converted to complexes declined rapidly towards zero between pH 6 and 8. At a fixed pH (between 5 and 7.5), fluoride uptake varied in accordance with Langmuir

model (maximum capacity ~ 1 mol/kg). The amount of substrate converted into $AlF_x$ complexes in acid media increased with decreasing pH and increasing initial fluoride concentration.

Ghorai and Pant (2004) concluded that removal of fluoride was the result of ion exchange as well as adsorption, which follows both Freundlich and Langmuir isotherms (Ghorai and Pant, 2004; Ghorai and Pant, 2005). AA has a great capacity for fluoride adsorption, which is dependent upon the crystalline form, activation process, solution pH, and alkalinity. Shimelis *et al*. (2006) also showed the importance of activation, comparing untreated hydrated alumina (UHA) and thermally treated hydrated alumina (THA) obtained from hydrolysis of locally manufactured aluminium sulfate.

The use of activated alumina in a continuous–flow system was reported to be an economical and efficient method for defluoridating water supplies (Ghorai and Pant, 2004), and an adsorption capacity of 1.45 mg/g at pH 7 can be achieved. The greatest disadvantage of fluoride removal by activated alumina is that the optimum fluoride removal capacity occurs only at a pH value of the solution below 6.0, which strongly limits the practical applications of the AA. The authors observed that adsorption of fluoride was retarded in acidic solutions because of the electrostatic repulsion and when equilibrium solution pH was greater than 7.0, the fluoride adsorption by alumina decreased due to the electrostatic repulsion of fluoride ions by the negatively charged surface of alumina and the competition for active sites by excessive amounts of hydroxide ions. In addition interference due to the presence of other anions/cations has been reported to affect fluoride removal capacities of AA (Li *et al*., 2001).

Ghorai and Pant (2004) investigated the removal of fluoride using activated alumina (AA) (Grade OA–25) in batch and continuous operations. An adsorption capacity of 1.45 mg/g was obtained at pH 7. The percentage fluoride removal increased in the pH range from 4 to 7 and decreased thereafter. Silicates and hydroxyl ions were considered to compete more strongly with $F^-$ ions for alumina exchange sites at pH > 7, whereas, at pH < 7, the soluble alumino–fluoro complexes were formed which in return accounts for the presence of aluminium ions in the treated water. Early saturation and lower percentage fluoride removal was observed at higher flow rates and at higher concentrations. There was a marginal decrease in the adsorption capacity after each regeneration cycle. Regeneration procedure resulted in 85% efficiency with the grade of AA studied. A loss of 5% in adsorption capacity of AA was observed after five cycles.

The point of zero charge (PZC) of $\alpha$–$Al_2O_3$ at 20 $^oC$ was found to occur at pH 9.2. Through mineral/solution equilibria, this PZC was determined to be close to pH 9.5 of minimum solubility of amorphous aluminium hydroxide, suggesting the formation of this species onto the adsorbent's surface. Zeta potential measurements indicated that fluoride adsorbed specifically onto $\alpha$–$Al_2O_3$ by replacing hydroxyl ions from positively charged surfaces and through hydrogen bonding under conditions close to and above the $pH_{PZC}$ (Bahena *et al.*, 2002).

Moreover, it has been reported that alumina begins to leach below pH 6 and poses severe threats to human health because aluminium and its fluoride complexes are known to cause Alzheimer's disease and the other health complications (Davison *et al*., 1982; Crapper *et al*., 1973; Miller *et al*., 1984; Martyn *et al*., 1989).

Schoeman and MacLeod (1987) regenerated AA by flushing with a solution of 4% sodium hydroxide, which displaces fluoride from the alumina surface. This procedure is followed by flushing with acid to re–establish a positive charge on the surface of the alumina. They observed a marginal decrease in the adsorption capacity after each regeneration cycle.

#### 2.1.1.2. Modified aluminium based adsorbents

***Alumina plus manganese dioxide***

To enhance the adsorption efficacy of activated alumina, researchers have also modified the alumina surface. Maliyekkal *et al*. (2006) reported that a new adsorbent manganese oxide–coated alumina (MOCA) was able to bring fluoride concentrations down to the statutory limit of 1.5 mg/L for drinking water and was faster–acting than activated alumina and had a greater fluoride load capacity (2.85 mg/g compared with 1.08 mg/g for activated alumina). The MOCA was effectively regenerated using 2.5% NaOH as eluent. Tripathy and Raichur (2008) found that manganese dioxide–coated activated alumina could bring fluoride concentration down to 0.2 mg/L when the initial concentration of fluoride in water is 10 mg/L.

Teng *et al*. (2009) prepared a novel hydrous–manganese–oxide–coated alumina (HMOCA) by coating hydrous manganese oxide onto alumina surface through a redox process and used it for defluoridation. The manganese oxides were amorphous and manganese existed mainly in +IV oxidation state. The prepared adsorbent could reduce fluoride concentration from 6.0 to 0.45 mg/L at an initial pH of 5.2 ± 0.05, while the fluoride removal efficiency was 45% for the virgin activated alumina under the same condition. The optimum initial pH range of fluoride adsorption by HMOCA was 4.0–6.0 with fluoride removal efficiency higher than 95%. The surface of HMOCA was considered negatively charged when the initial pH was above 6.0 since the $pH_{PZC}$

of HMOCA was found to be 5.9, which would prevent the movement of $F^-$ towards HMOCA surface due to the Coulombic repulsion. The presence of bicarbonate, sulfate, and phosphate showed negative influence on the adsorption of fluoride. The adsorbed fluoride could be desorbed by alkali solution.

***Alumina plus magnesium oxide***

Recently Maliyekkal *et al*. (2008) described a magnesia–amended activated alumina (MAAA) prepared by impregnating alumina with magnesium hydroxide and calcining the product at 450 $^oC$. MAAA adsorbed fluoride from drinking water more effectively than activated alumina. More than 95% removal of fluoride (10 mg/L) was achieved with in 3 h of contact time at neutral pH, bringing concentration down to only 0.5 mg/L. Adsorption of fluoride on to MAAA was found to be pH–dependent and a decrease in sorption was observed at higher pH. An optimum fluoride removal was observed in the pH range of 5.0–7.5. The maximum adsorption capacity for fluoride was 10.12 mg/g in the fluoride concentrations range from 5 to 150 mg/L. Most of the co–existing ions found in the natural water source studied had negligible effect on fluoride sorption by MAAA. However, higher concentrations of bicarbonate and sulfate reduced the fluoride adsorption capacity. The fluoride bearing MAAA was regenerated with 2% sodium hydroxide solution as eluent.

***Alumina plus iron oxide***

When aluminium and iron(III) hydroxides are co–precipitated from a chloride mixture in equimolar quantities using ammonia, the resulting mixed hydroxide, after aging and drying, is a better adsorbent for fluoride than either aluminium hydroxide or iron(III) hydroxide (Biswas *et al*., 2007).

Fourier transform infrared (FTIR) spectra indicate the presence of the Fe–O–Al bond. Scanning electron microscopy (SEM) showed an almost irregular surface morphology with high porosity, indicative of a high surface area. The monolayer adsorption capacity of the mixed hydroxide, derived from Langmuir isotherms, was greater than for the pure hydroxides.

Chubar *et al*. (2005) studied the anion adsorption capacity of an adsorbent precipitated from equimolar aluminium and iron(III) chloride by addition of ammonia. The anions investigated were fluoride, chloride, bromide and bromate. At pH 4, fluoride was the most strongly adsorbed at 88 mg $F^-$/g of adsorbent. Similar observations have been made in investigating adsorption of As(III) and As(V) anionic species.

Kamble *et al*. (2010) have reported the effectiveness of alkoxide–origin alumina, γ–alumina containing small amounts of $Fe_2O_3$ and $SiO_2$ as well as activated carbon in its pores, for defluoridation of drinking water. The maximum fluoride removal efficiency was observed in the pH range of 5–7. Carbonate, bicarbonate and sulfate reduced the fluoride sorption due to the change in solution pH and competition for active sorption sites. The reason for increased adsorption by the alkoxide–origin alumina was attributed to the increased electropositivity and the small hydrophobicity retained on the alkoxide origin alumina. The breakthrough adsorption capacity was found to be strongly dependent on the feed flow rate, inlet fluoride concentration and bed height. A maximum of 85% of retained fluoride was eluted with sulfuric acid solution ($1.0 \times 10^{-1}$ mol/L), but the regenerated adsorbent showed slightly less adsorption capacity as compared to fresh alkoxide origin alumina.

### 2.1.2. Calcium–based adsorbents

Extensive research has also been carried out for the removal of fluoride using various calcium salts as calcium has a good affinity for fluoride anion. Fan *et al*. (2003) studied fluoride adsorption on a wide array of minerals including fluorite, calcite, quartz, and iron–activated quartz and compared their fluoride uptake capacities. Badillo–Almaraz *et al*. (2007) reported that the best pH range for adsorption on hydroxyapatite is 7.0–7.5, where the mineral can adsorb 19 mg/g.

Turner *et al*. (2005) conducted fluoride removal studies using crushed limestone (99% pure calcite) by batch studies and surface–sensitive techniques from solutions with high fluoride concentrations ranging from 3 to ~ 2100 mg/L. With the help of surface–sensitive techniques, such as atomic force microscopy (AFM) and X–ray photoelectron spectroscopy (XPS) as well as zeta potential measurements, the authors were able to confirm that a combination of surface adsorption and precipitation reactions removed fluoride from aqueous systems; the degree of removal being dependent on calcite surface area. The results proved that fluoride adsorption occurred immediately over the entire calcite surface with fluoride precipitating at step edges and kinks, where dissolved $Ca^{2+}$ concentration was highest. The AFM and zeta potential measurements confirmed that adsorption was instantaneous because surface morphology was immediately affected.

Activated lime and ordinary quick lime were also evaluated for their performance as adsorbents for fluoride removal from aqueous solutions (Islam and Patel, 2007). The removal of fluoride was 80.6% at optimum conditions from the synthetic solution when initial fluoride concentration was 50 mg/L. The Langmuir maximum adsorption capacity of activated quick lime for fluoride

was 16.67 mg/g. Scanning electron microscopy (SEM) micrographs and X–ray diffraction (XRD) studies revealed that the removal of fluoride was mainly due to chemisorption and precipitation. The anions reduced the fluoride adsorption in the order, $PO_4^{3-} > SO_4^{2-} > NO_3^-$.

Jain and Jayaram (2009) used aluminium hydroxide impregnated limestone (AlLS) for the efficient removal of fluoride from contaminated drinking water. The Langmuir maximum sorption capacities of the limestone and AlLS adsorbents were found to be 43.10 mg/g and 84.03 mg/g, respectively in fluoride concentrations range from 0 to 100 mg/L. Fourier transform infrared (FTIR) studies indicated that the adsorption of fluoride onto AlLS was physisorption.

A natural calcium phosphate, hydroxyapatite ($Ca_5(PO_4)_3OH$), has been obtained from animal bones by charring, to remove organic matter. The major components of bone char are hydroxyapatite (> 95%), calcium carbonate and a small amount of carbon. The fluoride removal mechanism involves the replacement by fluoride of the hydroxide ion in hydroxyapatite. The method of preparation of bone char is crucial for its fluoride adsorption capacity and the treated water quality. Poor quality bone char can impart bad taste and odour to water. Exhausted bone char is regenerated using caustic soda. In the USA in the past, a few defluoridation plants were using bone char. Now they have been largely replaced by activated alumina. Bone char is considered as an appropriate defluoridating material in some developing countries, including Ethiopia. Field trials in Thailand, Sri Lanka and some African countries have shown very encouraging results (Priyanta and Padamasiri, 1996; Mjengera *et al*., 1997; Susannae Rajchagool and Chaiyan Rajchagool, 1997).

Johnson *et al.* (2011) have assessed the technical performance, user acceptance and optimal institutional setting of bone char–based community and household filters for sustainable implementation in Ethiopia. The bone char has an average adsorption capacity about 1.2 before treated water exceeds 1.5 mg $F^-$/L. Bhargava and Killedar (1992) have studied the fluoride adsorption on fishbone char. Several reasons have limited the use of bone char in developing country that include: cost, unreliable supply of animal bones, insufficient effectiveness to reduce fluoride level to acceptable concentration as well as social unacceptability. For instance, bone media are not acceptable in some parts of Ethiopia for cultural and religious reasons.

### 2.1.3. Carbon–based adsorbents

Abe *et al*. (2004) have reported the fluoride adsorption capacity of various carbon–based adsorbents in the order bone char > coal charcoal > wood charcoal > carbon black > petroleum coke. Ramos *et al*. (1999) studied adsorption of fluoride from an aqueous solution on plain and alumina–impregnated activated carbon. It was found that the aluminium impregnation of carbon increase the fluoride adsorption capacity by 3–5 times as compared to untreated carbon.

Continuous down flow adsorption mode at room temperature was also adopted to defluoridate drinking water using zirconium impregnated activated charcoals by Janardhana *et al*. (2007). Zirconium ion–impregnated coconut fiber charcoal (ZICFC) showed maximum fluoride uptake followed by groundnut shell and coconut shell charcoals due to its large surface area. ZICFC was found effective for 21 L (8.0 mg $F^-$/L) test solution and 6 L (2.47 mg $F^-$/L) tap water. Regeneration of ZICFC was conducted by elution with 0.02 M NaOH solution.

Gupta *et al*. (2009) developed a micro nano–hierarchal web consisting of activated carbon fibers (ACF) and carbon nano–fibers (CNF), impregnated with Al for the removal of fluoride from wastewater. It was observed that pre–treatment of the feed water was not required while using the Al–CNF for treating the wastewater with pH 5.0–8.0. Using a redox process, granular activated carbon (GAC) was coated with manganese oxides and the prepared adsorbent (GAC–$MnO_2$) was used for fluoride removal from aqueous solution (Ma *et al*., 2009). The adsorption capacities of the coated GAC obtained with a 0.3 M $MnCl_2$ exhibited maximum fluoride adsorption capacity in comparison with other coated GAC, and at least three times greater than those of uncoated GAC. The pH of the solution influenced fluoride removal, and the optimum equilibrium pH for fluoride adsorption was observed to be 3.0.

### 2.1.4. Natural materials as adsorbent

Various naturally occurring materials available abundantly free of charge have been explored as adsorbents for the removal of fluoride from water.

Moges *et al*. (1996) used fired clay chips as an alternative water defluoridating media. The maximum amount of fluoride removed after equilibration was ca. 90% and 80% for solutions kept at pH 3 and 9, respectively. The maximum adsorption capacity of the adsorbent for defluoridating 1-2 litres of water was found to be 0.2 mg fluoride $g^{-1}$ adsorbent. The structure of the clay plays a very important role in determining the charge on the clay surface and type of exchange that can occur with ions in solution. In general, the more positive the surface the better the sorption will be for negatively charged ions, such as fluoride. In general, it was observed by Agarwal *et al*. (2003) and Zhuang and Yu (2002) that firing and chemical pretreatment both improve the adsorption capacity of some clays and soils. Bjorvatn *et al*. (1996) studied the

defluoridation of water using soil samples from Ethiopia. It was reported that the soil samples from highland areas around Addis Ababa reduced the fluoride content of the water from 15 to 1 mg/L. Zevenbergen *et al*. (1996) studied the defluoridation of water using the Ando soil of Kenya. It was concluded that the use of Ando soils appears to be an economical and efficient method for defluoridation of drinking water. South African clays have also been used as adsorbents for defluoridation of water (Coetzee *et al*., 2003). Various clay types such as bauxite, laterite, palygorskite, bentonite and kaolinite were tested for fluoride adsorption. Clays consisting of substantial amounts of gibbsite or aluminium oxides exhibited best overall potential as fluoride adsorbents. pH adjustment and activation of clay substrates were found to improve the adsorption capacities of some clays. Fluoride removal was found to be adversely affected only in the presence of $HCO_3^-$. Adsorption occurred on the surface as well as through intraparticle diffusion pattern as X–ray diffraction studies confirmed the deposition of fluoride on the surface of the clay material. FTIR studies also showed the involvement of hydroxyl group present on the surface in the adsorption interaction. The adsorbed fluoride was found to desorb by washing the adsorbent with a solution pH of 12 for some clay materials.

The removal of fluoride was also studied using acid activated kaolinite clay by Gogoi and Baruah (2008). The activation of clay was performed with conc. $H_2SO_4$. The clay of 300 mesh size showed maximum adsorption of fluoride due to the availability of larger specific surface area on the adsorbent surface. The optimum pH for fluoride removal was pH 4. The Langmuir maximum adsorption capacity of the acid activated clay for fluoride ranged between 0.0450 and 0.0557 mg/g at different temperatures.

Ma *et al*. (2005) synthesized granular Zr–loaded bentonite (GZLB) prepared with polyvinyl alcohol in an attempt to remove fluoride from aqueous solutions. Regeneration by alum exhibited to increase the defluoridation capacity of prepared adsorbent. An adsorption capacity of 0.76 mg/g was obtained at pH 6.97 and inlet fluoride concentration of 6.34 mg/L. The uptake of fluoride in the presence of cations was found to be enhanced, which was explained due to the increase in the amount of positive charge on the oxide surfaces and/or forming of a positively charged surface. Used adsorbent could be regenerated by the alkali treatment. The fluoride uptake mechanism was explained through replacement or exchange of $OH^-$ ions from 10% La–bentonite surface, which was exhibited by the results of pH and regeneration studies.

Zeolites have also been used for the defluoridation of aqueous solutions. Onyango *et al*. (2004) investigated the fluoride sorption characteristics of zeolite F–9 containing surface–active sites created by exchanging $Na^+$–bound zeolite with $Al^{3+}$ or $La^{3+}$ as they show good affinity for fluoride. It was concluded by the authors that the uptake of fluoride by $Al^{3+}$–exchanged zeolite proceeded by an ion–exchange mechanism, while fluoride–$La^{3+}$–exchanged zeolite interaction proceeded by physical adsorption as revealed by the Dubinin–Radushkevitch (D–R) isotherm parameters. Fluoride removal from water was affected by the solution pH and bicarbonate content. Bicarbonate buffered the system pH to higher values and thus diminished the affinity of the active sites for fluoride sorption. Reduction in the performance of adsorbents was observed in natural groundwater samples compared with results obtained with demineralized water. Overall, researchers have also taken advantage of the large internal surface area, hydrophilicity and the ion–exchange ability of low–silica synthetic zeolites to create fluoride adsorption sites by pre–treating the zeolites with $Al^{3+}$ ions for defluoridation of water (Onyango *et al*., 2006). The uptake of fluoride for each zeolite was relatively constant between pH 4 and 8. From the results of D–R

model, initial pH effects and desorption studies, it was considered that the fluoride adsorption onto the zeolites proceeded by ion–exchange or chemisorption mechanism. Aluminium ion was not detected in water suggesting that it was strongly bound onto the zeolite structure. The Langmuir maximum equilibrium sorption was found to be 2.04–4.13 mg/g for various metal loaded zeolites.

Despite of local availability of natural materials, lower efficiency in removing fluoride is considered as a main limitation of natural materials.

### 2.1.5. Industrial wastes as adsorbent

Widespread industrial activities generate huge amount of solid waste materials as by–products. One of the beneficial uses of these wastes is to convert them as inexpensive adsorbents for water treatment. Various industrial wastes have been examined with or without modification for fluoride removal from water. The ability of fly ash (a thermal power plant waste) to remove fluoride from water and wastewaters was studied by Chaturvedi *et al*. (1990). The removal of fluoride was found favourable at low concentration, high temperature and acidic pH. The Langmuir maximum adsorption capacity of fly ash for fluoride ranged from 20.0 to 20.3 mg/g.

The industrial waste residue, generated during the manufacture of aluminium sulfate (alum) from kaolin by the sulfuric acid process was used as defluoridating media by Nigussie *et al*. (2007). The percentage of fluoride removal remained nearly constant within the pH range of 3–8. With further increase in the solution pH, the fluoride removal efficiency decreased and the declining trend became significant at pH values >10. The presence of positively charged and neutral sites at the surface of the adsorbent in the pH range up to 8 was mentioned as the reason for better

fluoride removal in that range. The adsorbent fluoride removal efficiency was affected significantly by bicarbonate ion concentrations and little or no effect by other anions such as phosphates, chlorides, sulfates and nitrates.

The removal of fluoride from aqueous solution using the original and HCl–activated red mud (an aluminium industry waste) has also been studied (Cengeloglu *et al*., 2002). The fluoride adsorption capacity of the activated form was found to be higher than that of the original form. The maximum removal of fluoride ion was obtained at pH 5.5. It was found that the required time for adsorption equilibrium of fluoride ions was 2 h. The removal of fluoride ion using red mud was explained on the basis of the chemical nature and specific interaction with metal oxide surfaces, and the results were interpreted in terms of pH variations. The Langmuir maximum adsorption capacity of activated red mud for fluoride was calculated to be 6.3 mg/g.

To take advantage of these properties of alum sludge, Sujana *et al*. (1998) examined its use as an adsorbent for the removal of fluoride from polluted waters. The data indicate that treated alum sludge surface sites were heterogeneous in nature and that fitted into a heterogeneous site binding model. The Langmuir maximum adsorption capacity for fluoride removal by alum sludge was reported to be 5.394 mg/g. For an increase in temperature from 307 to 337 K, and with 20 mg/L of initial fluoride concentration, an adverse effect was observed on the adsorption of fluoride. The adsorption decreased from 85 to 72% at pH 6.0 although the fluoride adsorption at a given temperature increased with time. This was attributed to the escaping tendency of the molecules from interface at high temperatures and thereby diminishing the extent of adsorption. Fluoride removal was found maximum at pH 6.0, and found to decrease sharply above that as a result of stronger competition from hydroxide ions on adsorbent surface. Also, adsorption was

found less in the acidic range which was proposed to be a result of the formation of weakly ionized hydrofluoric acid. Defluoridation with alum sludge in presence of phosphate and silicate at higher concentrations (10–50 mg/L) had an adverse effect on fluoride removal. The affinity sequence for anion adsorption on treated alum sludge was in the following order phosphate ≥ silicate > sulfate > nitrate.

Thus, using industrial waste materials for removal of fluoride from drinking water is promising because of their low cost and high fluoride uptake capacity. However, the applicability of those adsorbents in the field is not reported.

### 2.1.6. Nano–adsorbents

Nanotechnology has emerged as a promising technology in past decade in various fields. Likewise, use of nano–particles as adsorbents for water treatment is also gaining wide attention in recent years. Carbon nano–tubes (CNTs) have attracted huge interest since their discovery. Their small sizes, large surface area, high mechanical strength and remarkable electrical conductivities make them potential materials for a wide range of promising applications.

Li *et al*. (2001) used CNTs as support to deposit $Al_2O_3$ and explored the possibility of $Al_2O_3$/CNTs for removing fluoride from drinking water. The adsorption isotherms showed that the best fluoride adsorption on $Al_2O_3$/CNTs occurred in pH range of 5.0–9.0. The adsorption capacity for $Al_2O_3$/CNTs was about 13.5 times higher than that of AC–300 carbon, four times higher than that of γ–$Al_2O_3$ at equilibrium fluoride concentration of 12 mg/L. Nano–sized inorganic oxides have been reported to be excellent reagents in various separation technologies through selective adsorption. They are known to exhibit remarkable adsorption properties due to

their enhanced surface area and large interface volume depending on the chemistry of the constituent atoms (Bhatnagar *et al.*, 2011).

Pathak *et al*. (2003) successfully standardized the preparation of a variety of nano–sized inorganic oxides through thermolysis of a polymeric based aqueous precursor solution of the desired inorganic ions. The obtained $Fe_3O_4$, $Al_2O_3$ and $ZrO_2$ nano–sized oxide powders were incorporated in the matrix of activated charcoal through adsorption and used as the adsorbing bed for the removal of trace amounts of fluoride and various other pollutants. The charcoal embedded fine powders of the inorganic oxides have been able to remove fluoride/arsenite and arsenate ions from industrial wastewater up to 0.01–0.02 mg/L levels.

Wang *et al*. (2009) performed defluoridation experiments employing nano–scale aluminium oxide hydroxide as adsorbent, taking into account the advantage of higher surface area of nano–particles as compared to the traditional micron–sized materials. The maximum Langmuir defluoridation capacity of nano–AlOOH was found to be 32.59 mg/g. The adsorption of fluoride onto nano–AlOOH was strongly pH dependent. The fluoride adsorption increased with the rise in pH, reaching a maximum of 96.7% at pH 6.8, and then decreased with further increase in pH. The $pH_{PZC}$ of the adsorbent was reported as ca. 7.8, which was responsible for the sorption of fluoride at acidic pHs and low efficiency in alkaline medium was explained by the repulsion between the negatively charged surface and fluoride. The XPS analysis of the adsorbent indicated that the adsorption of fluoride at low pH ($pH < pH_{PZC}$) could be explained by a two–step protonation/ligand exchange reaction mechanism and exhibited participation of surface OH group in fluoride removal. Adsorption of fluoride at an initial $pH > 7.8$ was attributed to van der Waal forces and not by anion exchange, which was evident from the decrease in final pH. At pH

> 7.8, nano–AlOOH was said to function as a cation exchanger as it adsorbed the sodium ions present in solution, releasing protons which was then responsible for the resulting decrease in final pH. Only the presence of sulfate and phosphate significantly affected fluoride uptake by nano–AlOOH. Desorption studies showed that the fluoride could easily be desorbed at pH 13.

Patel *et al*. (2009) investigated the potential of CaO nano–particles for fluoride removal. Colloidal particles of CaO were synthesized by the sol–gel method in the study. The percentage removal of fluoride decreased from 98.0% to 89.0% with initial concentration (100 mg/L) for 298–353 K, although the fluoride adsorption at a given temperature increased with time. The main cause of decreased removal at higher temperature was attributed to the escaping tendency of the molecules from interface at higher temperature which diminished the extent of adsorption. The Langmuir maximum adsorption capacity for fluoride removal was 163.3 mg/g. Fluoride adsorption onto CaO nano–particles was explained on the fact that CaO was converted into $Ca(OH)_2$ in water, and adsorption of fluoride occurred by surface chemical reaction, where hydroxide ions of calcium hydroxide were replaced rapidly by fluoride ions with the formation of $CaF_2$. Fluoride adsorption was found to be almost constant in the pH range of 2–8. A progressive decrease in fluoride uptake above pH 8 was attributed to electrostatic repulsion of fluoride to the negatively charged surface and the competition for active sites by an excessive amount of hydroxyl ions. Competitive anions such as sulfate and nitrate did not affect the adsorption of fluoride by CaO nano–particles.

Zhao *et al*. (2010) combined the advantages of $Al(OH)_3$ and magnetic nano–particles to fabricate nano–sized adsorbents with high surface area, high affinity towards fluoride and good magnetic separability, to develop a new kind of magnetic fluoride adsorbent. This nano–sized adsorbent

prepared using hydrous aluminium oxide embedded with $Fe_3O_4$ nano–particle, was applied to remove excessive fluoride from aqueous solution by them (Zhao *et al*., 2010). The adsorbent exhibited strong adsorption of fluoride when the pH was between 5.0 and 7.0, which was ascribed to the electrostatic attraction between the positively charged surface and fluoride. The adsorption capacity calculated by Langmuir model was 88.48 mg/g at pH 6.5. Fluoride removal in presence of anion increased in the order $PO_4^{3-} < SO_4^{2-} < Br^- \approx NO_3^- \approx Cl^-$. Fluoride adsorption was driven by both electrostatic attraction and surface complexation which was confirmed by XPS data and experimental results.

The feasibility of nano–alumina was evaluated for fluoride removal from aqueous solutions (Kumar *et al*., 2011). The maximum adsorption capacity of nano–alumina for fluoride was found to be 14.0 mg/g at 25 $^oC$ with initial fluoride concentrations (1–100 mg/g). Maximum fluoride removal occurred at pH 6.15. Fluoride sorption was mainly influenced by the presence of $PO_4^{3-}$, $SO_4^{2-}$ and $CO_3^{2-}$.

**2.2. Field experiences of aluminium hydroxide–based adsorbents**

Filter materials may function quite differently in laboratory and field conditions. For example, a particular adsorbent which shows higher uptake of fluoride in the laboratory under batch conditions, may fail in field conditions. This may be because of a number of factors such as presence of competing effect of other competing anions, higher pH of the field water and so on. An Adsorbent may function well in all conditions but be too costly to treat highly contaminated water. Thus, any particular technology, may be suitable for one particular region, but may not meet the requirements for another.

There is no universal method appropriate for all social, financial, economic, environmental and technical conditions. None of the methods has been implemented successfully at a large scale in many parts of the world. The aluminium hydroxide–based adsorbents may face limitations in the practical application due to capital and running costs as well as the management of monitoring, regeneration and replacement. Secondly, unexpected fluoride capacity reduction might occur when the flow rate is out of control or the adsorbent grade, which is commercially available, did not meet the minimum requirement to obtain appropriate fluoride removal. Thirdly, water quality may deteriorate as a result of treatment through, for example, bacterial grow, or the release of pollutants from the adsorbent. Besides the limitations of adsorbents there are also major factors that need to be considered when planning defluoridation plants in large scale. These are regeneration of saturated media and safe disposal of spent media, which might encourage sustainable utilization of the defluoridation technologies.

### 2.2.1. Global scenario

Activated alumina (AA) technology is one of the most widely used adsorption methods for the defluoridation of potable water and many reports are available on large–scale installations (Clifford, 1990; Rubel and Wooseley, 1979). Defluoridation in such units is carried out under supervision of skilled personnel and treated water is supplied to townships. The quality of treated water from such facilities is assured by skilled operator.

AA was proposed for defluoridation of water and patented for domestic use already in 1936 (Fink and Lindsay, 1936). Since then AA has been subjected to several patents and due to commercial interests, it is one of the most advocated defluoridation methods. AA is a largely available industrial chemical. It is however not widely distributed at grass root level as alum is.

Activated alumina is the favourable technique for developing countries in case high fluoride removal efficiency and high capacity is needed as compared with other alternative defluoridation technologies.

According to Hao and Huang (1986) the fluoride removal capacity of alumina is between 4 and 15 mg/g. Experiences from the field however; show that the removal capacity is often about 1 mg/g (COWI, 1998). Thus there seems to be a vast difference in the synthesis and degree of activation of alumina products for field implementation. The other explanation may be due to variation in pH. The capacity of activated alumina is highly dependent on pH. The presence of competing ions in the natural groundwater is also affecting its adsorption capacity.

Furthermore, its use has been limited by difficulties of regeneration, the low capacity of less purified technical grade products and the relative high price. During the recent years the activated alumina became less costly and more popular, especially in middle income countries, where it is now a day possible to manufacture.

During 1980–1990, use of indigenously manufactured activated alumina for fluoride removal was reported by few laboratories in India. Venkateswara Rao and Mahajan (1988) reported the development and evaluation of domestic and hand pump units where activated alumina was used as the defluoridation medium. The hand pump based defluoridation plant which was developed by IIT Kanpur, in India used activated alumina manufactured by Associated Cement Company and Indian PetroChemicals Ltd. (IPCL) (Bulusu and Nawalakhe, 1990). The unit was designed to operate in the up–flow mode. 110 kg of AA of grade G–87 (IPCL), with a particle size range of 0.3–0.9 mm was used. The raw water fluoride concentration was in the range of 6–7 mg/L.

Regeneration of exhausted activated alumina was carried out in situ. This procedure required 8–10 h. Average yield of the safe water (< 1.5 mg/L fluoride) per cycle was around 25,000 litres. Seventeen defluoridation cycles were completed in a span of 4 years (maximum of three months for one cycle). There was no major maintenance problem during this period. There was no complaint from the users either regarding the design or the palatability of treated water.

An activated alumina plant was designed, constructed and commissioned in the rural area of Madibeng local municipality, North West province, South Africa. Fluoride in the feed water is removed from 6 to 8 mg/L to less than 1.5 mg/L. No reduction in plant output was experienced over 6 service cycles. Therefore, it appears that fouling of the activated alumina should not be a problem. Plant output varied between 940 and 1296 $m^3$ to a fluoride breakthrough of approximately 2.0 mg/L. No significant operational problems were experienced during commissioning and the plant is performing satisfactorily. Spent regenerant was disposed of into evaporation ponds. The capital and operational costs of the 200 $m^3$/day defluoridation plant are estimated at approximately 26,646 USD and 0.014 USD/$m^3$ treated water, respectively (Schoeman, 2009).

### 2.2.2. Ethiopian scenario

The aluminium hydroxide–based adsorbent for defluoridation of water in Ethiopia was first implemented using activated alumina in Wonji/Shoa Sugar Estate in 1962. The factory uses the Awash River for irrigating sugar cane but the drinking water supply system for the population of the estates uses high–fluoride borehole water. The Wonji/Shoa Sugar Estate had 6 defluoridation plants (one each at Wonji and Shoa factory village and 4 in the plantation villages).

The defluoridation plant which uses activated alumina consists of 2 units and 185 kg of the chemical is put into the first tank and the defluoridated water from the first tank is passed through the second tank (92.5 kg) to further reduce fluoride level. This is adequate for 6 months with daily regeneration using 25 kg/day of caustic soda. The final defluoridated water is pumped into a 500,000 cubic meter reservoir for distribution to the Wonji factory village and a plantation village.

The weighing and introduction of the chemicals is performed by an experienced technician who has the responsibility of constantly monitoring the process and regeneration through flushing with caustic soda.

For a daily production of 12,300 L of treated water; 3.6 kg activated alumina and 25 kg of caustic soda are required. The cost for AA and caustic soda were 16.27 and 3.98 Birr/kg, respectively. Both chemicals were imported from other countries (AA from Germany and caustic soda from Taiwan). The production cost of defluoridated water was estimated to be 12.9 Birr (1.5 USD/$m^3$) without considering the labour cost.

The Wonji/Shoa defluoridation plant has been stopped functioning, because the drinking water supply of Wonji was connected to the Adama treated surface water supply system dependent on the Awash River. Some of the constraints encountered during operation were shortage and high cost of chemicals, poor follow–up from technicians, low efficiency of activated alumina, and poor maintenance. Hence, the seek for locally available aluminium hydroxide–based adsorbent with high fluoride removal capacity, affordable price, produced easily and requires less intensive operation, monitoring and intervention, is unquestionable.

# Chapter 3

# 3. Materials and methods

## 3.1. Synthesis and characterization of aluminium hydroxide–based adsorbents

### 3.1.1. Synthesis of AO, AOMO and nano–AlOOH

#### 3.1.1.1. Synthesis of aluminium hydro(oxide) (AO)

The adsorbent (49.89 g), AO, was prepared by mixing locally available aluminium sulfate (100 g) ($Al_2(SO_4)_3.14H_2O$), which is produced by Awash Melkasa Aluminium Sulfate and Sulfuric Acid Factory in Ethiopia, in 500 mL of deionized water under continuous mixing conditions with magnetic stirrer until complete dissolution. The resulting lower pH (2.7) was adjusted to about pH of 7.0 using 2.0 M NaOH. The AO was treated at a temperature of 300 $^oC$ in a furnace (Carbolite, ELF Model, UK) for 1 h. It was then thoroughly washed with deionized water (repeated rinsing with up to 40 mL/g) to remove $Na_2SO_4$ (Shimelis *et al*., 2006; Mulugeta *et al.*, 2013).

#### 3.1.1.2. Synthesis of aluminium oxide–manganese oxide (AOMO) composite material

The AO adsorbent, which was synthesized previously, was used as a precursor material for the preparation of aluminium oxide–manganese oxide composite material (AOMO). The adsorbent (AOMO) was prepared in two steps (Maliyekkal *et al*., 2006; Tripathy and Raichur, 2008). In the first step, a mixture of 50 mL (4.58 g of $MnCl_2{\cdot}H_2O$ and 0.5 mL of 10 M NaOH) was poured over 50 g of AO in a heat–resistance dish, and heated to 150 $^oC$ for about 5 h in an oven. In the second step, the same mixture was again heated at 500 $^oC$ for 3 h in a furnace.

### 3.1.1.3. Synthesis of nanoscale aluminium oxide hydroxide (nano–AlOOH)

Aluminium nitrate ($Al(NO_3)_3 \cdot 9H_2O$, 95%) (Merck, Germany) and ammonium bicarbonate ($NH_4HCO_3$, 98%) (Merck, Germany) were used as starting materials. Aluminium nitrate and ammonium bicarbonate solutions, which were prepared by dissolving the salts in deionized water, were added drop-wise from two separate burettes to deionized water in a reaction vessel to precipitate aluminium cations as transparent gel-like hydroxides. The mixture was stirred and maintained at 70 $^oC$ and then, the pH of the precipitate was controlled in the range from 7.5 to 8.5 using $HNO_3$ and/or NaOH (Parida *et al*., 2009).

The following chemical reactions could occur during preparation:

$$NH_4HCO_3 + H_2O \rightarrow NH_4OH + H_2O + CO_2\uparrow$$

$$Al(NO_3)_3 + 3NH_4OH \rightarrow Al(OH)_3 + 3NH_4NO_3$$

$$Al(OH)_3 \rightarrow AlOOH\downarrow + H_2O$$

The precipitate was finally filtered, washed thoroughly with deionized water and subsequently with ethanol followed by acetone to avoid contamination with sodium ions. The collected precipitate was then dried at room temperature.

### 3.1.2. Characterization of AO, AOMO and nano–AlOOH

The samples (0.1 g) were digested in a microwave digester in a 3:1 mixture (4 mL) of 30% HCl and 65% $HNO_3$ for 80 min and then diluted to 100 mL using deionized water (USEPA, 2007). The elemental composition (Li, B, Na, Mg, Al, Si, P, Cl, K, Ca, V, Cr, Mn, Fe, Co, Ni, Cu, Zn, As, Se, Sr, Mo, Cd, Sn, Sb, Ba, La, W, Au, Hg, Ti, Pb, Th, U, Br, Bi, Cs, Nb) was determined by

ICP–OES (SPECTRO CIROS$^{CCD}$, Germany), ICP–MS (Agilent 7500CX, USA) and sulfate was determined by ion chromatography (Metrohm 761, Switzerland). The absolute density was determined using the Pycnometer (MicroMeritics AccuPyc 1330, USA). The surface area of the sample was determined by $N_2$ adsorption method (Thermofinnigan Sorptomatic 1900, Germany). The samples were first outgassed at 110 $^oC$ and then allowed to cool to room temperature. Thermogravimetric analysis (TGA) was used to measure the weight loss of the samples after placing them in a ceramic crucible and heated at a rate of 10$^o$/min from room temperature to 1000 $^oC$. The instrument used was Mettler Toledo AG–TGA/SDTA851e, Switzerland. The X–ray diffraction (XRD) patterns of the adsorbents were recorded by an X–ray diffractometer (X'pert PRO, PANalytica, The Netherlands) using Cu K$\alpha$ radiation ($\lambda$ = 0.1542 nm) with a 0.05$^o$/min step scanned from 5 to 80$^o$ in 2$\theta$ angle. Scanning electron microscopy (SEM) analysis was carried out using a NOVA NANOSEM (FEI Company, USA) equipped with GAD (gaseous analytical detector), with an accelerating voltage of 5 kV. The point of zero charge (PZC) was measured by potentiometric mass titrations technique (Bourikas *et al*., 2003). PZC was identified as the common intersection point (CIP) of the potentiometric curve of the blank solution with the corresponding curves of the impregnating suspensions containing 0.5, 1.0, and 1.5 g of the adsorbent in electrolytic solution (0.02 N $NaNO_3$ in 50 mL of deionized water). The experiment was performed, under an $N_2$ atmosphere and the aqueous suspensions were equilibrated for 1 h to reach an equilibrium pH value. Small amount of 1 M NaOH was added to make the pH around 10 and recorded as initial pH after 15–20 min. Then the solid suspensions were titrated by 0.1 N $HNO_3$, using 665 Dosimat (Metrohm, Switzerland). The pH of each suspension was then measured with 1 min time interval using a digital pH meter standardized by buffers (WTW Inolab pH/ION Level 2, Germany).

### 3.2. Batch adsorption studies of AO, AOMO and nano–AlOOH

Batch experiments were conducted in 500 mL Erlenmeyer flask under continuous mixing condition with magnetic stirrers at room temperature (23 ± 2 $^{o}$C). A sample was taken as required, filtered and analyzed immediately for its fluoride content. The defluoridation capacity and the fluoride removal efficiency at a given time under specified conditions were determined based upon the measurement of liquid phase concentration.

The amount of fluoride adsorbed per unit mass of the adsorbent at any time t ($q_t$, mg/g), and the fluoride removal efficiency (% R, determined as the fluoride removal percentage relative to the initial concentration) of the system, was calculated as:

$$q_t = \left(\frac{C_o - C_t}{m}\right) V \quad (1)$$

$$\% R = \left(\frac{C_o - C_t}{C_o}\right) x\ 100 \quad (2)$$

where, $C_o$ and $C_t$ are the fluoride concentrations in solution (mg/L) initially and at any time (t), respectively, m is the mass of the adsorbent (g) and V is the volume (L) of the solution. In Equation (2), when $C_t = C_e$ (fluoride concentrations remaining in the solution at equilibrium in mg/L), $q_t = q_e$ (equilibrium adsorption capacity in mg/g).

The batch adsorption experiments were conducted by Shimelis *et al*. (2006) using AO to remove fluoride from drinking water. The parameters considered were contact time and adsorbent dose, thermal pre–treatment of adsorbent, initial fluoride concentration and pH. The adsorption was rapid during the initial 20 min, but significant amount (> 90%) was removed within one hour at an optimum adsorbent dose of 1.6 g/L for initial $F^-$ concentration of 20 mg/L. The removal

efficiency of $F^-$ was increased with adsorbent dosage. Fluoride adsorption efficiencies increase with increase in the thermal treatment temperature up to 200 °C, but further increase in temperature resulted in decreased removal efficiency. High defluoridation efficiency was achieved using AO within a pH range of 4.0 to 9.0. The adsorption data at ambient pH were well fitted to the Freundlich isotherm model with a minimum capacity of 23.7 mg/g. The kinetic studies showed that the adsorption reaction of fluoride removal by hydrated alumina can be well described by a pseudo–second–order rate equation.

### 3.2.1. Effect of process parameters on fluoride removal efficiency of AOMO

To assess the effect of varying the proportions of manganese oxide on defluoridation performance of AOMO, the amount of $MnCl_2 \cdot H_2O$ in the solution was varied (8.8, 13.7, 19.1, and 25.2 g) in order to obtain 11, 16, 21, 26% manganese oxide in AOMO, respectively. 4 g/L of each adsorbent with a percentage of 0, 6, 11, 16, 21, and 26% of manganese oxide was mixed with 20 mg/L fluoride solution for a contact time of 3 h.

The effect of raw water pH was investigated with initial fluoride concentration of 20 mg/L and adsorbent dose of 4 g/L by varying the initial solution pH from 3 to 10, using 0.1 M HCl or 0.1 M NaOH. The optimum adsorbent dose was selected from previous study (Alemu *et al.*, 2014).

### 3.2.2. Effect of process parameters on fluoride removal efficiency of nano–AlOOH

The effect of adsorbent dose and contact time were studied by varying the dosage in the range of 0.4 to 2.0 g/L at constant initial fluoride concentration of 20 mg/L. The effect of dose of the adsorbent, initial fluoride concentration, contact time and raw water pH were investigated by varying any one of the parameters and keeping the other parameters constant.

The effect of initial fluoride concentration and contact time were investigated by varying fluoride concentrations from 5–30 mg/L at constant adsorbent dose of 1.6 g/L. The effect of raw water pH on the adsorption of fluoride on to the adsorbent was studied by varying the solution pH from 3–10. The pH was adjusted to the desired level either with 0.1 M NaOH or 0.1 M $HNO_3$. The pH was measured with pH/ion meter (WTW Inolab pH/ION Level 2, Germany) using unfilled pH glass electrode. The meter was calibrated each time before measurements were being performed by using pH calibration buffers.

### 3.2.3. Adsorption isotherms and kinetics of fluoride adsorption onto AOMO

Adsorption isotherm experiments were conducted using an adsorbent dose of 4 g/L and varying initial fluoride concentrations within the range between 5 and 70 mg/L at constant pH of 7. Kinetic study of the adsorption data is based on pseudo first–order and pseudo–second order reaction rates. Adsorption kinetics was determined using constant surface loadings of 1, 2 and 4 g/L corresponding to the initial fluoride concentrations of 10, 20 and 40 mg/L, respectively. Linear and non–linear regression methods were used to compare adsorption isotherm and kinetic parameters and fitness of the models. Three isotherm models (Freundlich, Langmuir, and Dubinin–Radushkevich) and two kinetics (pseudo–first order and pseudo–second order) models were selected. Graph Pad Prism versions 6.0 have been used for determining the linear and non–linear parameters. The error analysis was also performed using six different error functions (ASS, $S_{y.x}$, $\chi^2$, APE, HYBRID, and MPSD) to evaluate the applicability of each model isotherm and kinetic equations to the experimental data.

### 3.2.4. Adsorption isotherms and kinetics of fluoride adsorption onto nano–AlOOH

Isotherm experiments were conducted by mixing constant fluoride concentration of 50 mg/L with 9 series of different dosages varying from 1.0–20.0 g/L. The liquid–adsorbent mixture was agitated for 24 h to ensure equilibrium. The kinetic analysis of the adsorption data is based on reaction kinetics of pseudo–first order and pseudo–second order mechanisms. Adsorption kinetics was determined using constant surface loading of 25 mg/g (1.6, 0.8 and 0.4 g/L adsorbents for the corresponding fluoride concentration of 40, 20 and 10 mg/L, respectively).

## 3.3. Optimization of aluminium hydro(oxide) (AO)

### 3.3.1. Optimization of AO produced at different OH:Al

The different forms of AO, aluminium hydro(oxide), were prepared by adding NaOH (1.7 to 2.8 M) to 100 g of $Al_2(SO_4)_3 \cdot 14H_2O$ in 500 mL deionized water at the flow rate of ca 9.1 mL/min with vigorous stirring (650 rpm). The amount of NaOH was adjusted to give OH:Al ratio in the final suspension as 2.0, 2.2, 2.5, 2.7, 3.0 and 3.3. The precipitates were filtered, washed with deionized water, dried and heated at 300 $^{o}$C in a furnace (Carbolite, ELF Model, UK) for 1 h. The AO which was produced at 2.7 OH:Al ratios ($AO_{2.7}$) was selected for further studies in the present work.

### 3.3.2. Characterization and acid–base titration of AO produced at different ratios

#### 3.3.2.1. Characterization

The characterization studies were undertaken by following the same procedure mentioned in section 3.2. The adsorption capacity of each products were also determined by mixing 1.6 g/L of the adsorbents in 20 mg/L fluoride containing deionized water in 250 mL flask. These mixtures

were allowed to equilibrate for 60 min under continuous mixing conditions at room temperature (25 $^{o}$C) in the thermostatic cabinet.

#### 3.3.2.2. Acid–base titration

The acid–base titrations for the adsorbents were carried out at pH values between 5 and 10 with 0.5 g adsorbent in electrolyte solution (0.1 M NaCl, 50 mL) under $CO_2$–free conditions, at a constant temperature of 25 $^{o}$C. The titrants used were 0.1 M NaOH and 0.1 M HCl. Before titration, the samples were equilibrated with the electrolyte solution for an hour, gently stirring under a continuous stream of purified, nitrogen with 100% humidity (Kummert, 1979; Yang *et al*., 2007). The adsorbent was then rapidly titrated (60 s per titration step) to pH 10. The suspension was then equilibrated for 10 min prior to centrifugation to separate the solid from the solution. Both were then back titrated separately to pH of around 5. After 10 min, the procedure was repeated. The titration was performed by Dosimat (665 Metrohm, Switzerland), with a combined pH glass electrode (WTW Inolab pH/ION Level 2, Germany) calibrated using Gran titration method (Gran, 1952). This experiment was performed in duplicate.

### 3.3.3. Effect of co–existing anions on fluoride adsorption capacity of AO

The effect of anions ($HCO_3^-$, $SO_4^{2-}$, $Cl^-$, and $HPO_4^{2-}$) on fluoride adsorption was studied in batch mode in the presence of anions that commonly exist in groundwater (Tamiru, 1993). The solutions of the required concentration of anions (0–9 mmol/L) were prepared by dissolving the sodium salts of the respective anions in deionized water containing 20 mg/L fluoride. The pH of the solution was determined. Then, 1.6 g/L of AO was added and allowed to equilibrate for 60 min under continuous mixing conditions at room temperature (22 ± 2 °C). The residual fluoride concentration and pH of the solution were determined in the supernatant after overnight settling.

Experiments were performed in triplicate. The standard error of the mean (SEM) was calculated as SEM = SD/√n, where SD is the standard deviation and n is sample size (n = 3).

### 3.3.4. Mini–column experiments with AO

To evaluate the fluoride removal performance and possible release of contaminants from the filter material during continuous operation, columns of length 11 cm and internal diameter 3.4 cm were packed with AO filter material (1–2 mm particle size) and operated at constant fluoride concentrations (0 and 20 mg/L) and controlled flow rates (10 and 100 empty bed volumes per day) using peristaltic pump (ISMATEC, REGIO–CPF Analog, Switzerland). These experiments were conducted in deionized water (DIW) and in buffered solutions (10 mM $NaHCO_3$ and $P_{CO2}$ of 3000 ppm) to represent the pH and buffer conditions for Ethiopian groundwater in the Rift Valley (Reimann *et al*., 2003). The effluent of one of the columns was passed through a container containing calcite ($CaCO_3$, 125 g). This amount of $CaCO_3$ ensured a retention time of around 2.4 hours (10 eBV/day) to guarantee sufficient time for the neutralization processes to occur. The effluent of all columns was collected at defined time intervals and examined for pH, aluminium, sodium, sulfate, and fluoride concentration.

### 3.3.5. Granulation of waste AO powder

During synthesis of AO, approximately 49% yield was achieved and this was further crushed and sieved between 1–2 mm particle sizes for column experiments. Thus the AO powder, which was left after sieving, was granulated to minimize wastes and to reuse the AO powder for continuous experiments. Spray granulation was employed by putting the AO powder into the rotating plastic beaker while spraying few drops of water (Sathish *et al.*, 2012) and then the granules were sieved between 1–2 mm size for column experiments.

To evaluate the performance of the granulated AO for fluoride removal; a mini–column of length 6.0 cm and internal diameter 3.0 cm were packed with granulated AO adsorbent (1–2 mm particle size) and operated at constant fluoride concentration of 20 mg/L and controlled flow rate of 10 empty bed volumes (eBV) per day using peristaltic pump (ISMATEC, REGIO–CPF Analog, Switzerland). This experiment was conducted in buffered solutions (10 mM $NaHCO_3$ and $P_{CO2}$ of 3,000 ppm). The effluent from the mini–column was collected at defined time interval for fluoride and pH measurement.

### 3.4. Comparison of AO with aluminium hydroxide–based adsorbents

#### 3.4.1. Adsorbents

The activated alumina (AA) and pseudoboehmite (PB) were obtained from Albemarle Corporation, Germany. The activated alumina (Compalox$^R$ AN/V–812) has been used for catalytic and adsorptive applications. It has high porosity, large pore volume, high specific surface area (> 250 $m^2/g$), high crushing strength, and high adsorptive capacity for ions such as fluoride, chloride, phosphate, and arsenic. Granular activated alumina is thermally formed from boehmite, AlOOH (Weingartner *et al*., 1978) (Figure 4). Pseudoboehmite (PB) has also widespread utilized in the manufacturing of catalyst, due to their relative high surface area, porosity, crushing strength and thermal stability (Beiding *et al*., 1973). Preparation of pseudoboehmite is similar to that of AO. The elemental composition and surface area of the two adsorbents were summarized in Table 8 as it is reported from the literature (Weingartner *et al*., 1978; Beiding *et al*., 1973; Mulugeta *et al*., 2013). The characterization result of AO is also presented for comparison.

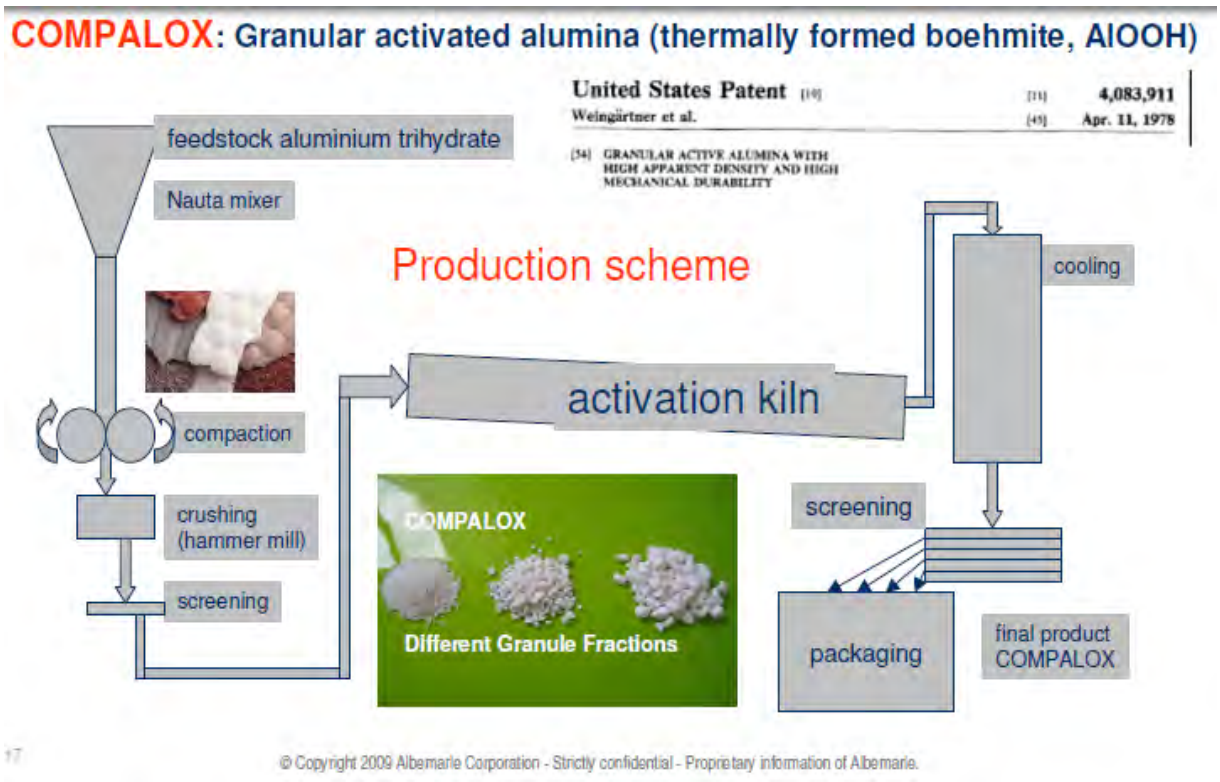


Figure 4. Thermal production of granular activated alumina (Compalox$^{R}$ AN/V–812) from boehmite.

### 3.4.2. Surface acidity of the adsorbents

The acid–base titrations for the adsorbents (AO, AA, and PB) were carried out following the same procedure stated in section 3.3.2.2.

### 3.4.3. Investigation of AO instability in batch experiments

A graphical demonstration of the instability of AO with amorphous and crystalline $Al(OH)_3$ was used for comparing the solubility curves of the hydroxides. The AO powder was suspended in deionized water containing an inert electrolyte (0.1 M NaCl) in closed plastic bottles with an oxide/water ratio of 1 g/100 mL for six days under continuous stirring at room temperature (25 $^{o}$C) (Carrier *et al*., 2007). The pH was adjusted from 3 to 11 by addition of either 0.1 M HCl or

NaOH throughout the experiments. The aluminium content was determined by ICP–MS (Agilent 7500CX, USA). These curves were calculated using the ChemEQL software (Muller, 1992).

### 3.4.4. Coordination geometry of Al species by $^{27}$Al–NMR

High resolution $^{27}$Al Magic Angle Spinning Nuclear Magnetic Resonance ($^{27}$Al MAS NMR) spectra of AO, AA and PB were recorded, to analyze the coordination geometry of the solid Al species that is formed, on a Bruker AVANCE–400 spectrometer operating at 104.3 MHz and equipped with high speed MAS probe head (2.5 mm zirconia rotor spinning up to 35 kHz). A relaxation delay of 1 s and pulse length of 0.3 μs were used to collect the $^{27}$Al MAS NMR spectrum. Chemical shifts are referenced with respect to an external $Al(NO_3)_3$ aqueous solution i.e., the resonance of $Al(H_2O)_6^{3+}$ was set to 0 ppm.

### 3.4.5. FTIR spectroscopy

The adsorbents (AO and AA) before and after fluoride adsorption of 10 mg/g, were blended with KBr, and then pressed into disks for FTIR analysis. Scans were taken from 400 to 4000 $cm^{-1}$ at 1 $cm^{-1}$ resolution, and the spectra were recorded on a FTIR spectrophotometer (Nicolet 8700, USA).

### 3.4.6. Comparison of fluoride breakthrough in continuous column experiments

To investigate the fluoride removal performance of AO, AA and PB by continuous operation, three columns of each with length 11 cm and internal diameter 3.4 cm were packed with the adsorbents. The amount of AO, AA and PB packed in these columns were 31, 100, and 41 g, respectively. The peristaltic pump (ISMATEC, REGIO–CPF Analog, Switzerland) was used to impel a synthetic buffered solutions (10 mM $NaHCO_3$ and $P_{CO2}$ of 3000 ppm) containing 20

mg/L fluoride concentration at a controlled flow rate of 10 empty bed volumes per day in the up flow mode through the columns. The effluent of all columns was collected at defined time intervals and examined for pH, aluminium, sodium, sulfate, and fluoride concentration.

### 3.4.7. Comparison of repetitive regeneration potential

The regeneration experiments were followed when the fluoride concentration in the effluent exceeds 1.5 mg/L and conducted using a sodium hydroxide solution. 0.01 M NaOH was used to regenerate AO and 0.25 M for AA and PB with flow rate of 8.3 mL/min for 60 min. For all cases, rinsing and neutralization by 0.02 M $H_2SO_4$ steps were followed with flow rate of 8.3 mL/min (60 min) and 16.7 mL/min (90 min), respectively (Schoeman, 2009). Multiple adsorption/desorption cycles were also executed up to three cycles.

## 3.5. Field implementation of AO in a pilot community defluoridation plant in rural Ethiopia

### 3.5.1. Study area

The AO community defluoridation pilot plant is located in Tsuchigragona, Dugda Woreda, East Shoa Zone, Oromia Region, Ethiopia (Latitude: $8^o$ 10’ 1.19’’ N; Longitude: $38^o$ 53’ 12.67’’ E). Tsuchigragona is a typical rural village in the Rift Valley region inhabiting approximately 3000 people. The village is about 145 km far from the capital, Addis Ababa. It is located in between Alem Tena and Meki town and about 8 km away from the main road (Figure 5).

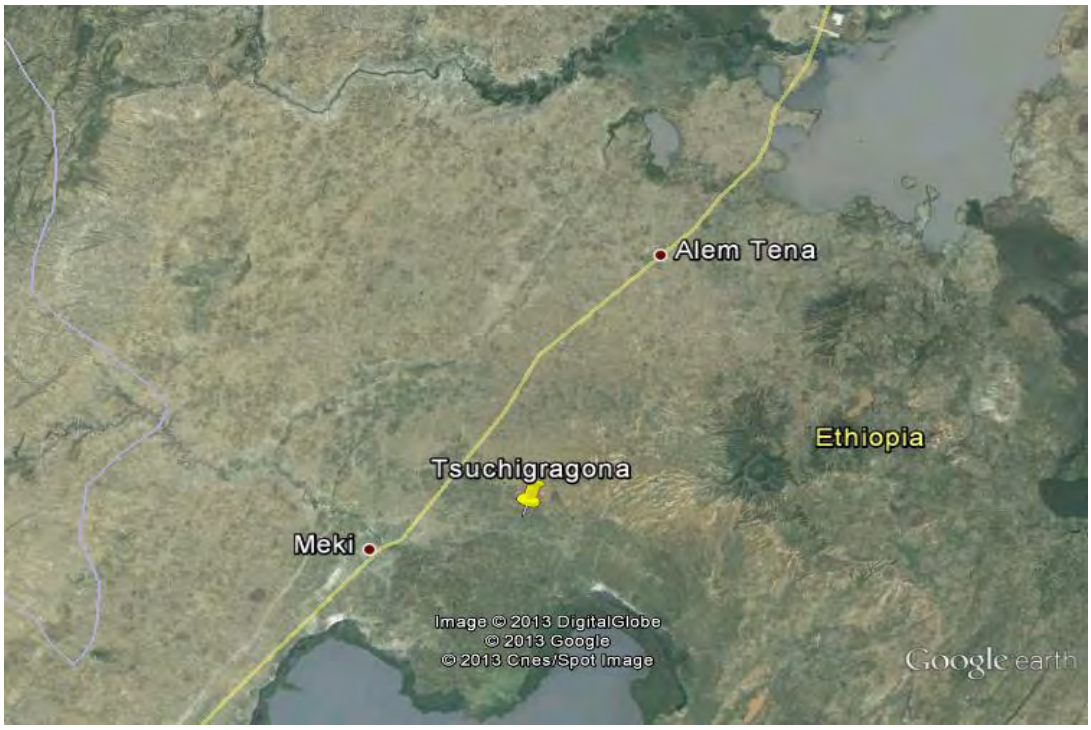


Figure 5. Areal map of the study area (Tsuchigragona).

The community AO defluoridation plant was commissioned in Tsutchigragona, Oromya Regional State, Ethiopia in July, 2011 and the second field test was conducted in May, 2012. The opening ceremony was attended by many beneficiaries of the project area as well as by roughly a dozen representatives from the Oromya region, the Ministry of Water and Energy, research institutions, and different non–governmental organizations (NGOs). In the study area, most people depend on water resources from one windmill and 40 hand–dug wells containing excessive level of fluoride above WHO guideline. The fluoride concentration in the particular field site where the study was conducted (windmill) was lied between 8 to 10 mg/L.

### 3.5.2. Pilot scale production of AO adsorbent

The AO was produced in pilot scale based on scaling up of the laboratory synthesis scheme. The raw materials aluminium sulfate and caustic soda were purchased from the local supplies Awash

Melkasa Aluminium Sulfate and Sulfuric Acid Factory and Abdoshe International P.L.C., respectively. The raw materials were bought at a cost of 10.2 Birr/kg and 20 Birr/kg for aluminium sulfate and caustic soda, respectively (Figure 6). The mass production of AO was carried out by daily laborers; after short training under the supervision of research assistance. The production process involves materials and equipments, which are obtained easily from the local markets (Figure 7). The calcite which was used after AO tank is collected from leftover of marble factory in Addis Ababa and crushed to the required particle sized (Figure 8).

Aluminium sulfate


Caustic soda

Figure 6. Raw materials for the production of AO.


Figure 7. Simple AO production process.

Marble leftover

Marble crusher


Figure 8. Calcite obtained after crushing the marble leftover.

### 3.5.3. Design and construction of AO community defluoridation plant

The field test was implemented based on intensive investigations underwent in laboratories both at Eawag (Switzerland) and Addis Ababa University (Ethiopia). The principal variables which affect the performance of the adsorbent were flow rate, sulfate, pH of raw water and aluminium leached from the adsorbent. A design of the community defluoridation plant is presented in Figure 9.

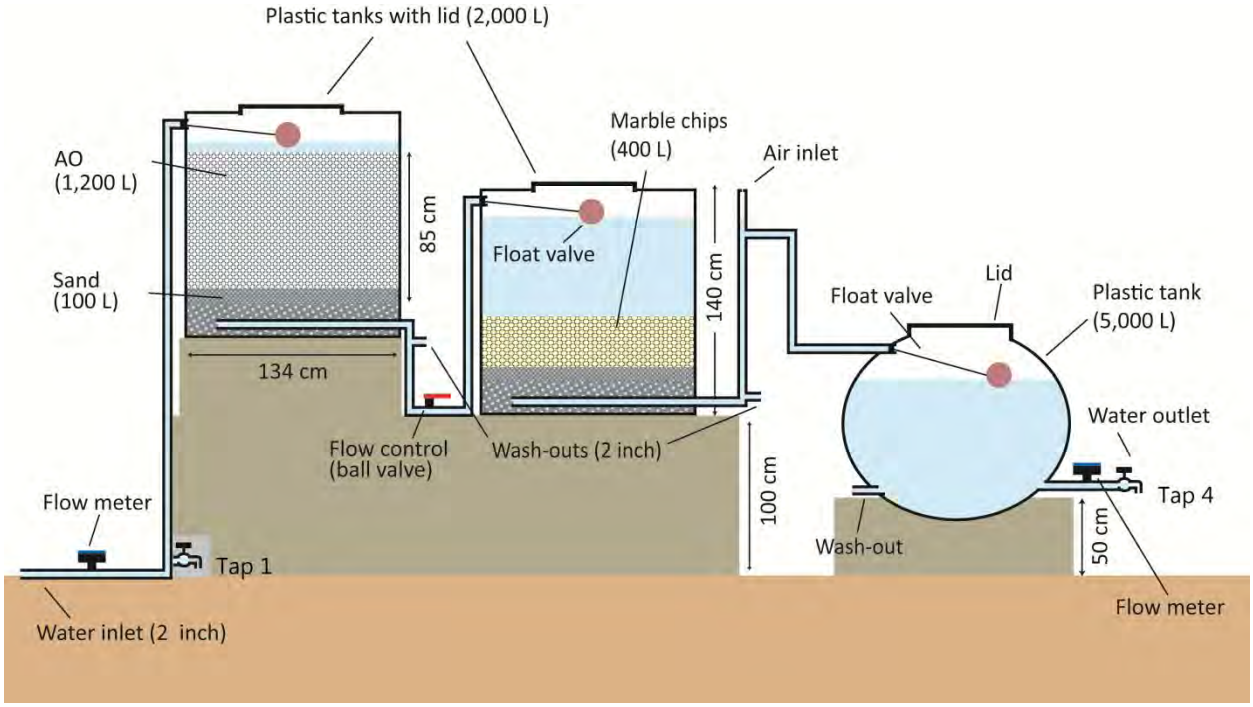


Figure 9. The design of AO community defluoridation pilot plant implemented in Tuchigragona, Oromya Regional State, Ethiopia.

The groundwater is pumped out by the help of windmill and hence requires no electricity. The fluoride content of the groundwater was ranging from 8 to 10 mg/L and it was treated by passing it through the plastic Tank A, which was packed by AO media and Tank B, containing calcite (Marble tank). The flow rate was adjusted to about 3 L/min by using flow control ball valve, which was fixed between Tank A and Tank B. The post treatment filter Tank B was added to assure that pH and aluminium concentration in the treated water with in the acceptable level. During the first day of operation, Tank A was allowed to fill then was drained several times (until the electrical conductivity of the water was below 1500 μs/cm) to wash the sulfate form AO adsorbent and 10,000 L of raw water (ca 20 L/min flow rate) was used for washing. A 5000 L plastic tank was used to store the treated water. The AO community defluoridation pilot plant

was run twice by replacing the spent with fresh media in the second round and with some plant design modification.

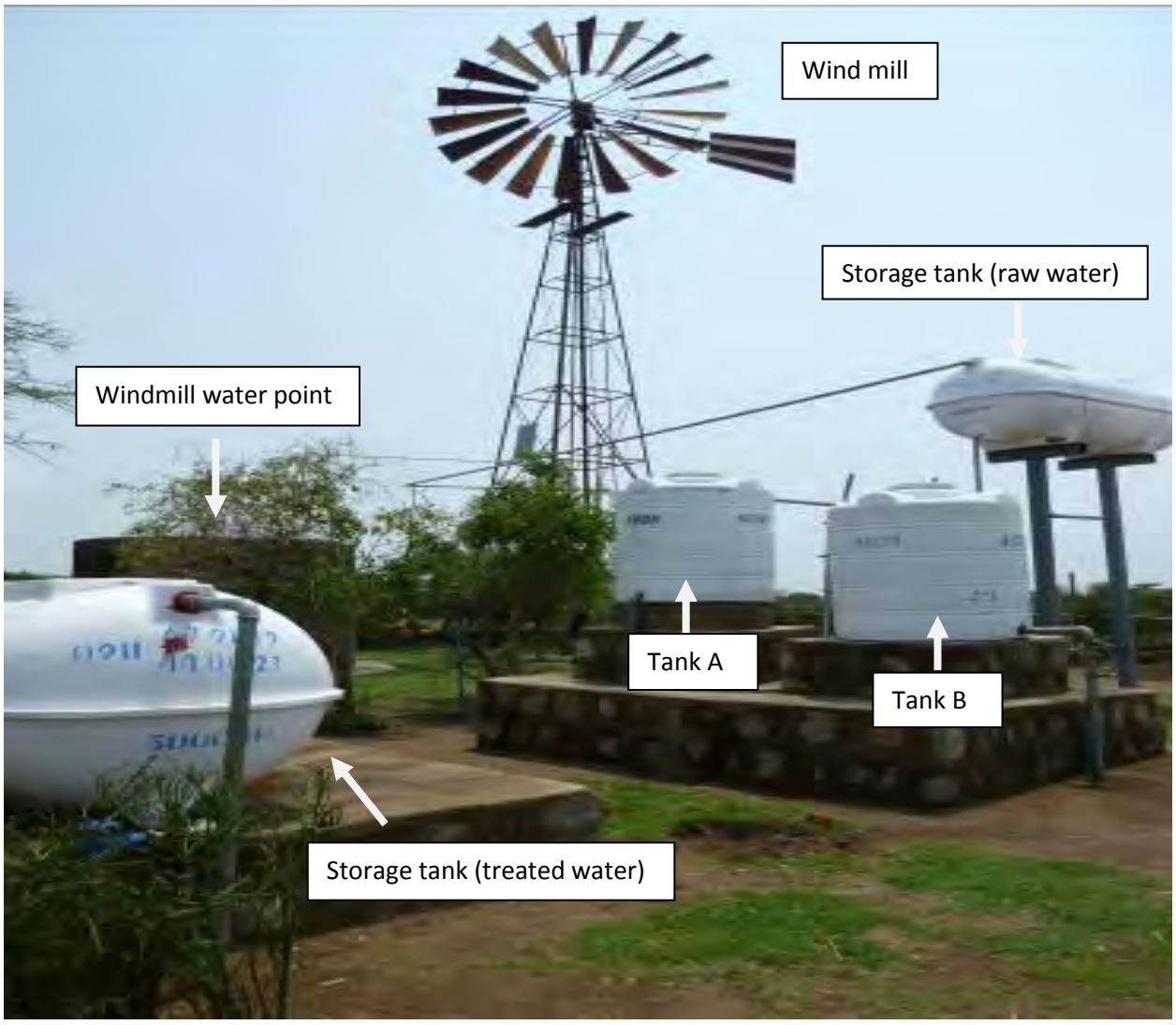


Figure 10. AO community defluoridation pilot plant implemented in Tuchigragona.

Monitoring of the community defluoridation plant was performed by collecting influent and effluent samples once per week. Temperature, pH, EC and turbidity of the raw water (Tap 1) and treated water (Tap 2, between Tank A and B; Tap 3, between Tank B and treated water storage tank; and Tap 4, treated water) were measured onsite. The water meter readings were also

recorded during which samples were taken. However, fluoride, aluminium, sulfate and other contaminates were measured offsite both at Eawag and AAU. Samples were collected in two 30 mL plastic vials, one preserved with $HNO_3$ and the other without acidification. The samples were stored in a refrigerator until they were sent to Eawag, Switzerland for analysis of Al, $SO_4$, Ca, As, U, Se and other contaminants. Samples were filtered prior to analysis using 0.45 μm membrane filters. A pH/ISE meter (Orion Model, EA 940 Expandable Ion Analyzer, USA) equipped with combination fluoride–selective electrode (Orion Model 96–09) was employed for the determination of fluoride in Addis Ababa University, Ethiopia. Sulfate was measured by ion chromatography (Metrohm 761, Switzerland). ICP–MS (Agilent 7500CX, USA) was used to measure Al, Ca, As, U, Se and other ions.

The capital and operational cost of AO defluoridation plant were estimated based on information collected from field experience. Construction cost for defluoridation plant and costs for purchasing machineries and materials required to produce AO were included as capital cost. The operational cost was calculated based on the cost of raw material for production of AO and man power.

# Chapter 4

# 4. Results and discussions

## 4.1. Characterization results of AO, AOMO, and nano–AlOOH

### 4.1.1. Physical and chemical characteristics of AO

The elemental composition of the AO is summarized in Table 2. The major components that make up more than 96% of the solid phase are aluminium, sulfate, and sodium, while the minor components are iron, silicon, potassium, calcium, manganese, and magnesium. From the analysis, the chemical formula of AO could be formulated as $Al(OH)_{2.8}(SO_4)_{0.1}$ (though the presence of unreacted alum and $Al(OH)_3$ cannot be excluded even though the later was expected as a major product). Therefore, the presence of sulfate and small amount of iron in AO would contribute to the higher fluoride adsorption capacity. The sulfate that is associated with Al (0.94 mmol/g) is responsible for the acidity of the adsorbent and hence high fluoride uptake by AO, whereas sulfate content associated with Na (0.68 mmol/g) might be further reduced if the washing efficiency improved. The AO material appears brownish in color since it consists of Fe (0.44 mmol/g) as iron oxide.

Table 2. Elemental composition, surface area (SA), density and point of zero charge (PZC) of AO, AOMO and nano–AlOOH.

| Adsorbents | Concentration | Al | Mn | Na | $SO_4$ | SA ($m^2/g$) | Density ($g/cm^3$) | PZC |
|---|---|---|---|---|---|---|---|---|
| AO | mg/g | 288 | 0.39 | 31 | 155 | 37.7 | 2.39 | 9.57 |
| | mmol/g | 10.7 | 0.01 | 1.35 | 1.61 | | | |
| AOMO | mg/g | 255 | 122 | 102 | 85.8 | 30.7 | 2.78 | 9.54 |
| | mmol/g | 9.44 | 2.22 | 4.43 | 0.89 | | | |
| nano–AlOOH | mg/g | 339 | 0.02 | 6.9 | 3.3 | – | 2.18 | 9.80 |
| | mmol/g | 12.6 | $3.6x10^{-4}$ | 0.3 | 0.034 | | | |

XRD analysis (Figure 11) could not identify any crystalline structures and showed AO to be an amorphous compound. Representative low–magnification SEM image (16 000×) of the sample indicated the presence of a few $Na_2SO_4$ aggregates and an amorphous Al–hydroxide network of fibres with a size range of 200–300 nm (Figure 12). It was not possible to differentiate between the presence of $Al(OH)_3$ and traces of alum or solid solutions of $Al(OH)_3$ with sulfate containing hydroxide phases. The results of density measurement showed that the density of AO was 2.39 $g/cm^3$, that is lower than the density of $\gamma$–$Al_2O_3$ (3.67 $g/cm^3$) (Temuujin *et al*., 2000). The surface of AO was positively charged when solution pH was below its PZC (9.57), facilitating fluoride adsorption through the electrostatic attraction between the fluoride ions and adsorbent.

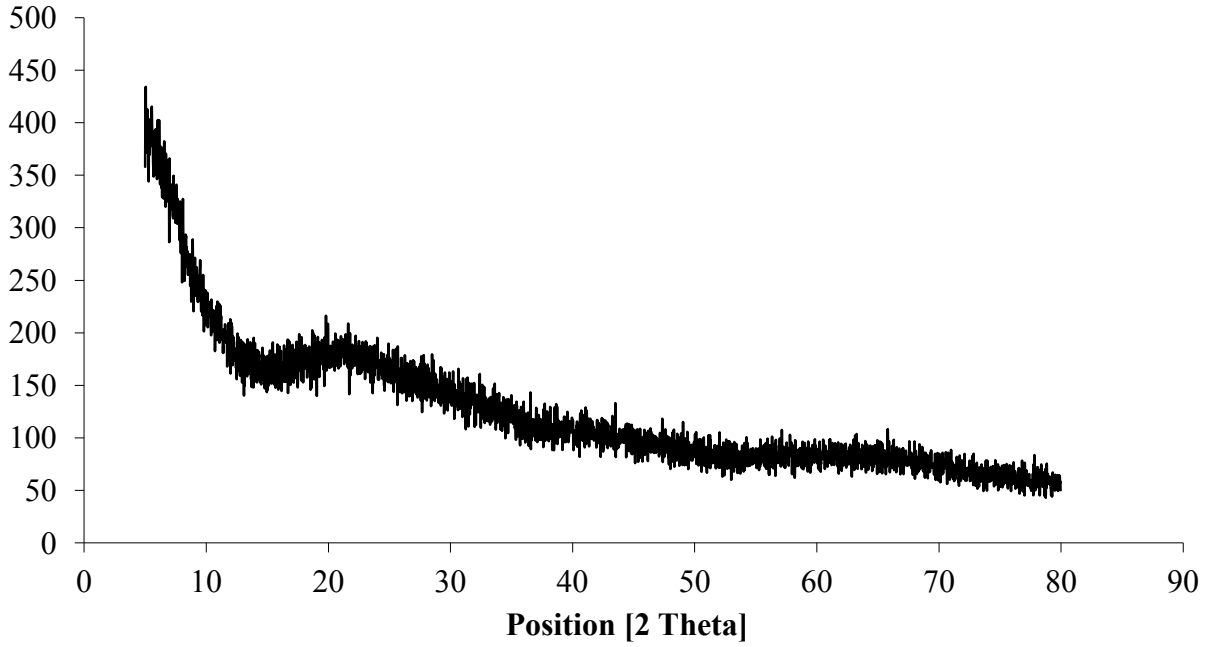


Figure 11. X–ray diffractogram of AO.

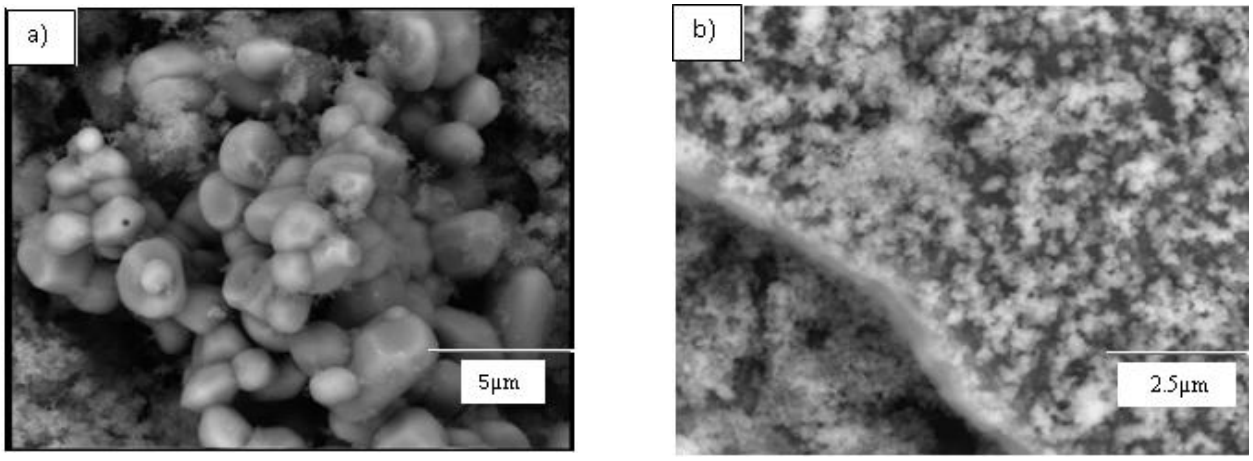


Figure 12. SEM photographs of AO (magnification; a) 16,000X and b) 30,000X), showing $Na_2SO_4$ on the left and amorphous Al hydroxide on the right.

### 4.1.2. Physical and chemical characteristics of AOMO

The elemental composition of AOMO in comparison with AO and nano–AlOOH is summarized in Table 2. The major components that make up more than 97% of the solid phase (AOMO) are aluminium, manganese, sodium, sulfate and the minor components are iron, silicon, potassium, calcium and magnesium (assuming Al to be present as $Al(OH)_3$). The remainder is primarily composed of Fe (13.9 mg/g). All other elements were present in concentrations below 3.0 mg/g. Therefore, the presence of sulfate, manganese and a small amount of iron in AOMO would contribute to the higher fluoride adsorption capacity. The AOMO material appears dark brownish (brown–black) in color since it consists of Mn and Fe as manganese and iron oxides.

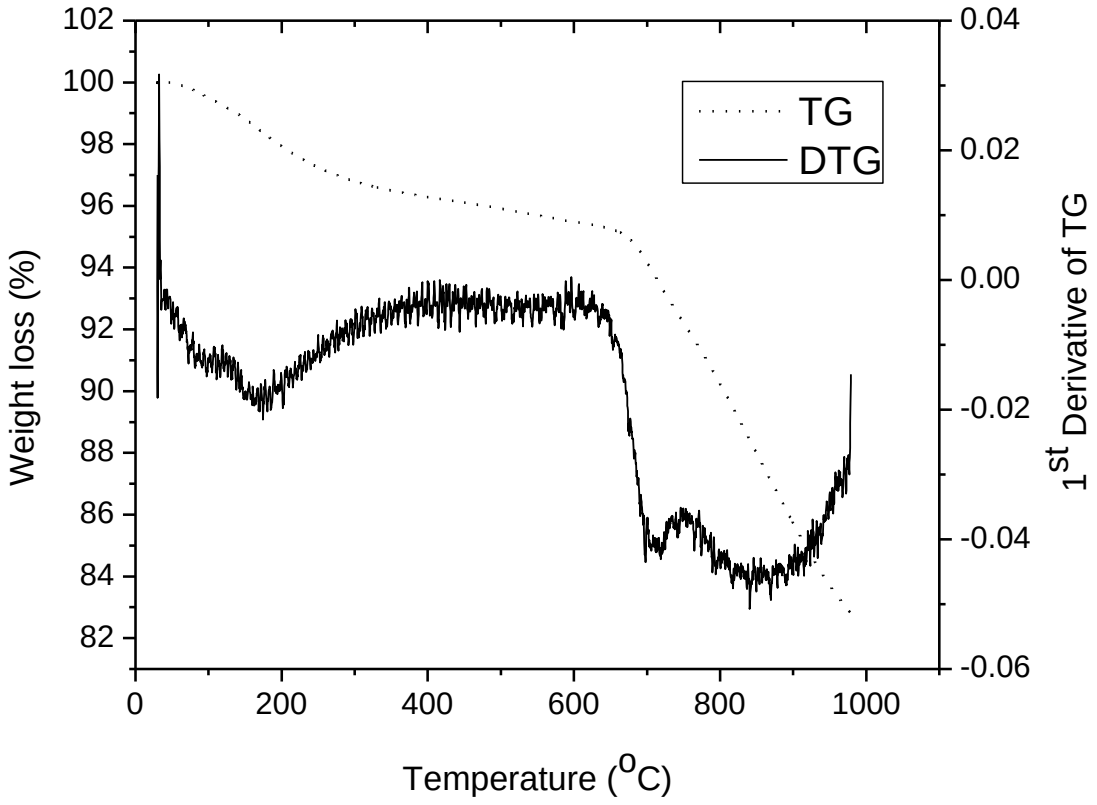


Figure 13. Thermogravimetric curve, TG (solid line) and derivative of thermogravimetric curve, (DTG) (dotted line) of AOMO.

Figure 13 shows the TGA curve of AOMO. The first step ranges from 70–350 $^{o}$C with a weight loss of 2.8% correspond with the evolution of all the water (70–120 $^{o}$C) and formation of manganese dioxide and aluminium oxyhydroxide compounds (120–350 $^{o}$C) (Shaheen and Selie, 2000). The second step ranges from 640–980 $^{o}$C with weight loss of 10.8% corresponding to the reduction of manganese dioxide to manganese trioxide and the complete decomposition of aluminium oxyhydroxide to aluminium oxide (640–760 $^{o}$C); it can also represent the conversion of $Mn_2O_3$ to $Mn_3O_4$ and the formation of $MnAl_2O_4$ as the result of solid–solid interaction between the corresponding oxides (Shaheen and Hong, 2002). The TGA result is supported by the XRD investigation of the sample. The XRD pattern (Figure 14a) confirms the existence of poorly crystalline $MnO_2$ and $Al_2O_3$ phases are present. This might be attributed to the presence of aluminium oxide that leads to increase in the degree of dispersion of $MnO_2$ on its surface thus hindering their grain growth (Shaheen and Hong, 2002). The SEM image is shown in Figure 14b, and AOMO had a significantly rough surface and lots of pores. The measurement of PZC showed that the surface of AOMO was positively charged when solution pH was below its PZC (9.54), facilitating fluoride adsorption through the electrostatic attraction between fluoride and adsorbent (Alemu *et al.*, 2014).

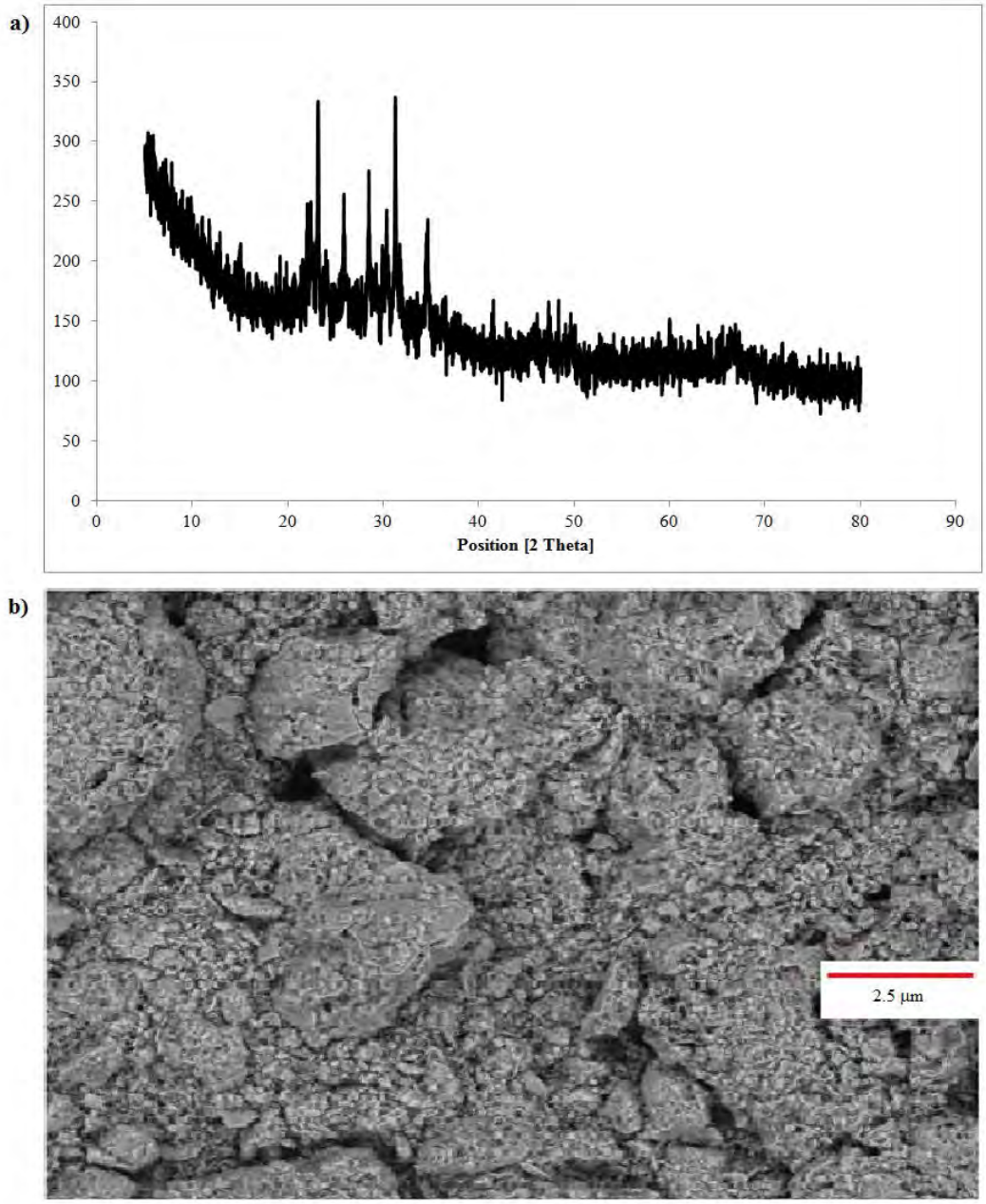


Figure 14. a) X–ray diffractogram of AOMO and b) SEM images of AOMO (magnification; 1000X).

### 4.1.3. Physical and chemical characteristics of nano–AlOOH

The elemental composition analysis (Table 2) of the adsorbent showed the presence of AlOOH (97.6%), $Na_2O$ (1.2%), $SiO_2$ (0.37%), $Fe_2O_3$ (0.31%), CaO (0.14%) and the rest constituted by compounds of K, Mg, Sr, Zn and Cu. The presence of a relatively high amount of Na might be attributed to the NaOH solution used for adjusting the pH during the synthesis of nano–AlOOH. The absolute density of nano–AlOOH was found to be 2.18 g/cm$^3$, and is smaller than that of boehmite, 3.01 g/cm$^3$ (Wefers and Misra, 1987). Based on this result, it can be concluded that nano–AlOOH may have more pore spaces, and hence higher surface area which make it an effective defluoridating agent. The measurement of PZC showed that the surface of nano–AlOOH was positively charged when the solution pH was below its PZC (9.80).

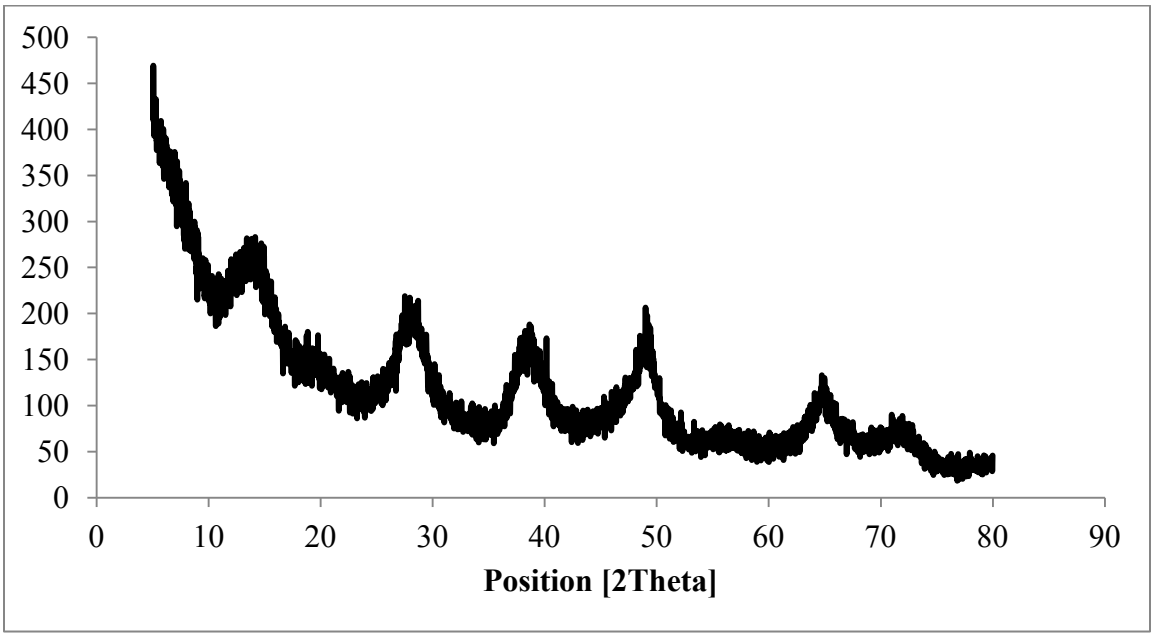


Figure 15. The X–ray diffraction pattern of nano–AlOOH.

The X–ray diffraction (XRD) pattern (Figure 15) of nano–AlOOH showed broad peaks for two-theta values between (10–15, 25–30, 35–40, 45–50 and 60–70), which indicates high crystalline order of the synthesized compound. This is consistent and matched with XRD results of nano–sized AlOOH synthesized by other researches (Parida *et al*., 2009; Wang *et al*., 2008). In addition to that, the XRD pattern showed broadening of the peaks, indicative of the ultra fine nature of the crystallite. The crystallite size calculated using Scherrer's formula (Equation 3) was about 3.7 nm (Scherrer, 1918).

$$L = \frac{K}{\text{Cos}} \tag{3}$$

where, L is the crystallite size, K is the Scherrer constant (0.94, for FWHM of spherical crystallites), is the XRD radiation wavelength in nm ( = 0.1542 nm), is the Full Width at Half Maximum (FWHM) in radians, and 2 is the diffraction angle.

As it can be seen in Figure 16, the dehydration of the aluminium oxide–hydroxide appears to occur in three steps with a total weight loss of approximately 31.0%. The first two endothermic effects at 100–300 $^{o}$C that resulted in 2.94 mg (19.8 wt %) weight loss could be attributed to the removal of physically adsorbed water, and the third step at 340–500 $^{o}$C which resulted in 1.67 mg (11.2 wt %) weight loss could be due to the conversion of AlOOH into $Al_2O_3$.

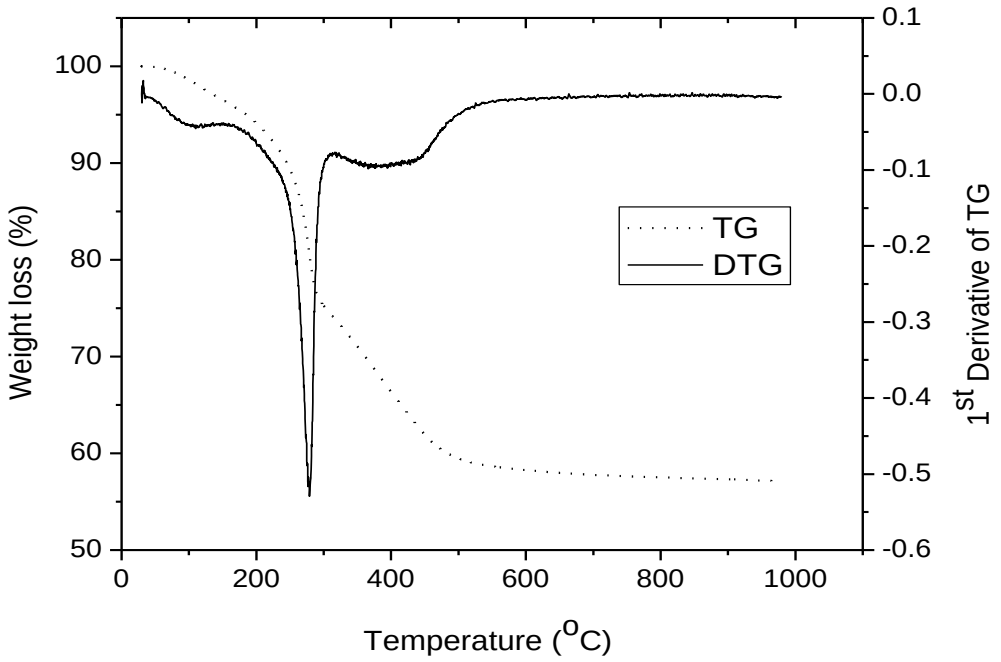


Figure 16. Thermogravimetric curve, TG (dotted line), and derivative of thermogravimetic curve, DTG (solid line) of nano–AlOOH.

## 4.2. Batch adsorption studies of AOMO and nano–AlOOH

The use of acid AO adsorbent directly while maintaining the high fluoride uptake capacity was successful. However, optimization of the synthesis of AO at different ratios and chemical activation of AO using $MnO_2$ had a positive impact on the performance of AO, in terms of dissolution of aluminium and adsorption capacity. In addition, performance comparison experiments under batch mode with AOMO and nano–AlOOH will help to understand the adsorption mechanism fluoride onto AO.

### 4.2.1. Factors affecting fluoride adsorption onto AOMO

#### *4.2.1.1. Effect of manganese oxide proportion*

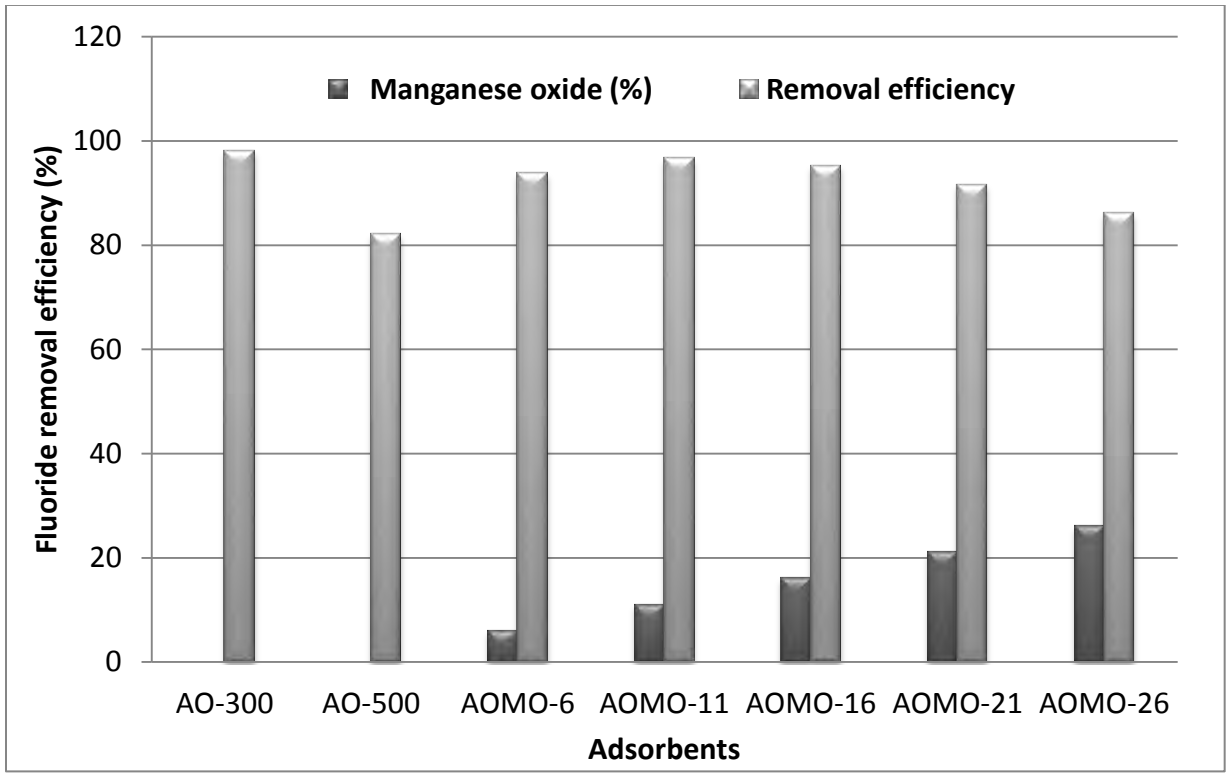


Figure 17. Effect of thermal treatment and percentage of manganese oxide on fluoride removal efficiency of AOMO (adsorbent dose = 4 g/L, initial fluoride concentration = 20 mg/L, contact time = 180 min, pH = 7.0 ± 0.20).

As it can be seen from Figure 17, fluoride removal efficiency of AO–300 (aluminium hydro(oxide), treated at 300 $^{o}$C) is much higher than that of AO–500. This is due to the fact that AO–500 has lost a considerable amount of hydroxyl groups compared to AO–300, which accounts for reduction in fluoride removal efficiency. It can also be seen that fluoride removal efficiency is higher with manganese oxide proportion ranges from 11–16% and then decreased for 21 and 26%. An increase in fluoride removal efficiency with percentage of manganese oxide in the adsorbent is possibly due to the formation of porous manganese oxide on the outside and inner surfaces of aluminium oxide. As more and more manganese oxide is formed especially on the inner surfaces of the base material, surface area available per unit mass of the adsorbent for the adsorption may decrease and may result in low fluoride removal efficiency. An adsorbent with 11% manganese oxide showed relatively greater fluoride removal efficiency, thus used for further study as AOMO (Alemu *et al.*, 2014).

#### 4.2.1.2. Effect of solution pH

The experimental results of the effect of solution pH on the adsorption of fluoride are shown in Figure 18. Strong dependence of removal efficiency on pH is observed within a pH range studied. Surface charge of an oxide mineral in aqueous systems will change with changing pH and would be hydroxylated to develop a surface condition in which there is an uneven charge distribution over the surface (Agarwal *et al*., 2003). Thus, significant and rapid removal of fluoride in the acidic pH range and decreased removal at high pH can be explained due to ion–exchange adsorption mechanism. Protonation of the oxide surface followed adsorption of fluoride through ligand exchange can explain the overall adsorption process.

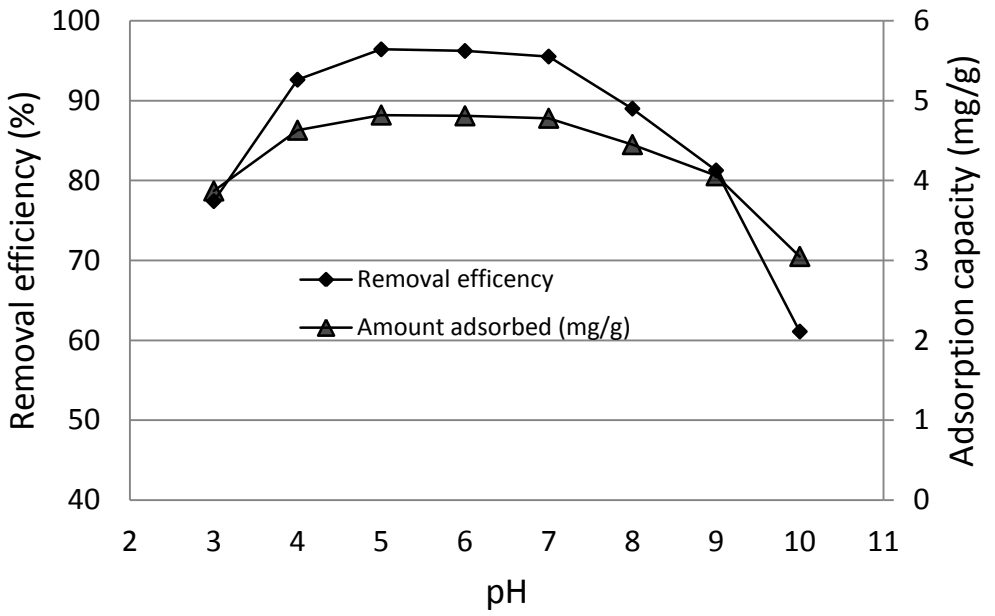


Figure 18. Effect of initial solution pH on fluoride removal efficiency (initial $F^-$ concentration = 20 mg/L, adsorbent dose = 4 g/L, contact time = 120 min).

Figure 18 shows that initially the adsorption of fluoride increased from pH 3 to 5 reached maximum of about 96.4% at pH 5. Then very slight change in fluoride removal was observed up to pH around 7.0. The high removal efficiency in the acidic pH range is due to the existence of positive sites and neutral sites on the surface of the adsorbent that facilitates for more fluoride ions to bind on the surface thereby resulting in high efficiency in fluoride removal. After pH 8, fluoride adsorption decreased sharply and as low as 61.1% was removed at pH 10. The low adsorption efficiency of the media at higher pH values is attributed to the strong competition of hydroxide ions on the adsorbent surface for the adsorption sites as well as the repulsion of fluoride ions by the negatively charged surface of the adsorbent. At lower pH, the adsorption efficiency is less, which is possibly due to the formation of positively charged AlFx complexes.

### 4.2.2. Factors affecting fluoride adsorption onto nano–AlOOH

#### 4.2.2.1. Effect of adsorbent dose and contact time

The removal of fluoride ions by nano–AlOOH increases with an increase in the amount of adsorbent as shown in Figure 19. For all these runs, initial fluoride ion concentration was fixed at 20 mg/L. The amount of adsorbent dose was varied between 0.4 and 2 g/L in aqueous solution at their optimal pH values.

The result shows that, the reaction was very fast during the initial 30 min, and a contact time of about 60 min is enough to remove 95% of the fluoride in solution with an adsorbent dose greater than or equal to 1.6 g/L, at room temperature of 22 ± 2 $^{o}$C. This indicates that longer contact time may not have much effect.

The rate of removal of fluoride is fast during the first 5 min. After 30 min, the rate of removal of fluoride decreases and reaches equilibrium within 120 min. When the AOMO dose was increased, beyond 4 g/L, there was no significant change in the percentage of fluoride removed. Thus, 4 g/L was considered as optimum adsorbent dose for AOMO (Alemu *et al.*, 2014).

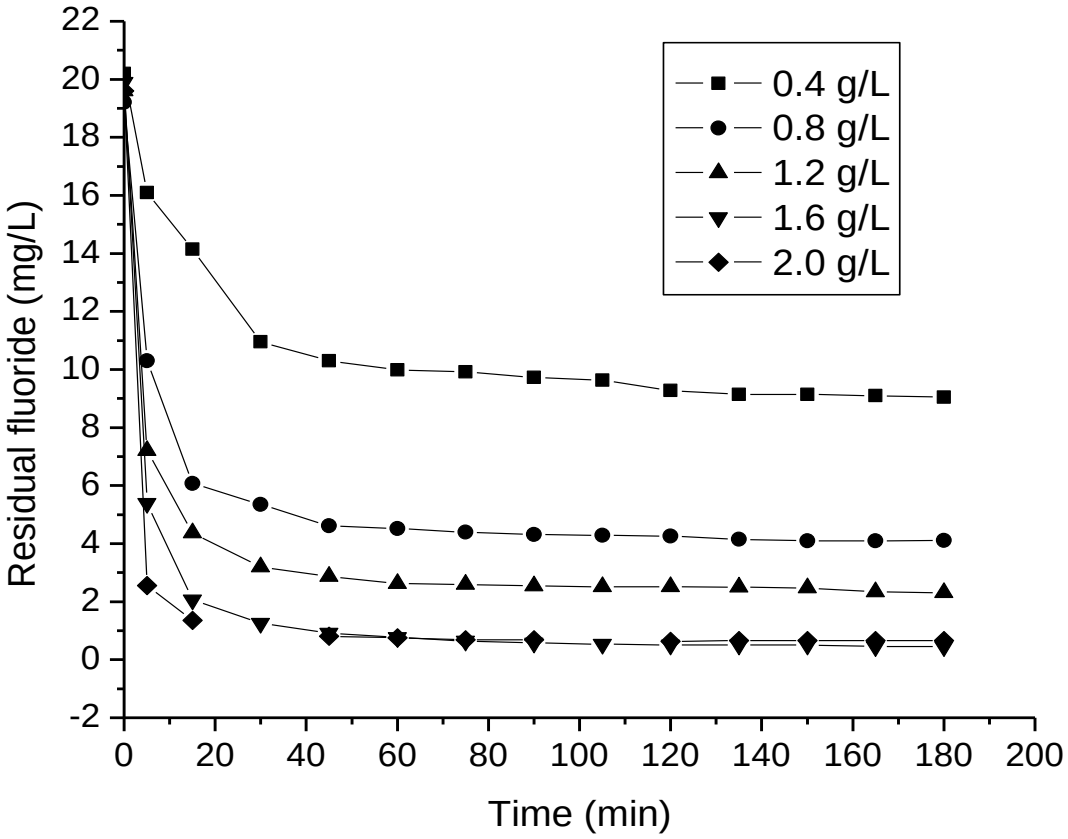


Figure 19. Residual $F^-$ concentration as a function of time for different dose of nano–AlOOH ($C_o$ = 20 mg/L).

The defluoridation efficiency (%) was significantly increased with dose as reflected by the measured residual fluoride concentration (Figure 20). The percent removal of fluoride increases significantly up to adsorbent dose of 1.6 g/L; however, no significant change was observed beyond this dose under the experimental conditions used. The increase in fluoride removal efficiency was due to the large number of available $F^-$ binding sites resulting from the increase in adsorbent dosage. Thus, 1.6 g/L of adsorbent dose was taken as an optimum dose for further experiments.

Conversely, the adsorption capacity decreases with increasing dose (Figure 20), this is possibly due to constant initial $F^-$ concentration. To maintain reasonable capacity and high fluoride removal efficiency, the surface loading (i.e., the mass ratio of fluoride to adsorbent dose) should be lower than the optimum value (i.e., the surface loading for optimum fluoride removal, about 90%, obtained from Figure 21 is 13.25 mg/g or less). A dose of 1.6 g/L corresponding to the capacity of about 11.88 mg $F^-$/g of adsorbent was considered for further adsorption experiments, which is greater than the reported surface loading of micronized AlOOH (11.25 mg $F^-$/g of adsorbent) for the corresponding dose of 1.6 g/L (Shimelis *et al*., 2006).

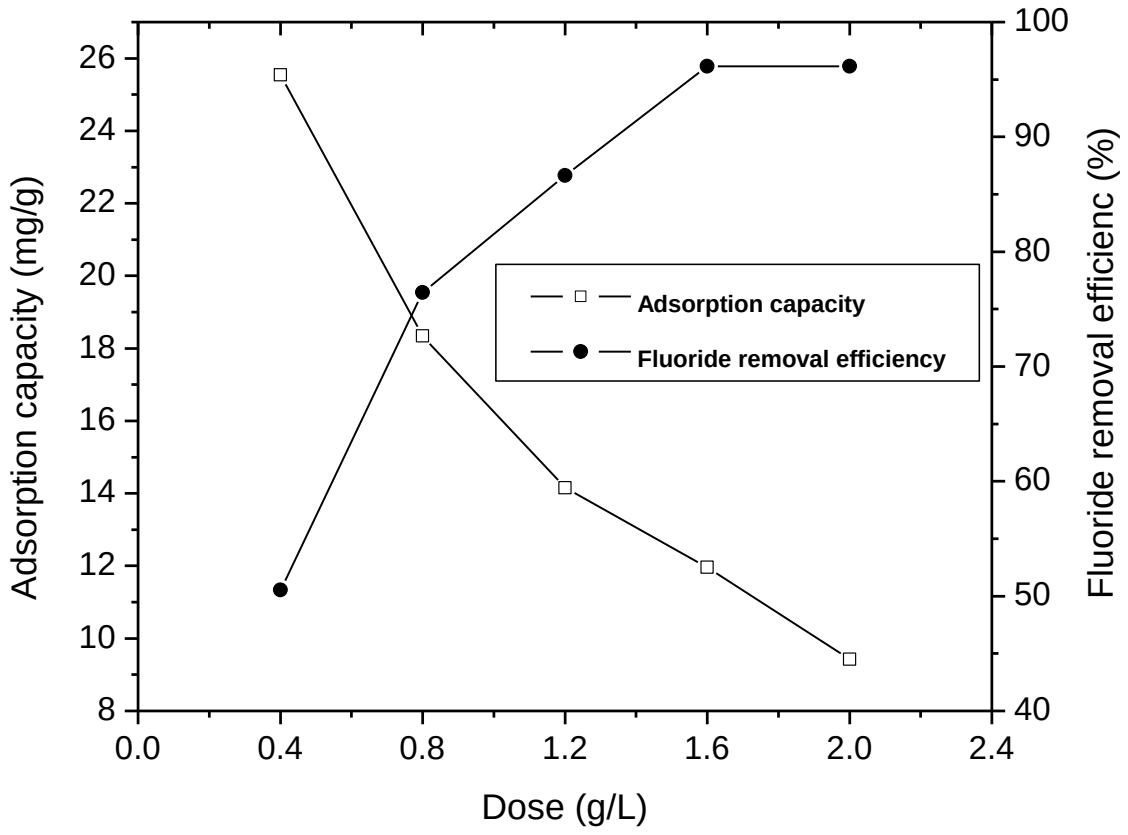


Figure 20. Capacity and efficiency (%) as a function of adsorbent dose ($C_o$ = 20 mg/L, contact time = 60 min).

#### 4.2.2.2. Effect of initial fluoride concentration

As shown in Figure 21, the efficiency increases with decreasing initial fluoride concentration at the initial stage of adsorption. It can be observed that the adsorption of fluoride from water is relatively more rapid at lower initial concentrations. This is due to the utilization of more accessible energetically active sites on the adsorbent surface. Thus the initial fluoride concentration had an influence on the equilibrium sorption time, and significant fluoride removal efficiency (> 90%) was observed when the initial fluoride was less than or equal to 20 mg/L for a contact time of 60 min. However, adsorption of more concentrated fluoride solution approached equilibrium slowly.

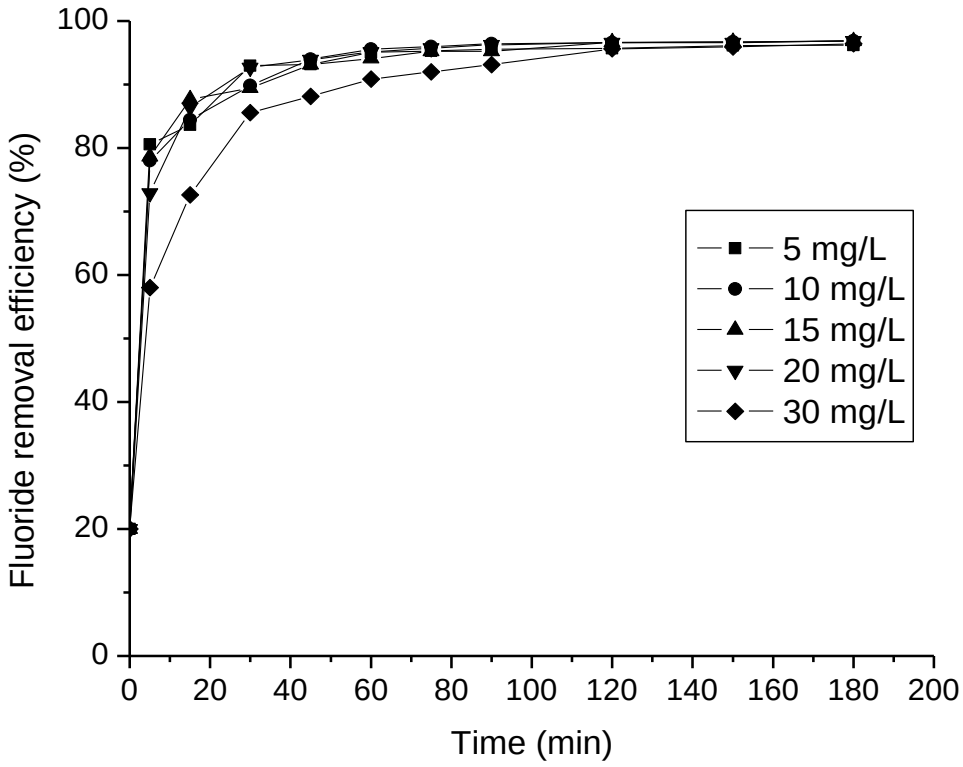


Figure 21. Effect of initial fluoride concentration on fluoride removal efficiency as a function of contact time (dose = 1.6 g $L^{-1}$).

#### 4.2.2.3. Effect of solution pH

Figure 22 shows the influence of initial solution pH on the fluoride removal efficiency of the adsorbent. It is evident that the percentage of fluoride removal increases as the pH of the solution increases from of 3–8 and reaches a maximum at pH = 7.0. Further increase in the solution pH from 8–10 decreases the fluoride removal efficiency and it becomes significant after pH of 9. This is consistent with the work of (Parida *et al*., 2009; Wang *et al*., 2008). The fluoride adsorption capacity of this medium is more enhanced in the pH range from 5 to 8, possibly due to the development of positive sites at the surface of the adsorbent. The decrease in the fluoride removal below pH 5 is possibly due to the protonation of the fluoride ion. On the other hand, at a pH above 8, fluoride removal efficiency decreases possibly due to the development of negative charges on the adsorbent surface and/or stronger competition from hydroxide ions. Nano–AlOOH has a $pH_{pzc}$ of 7.8, which means that the surface of the adsorbent presents a net positive charge when $pH \leq 7.8$. Therefore, the high efficiency in pH less than 8 can be attributed to the gradual increase in attractive forces, and low efficiency in alkaline medium can be explained by the repulsion between the negatively charged surface and fluoride.

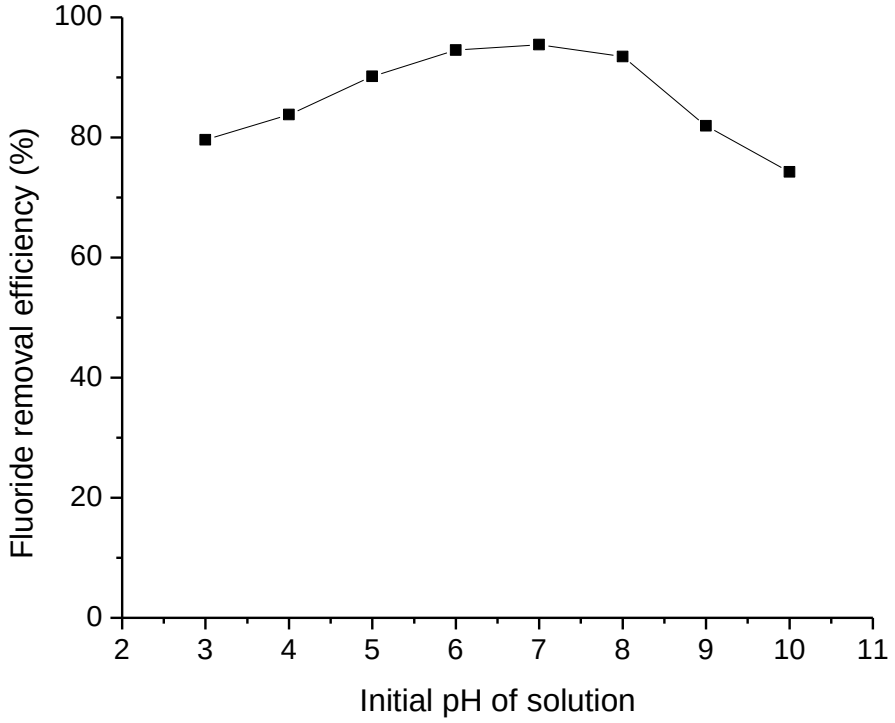


Figure 22. Effect of initial solution pH on fluoride removal efficiency of the media (dose = 1.6 g/L, $C_o$ = 20 mg/L, and contact time = 60 min).

### 4.2.3. Adsorption isotherms and kinetics of fluoride adsorption onto AOMO and nano–AlOOH

#### 4.2.3.1. Adsorption isotherms and kinetics of fluoride adsorption onto AOMO

The determined coefficients for isotherm and kinetic models are shown in Table 3 and 4, respectively. Figure 23 and 24 were drawn using the experimental and predicted value by linear and non–linear regression methods for isotherm and kinetics models, respectively. The error analysis was also performed using six different error functions (ASS, $S_{y.x}$, $\chi^2$, APE, HYBRID, and MPSD) to evaluate the applicability of each model isotherm equation to the experimental data (Table 5).

Table 3. Linear and non–linear isotherm equations and parameters.

| Isotherms | Linear | | | Non–linear | | |
|---|---|---|---|---|---|---|
| Langmuir | $\frac{C_e}{q_e} = \frac{1}{q_m} + \frac{C_e}{q_m}$ | | | $q_e = \frac{q_m b C_e}{1 + bC_e}$ | | |
| | Parameters | | | | | |
| | $q_m$ (mg/g) | b (L/mg) | $R^2$ | $q_m$ (mg/g) | b (L/mg) | $R^2$ |
| | 18.62 | 0.3834 | 0.9712 | 19.19 | 0.3300 | 0.9772 |
| Freundlich | $\log(q_e) = \log(K_F) + \frac{1}{n}\log(C_e)$ | | | $q_e = K_F C_e^{1/n}$ | | |
| | Parameters | | | | | |
| | $K_F$ (mg/g) | n | $R^2$ | $K_F$ (mg/g) | N | $R^2$ |
| | 4.481 | 1.668 | 0.9529 | 4.942 | 1.946 | 0.9895 |
| Dubinin–Radushkevich (D–R) | $\ln q_e = \ln q_s -$ $^2$ | | | $q_e = (q_s)\exp(-$ $^2)$ | | |
| | Parameters | | | | | |
| | $q_s$ (mg/g) | E (kJ/mol) | $R^2$ | $q_s$ (mg/g) | E (kJ/mol) | $R^2$ |
| | 99.87 | 9.71 | 0.9645 | 16.21 | 27.08 | 0.9528 |

From Table 3, it was observed that the correlation coefficient value for the linear form of Langmuir is higher ($R^2$ = 0.9712) than Freundlich and Dubinin–Radushkevich isotherms. However, the non–linear isotherm correlation coefficient for Freundlich ($R^2$ = 0.9712) is higher than the linear as well as the non–linear forms of Langmuir and Dubinin–Radushkevich isotherms. Therefore, non–linear model could be the best representation of the experimental data as compared with linear models. It is clear that transformations of the non–linear Langmuir isotherm equation to linear forms implicitly alter the error structure and may also violate the error variance and normality assumptions of the standard least–squares method (Ho and Wang, 2004). The error analysis performed for non–linear isotherms also indicates that Freundlich isotherm was the one with the lowest value (Table 5). Thus, from the values' of correlation coefficient and error analysis, non–linear Freundlich isotherm model was found to be the best

representative of adsorption of fluoride by AOMO (Alemu *et al.*, 2014). Considering the theoretical bases of the Freundlich model, the studied separation process could be described either as non–ideal and reversible sorption, not restricted to monolayer formation on heterogeneous surface, or as multilayer sorption with non–uniform distribution of adsorption heat and affinities over the heterogeneous surface (Foo and Hameed, 2010).

Table 4. Linear and non–linear kinetic equations and parameters.

| Kinetic | Linear | | | Non–linear | | |
|---|---|---|---|---|---|---|
| Pseudo–first order | $\log(q_e - q_t) = \log q_e - \frac{K_1 t}{2.303}$ | | | $q_t = q_e\,(1 - \exp^{-K_1 t})$ | | |
| | Parameters | | | | | |
| Initial $F^-$ and adsorbent dose | $q_e$ (mg/g) | $K_1$ | $R^2$ | $q_e$ (mg/g) | $K_1$ | $R^2$ |
| 10 mg/L $F^-$ and 1 g/L dose | 1.893 | $7.28 \times 10^{-3}$ | 0.8224 | 8.442 | 0.1119 | 0.9812 |
| 20 mg/L $F^-$ and 2 g/L dose | 1.639 | $9.92 \times 10^{-3}$ | 0.8952 | 9.038 | 0.1674 | 0.9838 |
| 40 mg/L $F^-$ and 4 g/L dose | 1.334 | $7.73 \times 10^{-3}$ | 0.7895 | 9.383 | 0.1939 | 0.9858 |
| Pseudo–second order | $\frac{t}{q_t} = \frac{1}{K_2 q_e^2} + \frac{1}{q_e} t$ | | | $q_t = \frac{K_2 q_e^2 t}{1 + K_2 q_e t}$ | | |
| | Parameters | | | | | |
| Initial $F^-$ and adsorbent dose | $q_e$ (mg/g) | $K_2$ | $R^2$ | $q_e$ (mg/g) | $K_2$ | $R^2$ |
| 10 mg/L $F^-$ and 1 g/L dose | 8.73 | $2.20 \times 10^{-2}$ | 0.9999 | 8.726 | 0.0220 | 1.0000 |
| 20 mg/L $F^-$ and 2 g/L dose | 9.29 | $3.67 \times 10^{-2}$ | 0.9998 | 9.285 | 0.0324 | 1.0000 |
| 40 mg/L $F^-$ and 4 g/L dose | 9.19 | $4.54 \times 10^{-2}$ | 0.9998 | 9.615 | 0.0374 | 1.0000 |

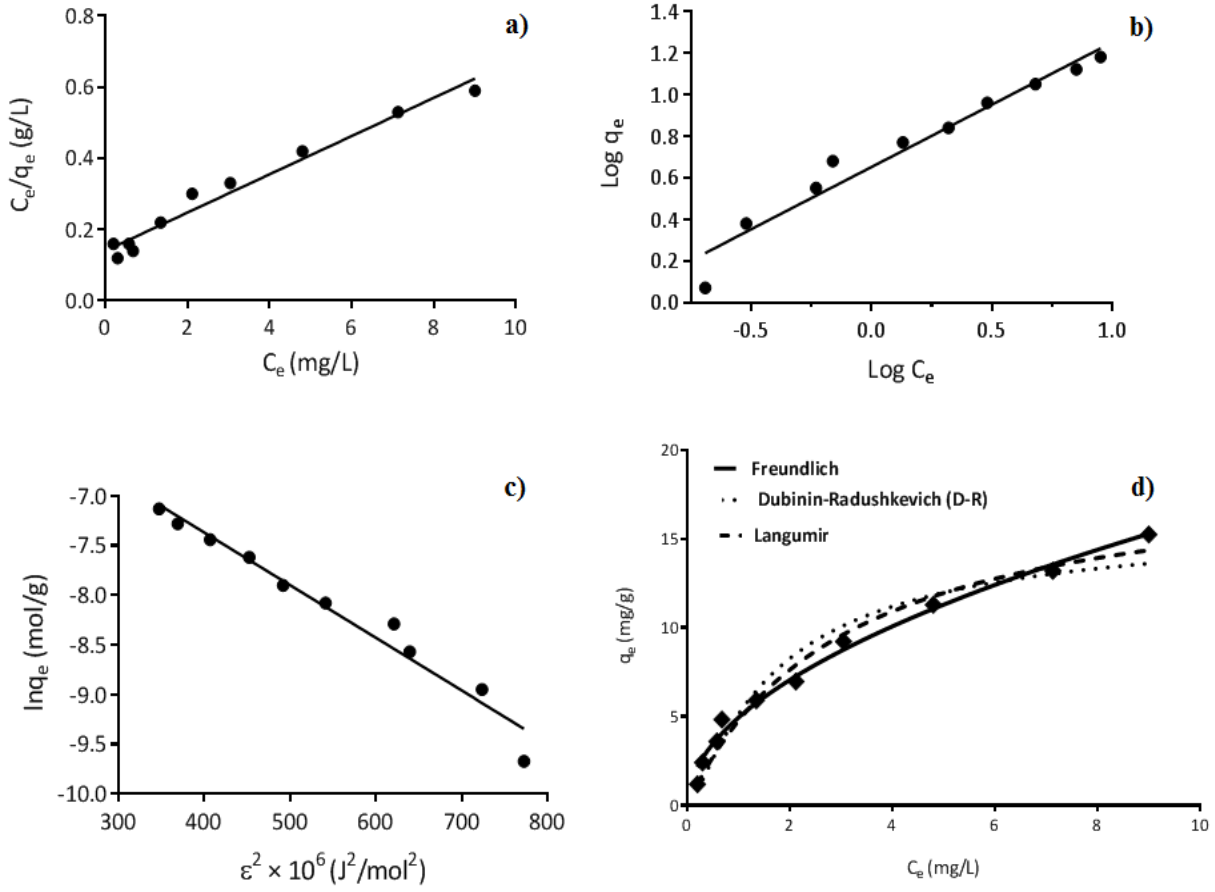


Figure 23. Linear and non–linear isotherm models for the adsorption of fluoride by AOMO (a) linearized Langmuir, (b) linearized Freundlich, (c) linearized Dubinin–Radushkevich and (d) non–linear isotherms (adsorbent dose = 4 g/L, contact time = 4 h, pH = 7.0 ± 0.2) (Alemu *et al.*, 2014).

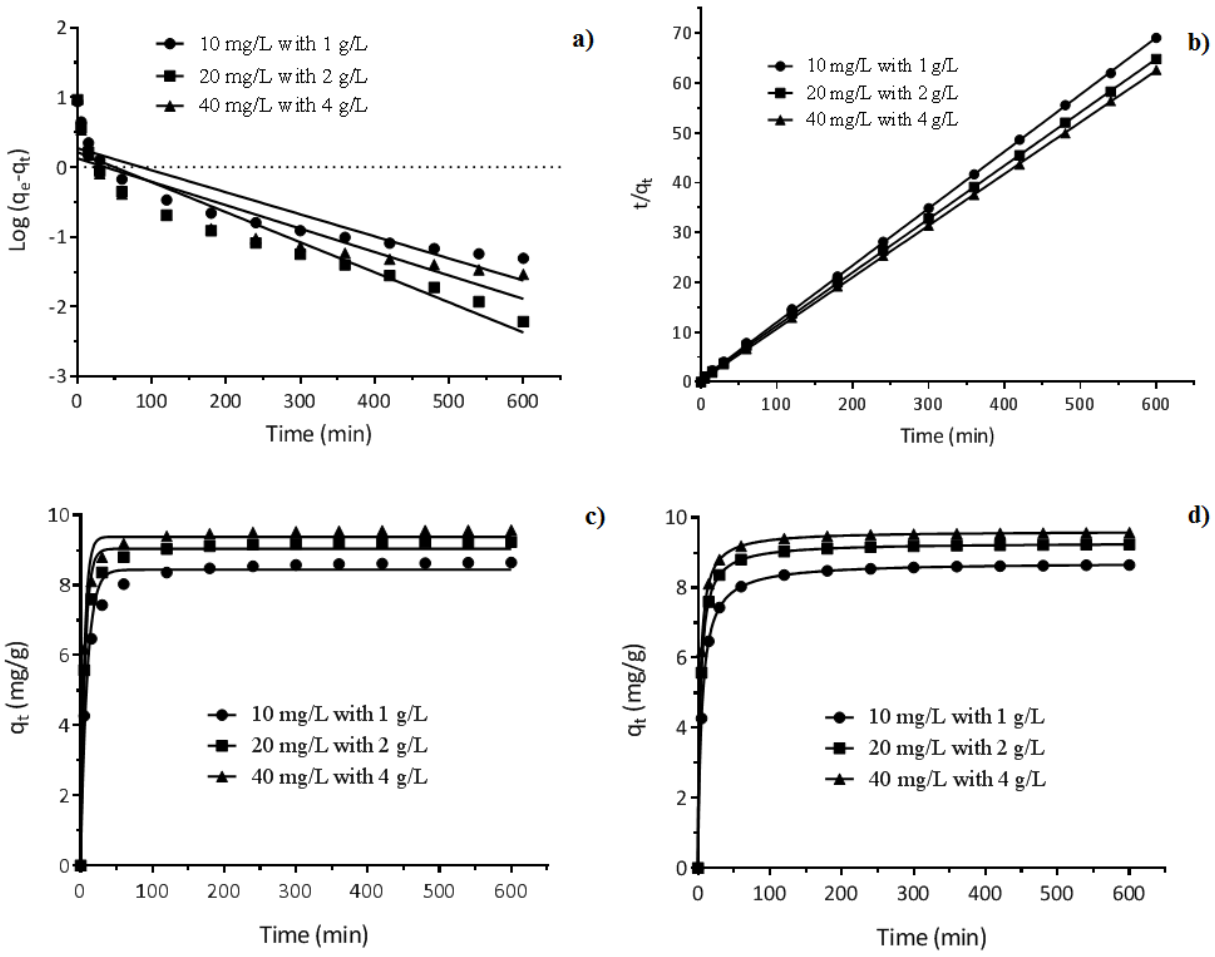


Figure 24. a) linear and c) non–linear pseudo–first order and b) linear and d) non–linear pseudo–second order kinetics for the adsorption of fluoride on AOMO with initial fluoride concentrations of 10 mg/L, 20 mg/L and 40 mg/L, to adsorbent doses of 1.0, 2.0 and 4 g/L, respectively (pH = 7.0 ± 0.2, contact time = 10 h).

Table 5. Comparison of linear and non–linear models using error functions.

| Error functions | Regression methods | Isotherm models | | | Kinetic models | |
|---|---|---|---|---|---|---|
| | | Langmuir | Freundlich | D–R | Pseudo–first order | Pseudo–second order |
| ASS (Absolute sum of squares) $ASS = \sum_{i=1}^{n}(q_{e,cal} - q_{e,meas})^2$ | Linear | **0.0074** | 0.0521 | 0.2049 | 1.431 | **0.6289** |
| | non-linear | 4.569 | **2.110** | 9.464 | 1.353 | **0** |
| $S_{y.x}$ (Sum of the squares for the residuals) $S_{y.x} = \sqrt{\frac{SS}{df}}$ | Linear | **0.0304** | 0.0807 | 0.1600 | 0.3441 | **0.2241** |
| | non-linear | 0.7557 | **0.5136** | 1.088 | 0.3356 | **0** |
| $\chi^2$ (Chi–square) $\chi^2 = \sum_{i=1}^{n}\frac{(q_{e,cal} - q_{e,meas})^2}{q_{e,meas}}$ | Linear | 0.0344 | 0.4364 | **-0.023** | **-0.2067** | 0.1143 |
| | non-linear | **0.8460** | 0.9784 | 1.608 | 0.3207 | **0.0011** |
| APE (Average percentage errors) $APE = \frac{100}{n}\sum_{i=1}^{n}\left\lvert\frac{q_{e,meas} - q_{e,cal}}{q_{e,meas}}\right\rvert$ | Linear | 10.79 | 29.09 | **1.2** | 65.85 | **3.9777** |
| | non-linear | **10.07** | 12.67 | 17.1 | 4.731 | **0.1423** |
| HYBRID (Hybrid fractional error function) $HYBRID = \frac{100}{n-p}\sum_{i=1}^{n}\frac{(q_{e,meas} - q_{e,cal})}{q_{e,meas}}$ | Linear | -3.777 | **-25.60** | -0.019 | 66.62 | **-2.404** |
| | non-linear | 6.653 | **-9.432** | 9.7982 | 2.046 | **-0.174** |
| MPSD (Marquardt's percent standard deviation) $MPSD = 100\sqrt{\frac{1}{n-p}\sum_{i=1}^{n}(\frac{q_{e,meas} - q_{e,cal}}{q_{e,meas}})^2}$ | Linear | 259.2 | 102.9 | **4.284** | 232.9 | **14.06** |
| | non-linear | 2278 | **44.79** | 60.32 | 16.73 | **0.503** |

Note: The bold values indicate the lowest value within three isotherm and two kinetic models, respectively.

#### 4.2.3.2. Adsorption isotherms and kinetics of fluoride adsorption onto nano–AlOOH

The experimental data of equilibrium isotherm for fluoride adsorption were modeled using the most frequently used isotherms, such as Freundlich, Langmuir, Dubinin–Radushkevich (D–R) and Temkin isotherm.

The linear plot of $C_e/q_e$ versus $C_e$ (Figure 25) indicates the applicability of Langmuir adsorption isotherm. The correlation coefficient obtained from Langmuir isotherm was the highest compared to the values obtained from Freundlich, D–R and Temkin isotherms (Table 6). Therefore, the Langmuir isotherm is the best–fit isotherm for the adsorption of fluoride onto this adsorbent under the experimental conditions used in this study.

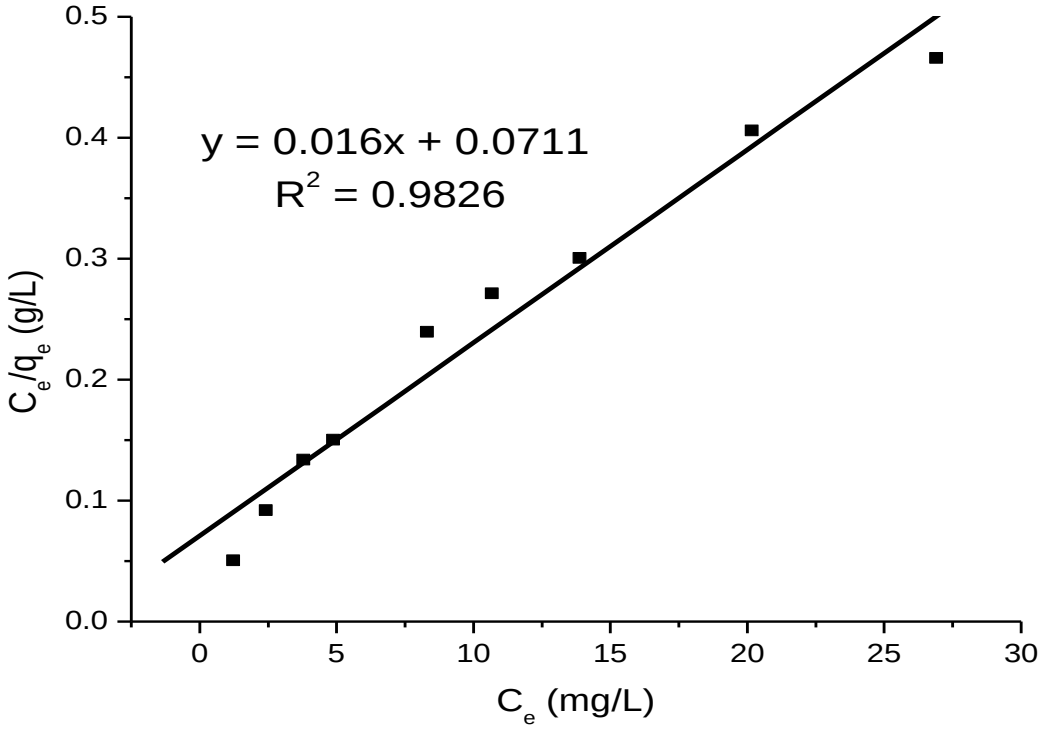


Figure 25. Linearized Langmuir isotherm of the adsorption process ($C_o$ = 50 mg/L, contact time = 24 h, and pH = 7).

Table 6. Langmuir, Freundlich, Dubinin–Radushkevich (D–R), and Temkin model constants at pH = 7 and 25 $^{o}$C.

| Isotherm models | Constants | | Correlation coefficients ($R^2$) |
|---|---|---|---|
| Langmuir | $q_{max}$ (mg/g) | B (L/mg) | |
| | 62.5 | 0.225 | 0.9826 |
| Freundlich | $K_F$ (mg/g) | 1/n (L/mg) | |
| | 20.75 | 0.286 | 0.9778 |
| Dubinin–Radushkevich (D–R) | $q_{max}$ (mg/g) | E (kJ/mol) | |
| | 112.8 | 13.15 | 0.9754 |
| Temkin | $K_T$ x $10^3$ (L/mg) | $RT/b_T$ x $10^{-3}$ | |
| | 92.75 | 0.56 | 0.9614 |

Figure 26 shows the average pseudo–second order plot of fluoride adsorption kinetics on the adsorbent each with the same initial load. Thus the three rate constants of an adsorbent averaged to get a single rate constant (2.22 g/min·mg) (x $10^{-3}$), and the correlation coefficient was found to be near to unity. Therefore, the pseudo–second order model is suitable to describe the adsorption kinetics of nano–AlOOH.

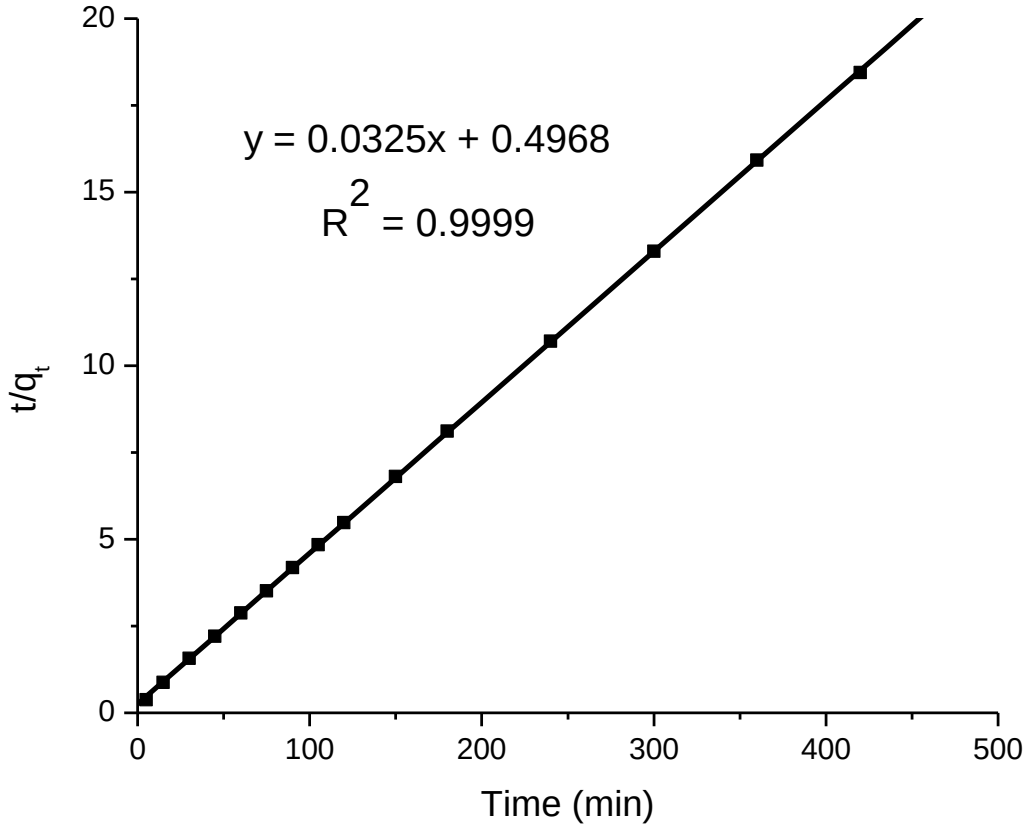


Figure 26. Average pseudo–second order plot of fluoride adsorption kinetics on adsorbents each with the same initial load (pH = 7.01–7.18, contact time, 10 h).

### 4.3. Fluoride adsorption performance of aluminium hydro(oxide) (AO)

AO was superior than the above adsorbents (AOMO and nano–AlOOH) in terms of adsorption capacity, availability of raw material, mode of field implementation, ease of operation and so on. Therefore, optimization and further studies of the AO adsorbent were required.

### 4.3.1. Fluoride uptake capacity of AO synthesised at different ratios

The effect of OH:Al ratio on the fluoride adsorption capacity, surface properties (acid and surface site concentration) and composition of AO is presented in Figure 27 and Table 7. The adsorption capacity of materials synthesised at OH:Al ratios of 2.5 and 2.7 is relatively higher than the rest of AO products, which is also revealed by acidity and surface site concentrations of AO. This is mainly because of optimum amount of sulfate associated with aluminium (Table 7) and hence higher surface acid site concentration which may play a significant role in the removal of fluoride.

Table 7. Composition of AO synthesised at different OH:Al ratios.

| Sample Name | OH:Al | Yield (g) | Adsorption capacity (mg/g) | Elemental composition | | | | *Normalized fluoride removal efficiency (%) |
|---|---|---|---|---|---|---|---|---|
| | | | | Al mmol/g | $SO_4^{2-}$ mmol/g | Na mmol/g | Fe mmol/g | |
| $AO_{2.0}$ | 2.0 | 30.7 | 7.60 | 5.10 | 4.2 | 0.28 | 0.08 | 59 |
| $AO_{2.2}$ | 2.2 | 36.4 | 7.91 | 7.50 | 4.1 | 0.32 | 0.12 | 61 |
| $AO_{2.5}$ | 2.5 | 49.0 | 12.2 | 10.7 | 3.2 | 0.00 | 0.15 | 95 |
| $AO_{2.7}$ | 2.7 | 45.7 | 12.0 | 10.9 | 2.2 | 0.00 | 0.15 | 94 |
| $AO_{3.0}$ | 3.0 | 47.2 | 3.94 | 13.7 | 0.3 | 0.01 | 0.19 | 30 |
| $AO_{3.3}$ | 3.3 | 32.9 | 2.81 | 15.7 | 0.1 | 0.19 | 0.28 | 21 |

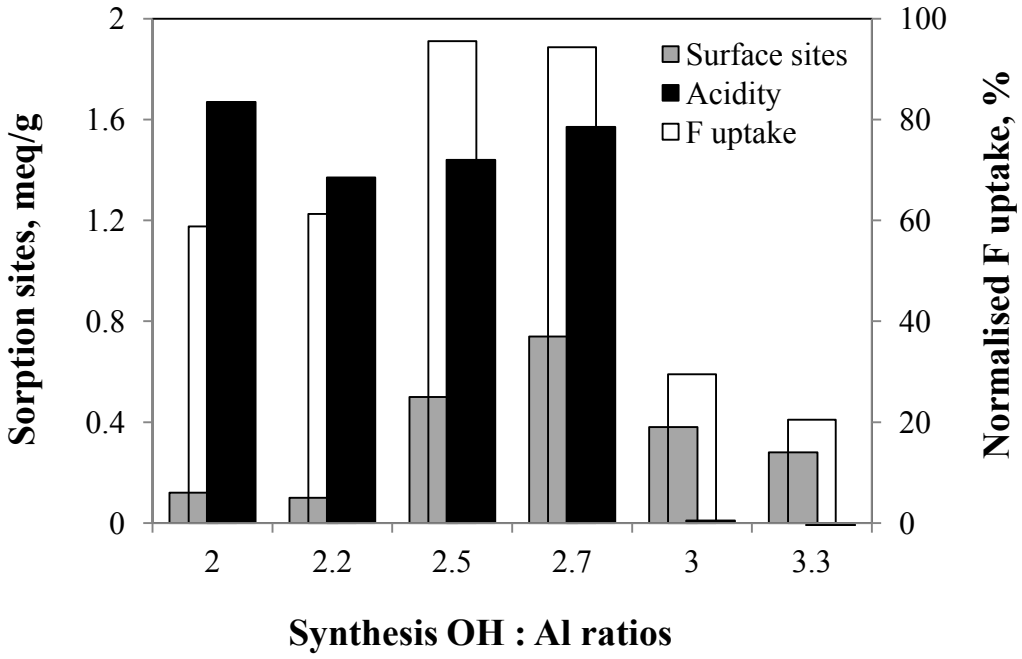


Figure 27. Fluoride uptake and binding sites as a function of OH:Al synthesis ratios.

### 4.3.2. Effect of co–existing ions on fluoride uptake

The effect of coexisting anions on the fluoride removal efficiency by AO is shown in Figure 28. In the absence of other anions, over 90% of fluoride was adsorbed and the residual pH was 4.76 when no competing ions were present. The results also show that $Cl^-$ and $SO_4^{2-}$ have no significant effect on fluoride adsorption. A decrease in fluoride uptake is noted for $HCO_3^-$, but this is most likely to be related to an increase in pH with increasing $HCO_3^-$ content, as the uptake is similar, for a given pH value, to solutions where $OH^-$ has been added. Phosphate, however, appears to compete with fluoride. With the addition of 500 mg/L $HPO_4^{2-}$, fluoride uptake is reduced from around 95 to 75%. These observations are in agreement with the literature. Maliyekkal *et al*. (2008) have also reported a similar observation for the removal of fluoride using a new adsorbent material, magnesia amended activated alumina. As can be seen from Figure 28, the error is within the acceptable range.

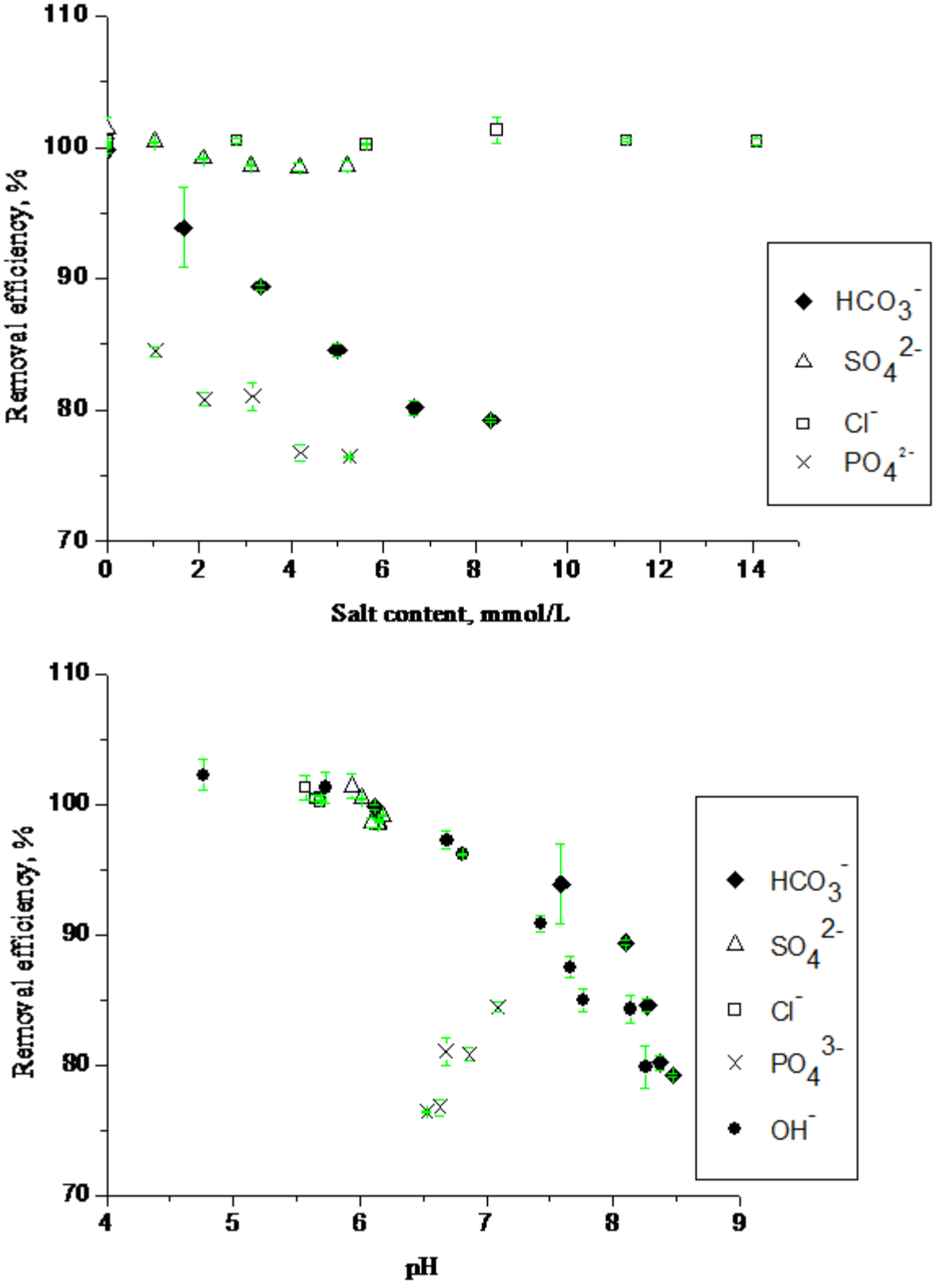


Figure 28. Effect of co–existing anions on fluoride removal efficiency of AO.

### 4.3.3. Fluoride removal performance of AO in packed bed column

The first set of experiments were run at a flow rate of 100 eBV/day using deionized water to follow the pH during column experiments with and without fluoride (0 and 20 mg/L) and to observe the release of potential contaminants. Figure 29 shows that in the absence of fluoride the pH of the column effluent was consistently around 4. Aluminium was released to the treated water at a level above the USEPA guideline value of 0.2 mg/L (USEPA, 2008) within the first 50 eBV, but then declined presumably because readily soluble aluminium salts were flushed out of the column. The sodium and sulfate content of the effluent was high (1500 and 6000 mg/L, respectively) during the first flush (< 10 eBV for Na and 20 eBV for $SO_4^{2-}$) and then dropped to below the WHO taste threshold limits (200 mg/L and 250–1000 mg/L for Na and $SO_4$, respectively) (WHO, 2011).

In the presence of fluoride, the pH values of the treated water were higher, with an initial minimum of 4.4 but with constantly increasing values thereafter. The higher pH values may be explained by the exchange of fluoride for hydroxide groups at the AO surface. The fluoride adsorption capacity to 1.5 mg/L (the WHO guideline value) was about 26.2 mg $F^-$/g AO, which is 6 times greater than the values reported for activated alumina, 3.8–4.5 mg $F^-$/g AA (WHO, 2011; Barbier and Mazounie, 1984).

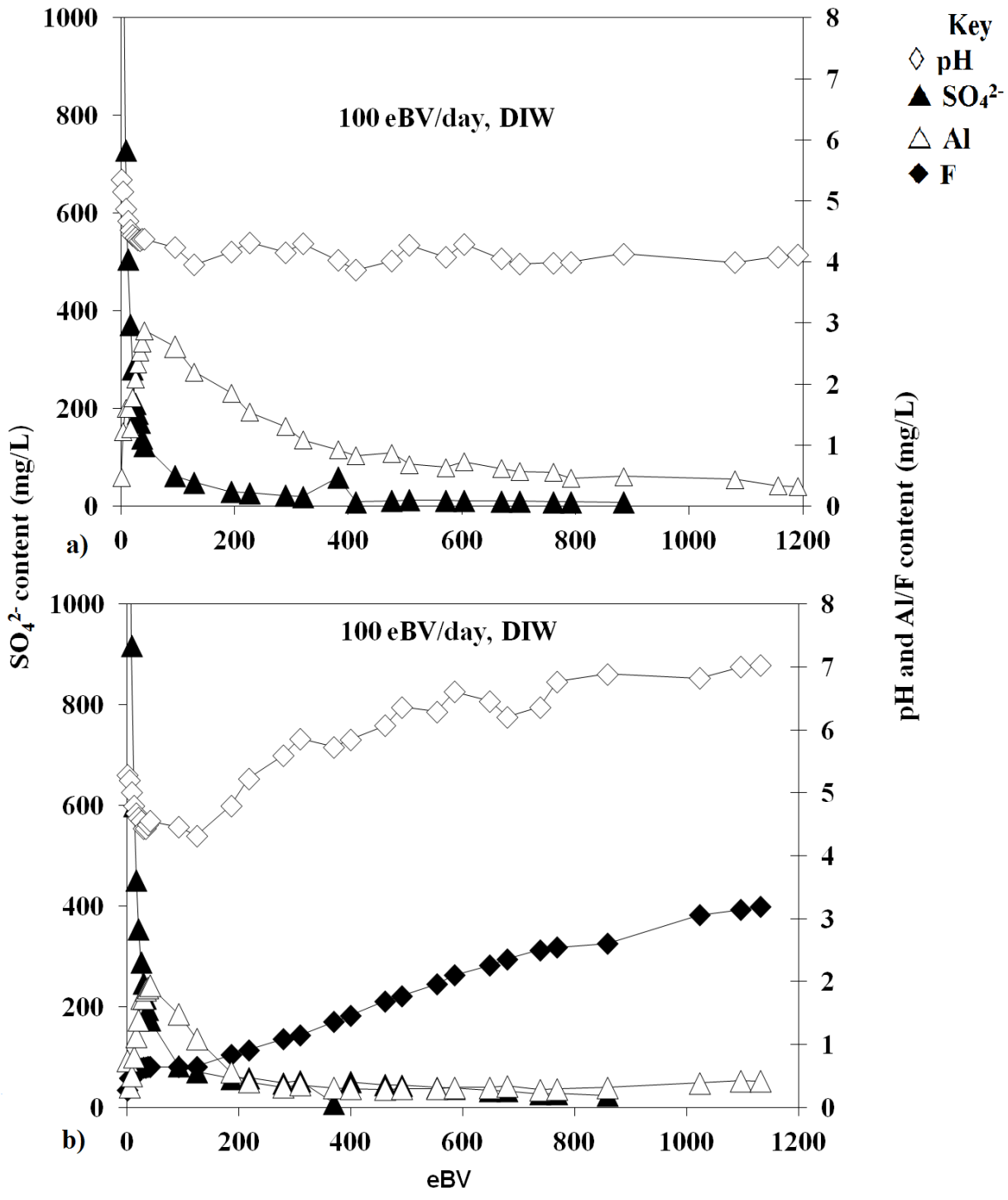


Figure 29. Fluoride removal from deionized water with influent fluoride concentration of a) 0, and b) 20 mg/L at flow rate of 100 empty bed volume/day.

The second set of experiments was performed with water buffered with 10 mM $NaHCO_3$ and 3000 ppm $CO_2$ (around pH 8) to represent Ethiopian groundwaters from the Rift Valley. At a flow rate of 100 eBV/day the pH remained consistently above 6 but the fluoride adsorption capacity to 1.5 mg/L was reduced to 4.65 mg/g (Figure 30a), demonstrating the pH dependence of the sorption process. At a flow rate of 10 eBV/day (Figure 30b), the fluoride uptake to 1.5 mg/L increased significantly to around 9 mg/g. However the pH was initially quite low (pH 4.7) and coincided with dissolved aluminium concentrations of 0.61 mg/L in the treated water. Aluminium concentrations of up to 2 mg/L were observed in the presence of fluoride after breakthrough even at the pH of around 8. Given the relative insolubility of $Al(OH)_3$ in the neutral pH range, this observation can possibly be ascribed to the solubilisation of aluminium through complex formation with fluoride. As previously observed, residual sodium sulfate was washed out within the first 20 eBVs. The sulfate concentrations remained above 400 mg/L for the first 50 eBVs and were probably released as the AO was neutralized by the release of $OH^-$ ions during fluoride sorption.

With calcite post–column treatment (Figure 30c) the pH value of the treated water was stabilised at between 7.5 and 8.5 and no early release of dissolved aluminium was observed. The fluoride adsorption capacity was about 7.7 and 15.5 mg/g until breakthrough concentration (1.5 mg/L) and complete exhaustion, respectively. Dissolved calcium in the treated water indicated that the calcite neutralises the treated water and precipitates dissolved aluminium. However the calcite column did not remove aluminium–fluoride complexes. There was an additional benefit that $SO_4^{2-}$ was also removed to acceptable limits (< 500 mg/L) in the first flush (< 8 eBV), most likely due to its precipitation in the form of gypsum ($CaSO_4 \cdot 2H_2O$).

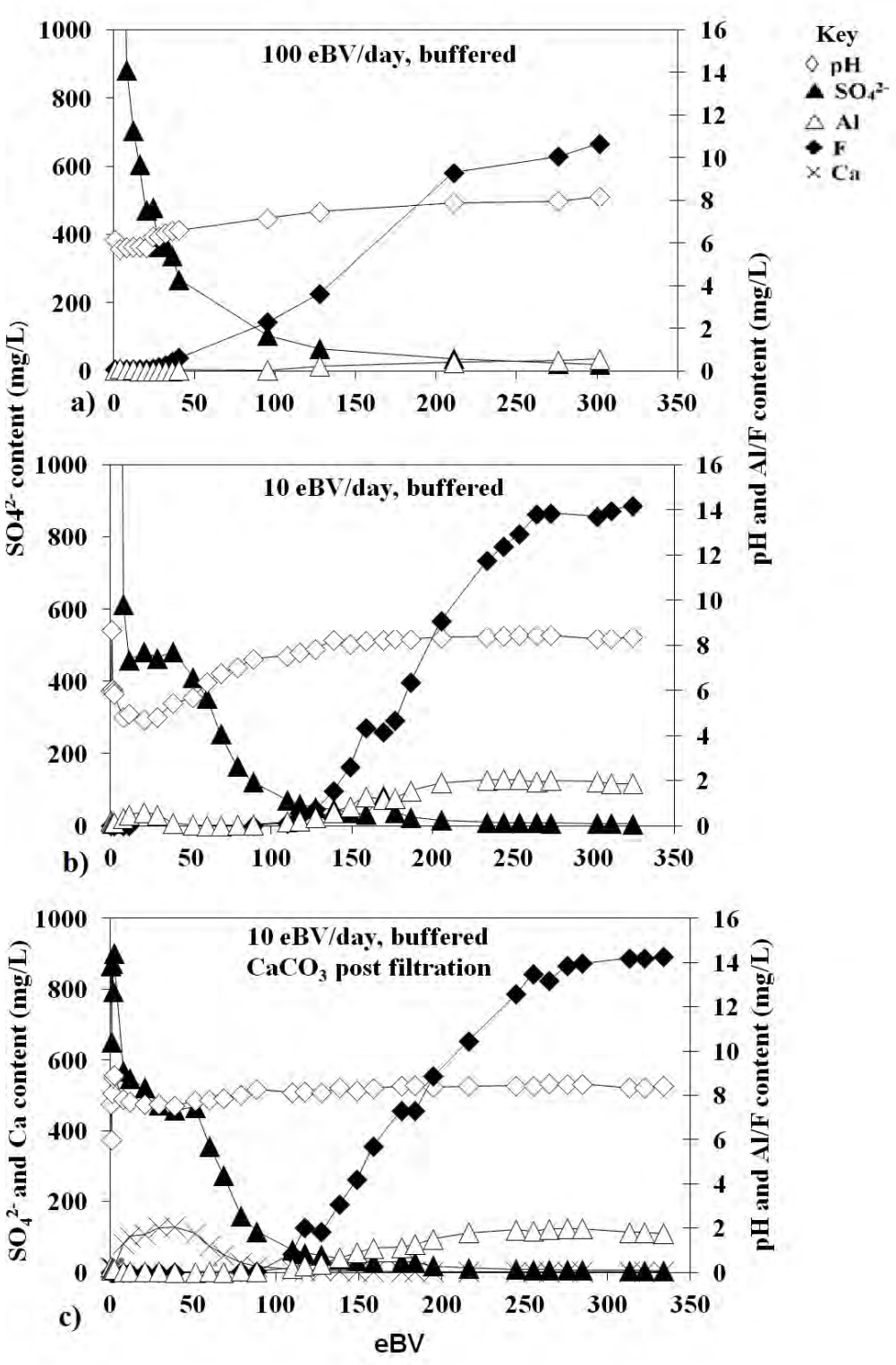


Figure 30. Fluoride removal from raw water with influent fluoride concentration of 20 mg/L at flow rate: (a) 100, (b) 10, (c) 10 empty bed volume/day.

### 4.3.4. Performance of granulated AO powder

The breakthrough curve for granulated AO is shown in Figure 31. The adsorption capacity of granulated AO adsorbent under optimum operating conditions (flow rate, 10 eBV/day and fluoride concentration, 20 mg/L) was 7.2 mg/g, which is comparable with AO adsorbent reported in Figure 30c. The pH of the treated water was within the range of 5.88 and 8.64. Therefore, the granulated AO adsorbent could be used directly or after coated with high surface area materials at community defluoridation plants.

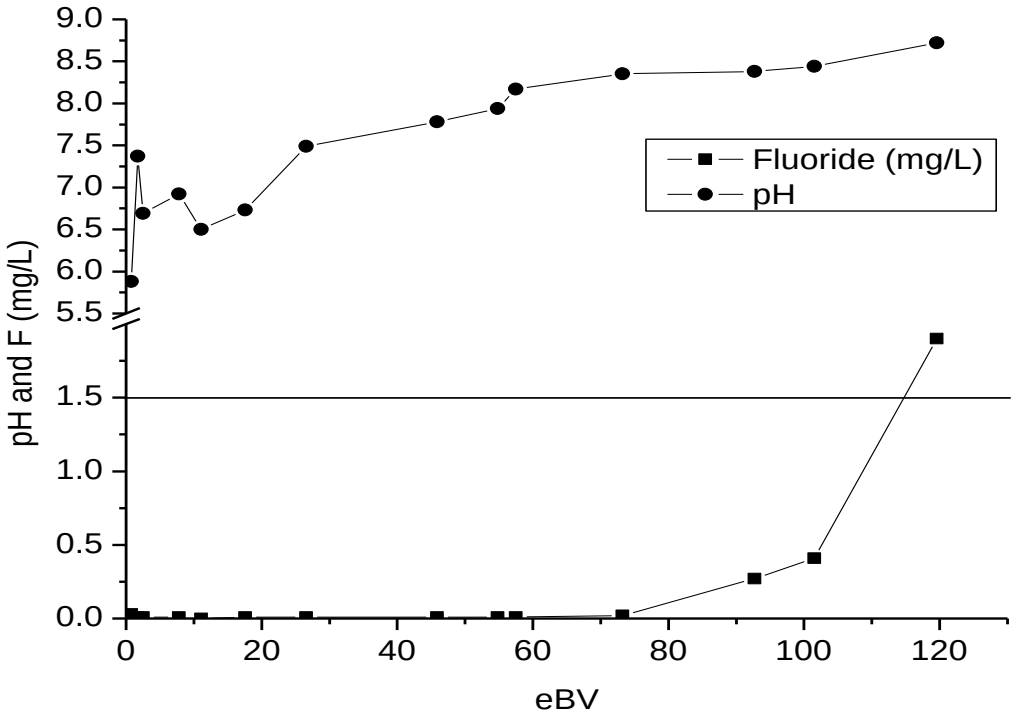


Figure 31. Breakthrough curve for granulated AO with influent fluoride concentration of 20 mg/L and at flow rate of 10 eBV/day.

## 4.4. Comparison of surface properties, elemental composition, and geometry of AO with aluminium hydroxide–based adsorbents

### 4.4.1. Surface acidity and elemental composition

The surface acidity and surface site concentrations of AO, AA and PB determined by acid–base titration are shown in Table 8. The acidity and surface site concentration of AO is higher than the corresponding AA and PB adsorbents, which may account for the higher fluoride removal capacity of AO. The results from Table 8 indicate that higher surface area and $Al_2O_3$ composition do not ensure better fluoride removal performance for aluminium hydroxide–based adsorbents (AA and PB). However, the sulfate proportion is still higher for AO.

Table 8. Acidity and surface site concentration, surface area, and elemental composition of AO, AA and PB.

| Adsorbents | Surface area ($m^2/g$) | Elemental composition % | | | | | Acidity | Surface site conc. |
|---|---|---|---|---|---|---|---|---|
| | | $Al_2O_3$ | $Na_2O$ | $SO_4$ | $Fe_2O_3$ | Total % | (meq/g) | (meq/g) |
| Activated alumina (AA) (Compalox$^R$ AN/V–812), Germany | 250 | 90.0 | 0.35 | – | 0.01 | 90.1 | –0.24 | 0.20 |
| Pseudoboehmite (PB), Germany | 300 | 95.0 | 0.1 | 0.2 | 0.02 | 95.3 | –0.23 | 0.39 |
| Aluminium hydro(oxide) (AO), Ethiopia | 37.7 | 78.3 | 0.01 | 19.4 | 2.20 | 99.9 | 1.57 | 0.74 |

### 4.4.2. Solubility of Al–hydroxide–based adsorbents

The solubility curve for AO, amorphous and crystalline aluminium hydroxide is shown in Figure 32. The curve for AO bears closer resemblance to that of amorphous $Al(OH)_3$ than crystalline $Al(OH)_3$; however, the solubility diagrams may vary when other environmental factors, such as $SO_4^{2-}$, are considered in AO (Letterman and Asolekar, 1990; Bi *et al*., 2004). Sulfate ion strongly

affects speciation. This is due to its chemical behavior. Firstly, it binds strongly to the aluminium complexes and secondly, it can be bound through different mechanisms (Ramo *et al*., 2008). It can function as a terminal ligand and bind to an aluminium atom in either a mono–, bi–, or even tridentate fashion or it can function as a bridging ligand between two or more aluminium atoms. In the studies of Ramo *et al*. (2008), sulfate ions were found to bind strongly to the aluminium hydroxides in aquatic environments. Furthermore, the sulfate ion not only competes with aqua ligands for the vacant coordination positions in the first solvation shell, but can also trigger topological changes in the aluminium complex cores. The dissolution of aluminium in AO is minimized in the pH range of 5 to 8, while for crystalline and amorphous $Al(OH)_3$ it is within the range of 8 to 10 and 5 to 9, respectively. The maximum of stability with respect to dissolution for AO is located at pH 7, with a dissolution curve steeper both at decreasing pH (<5) and at increasing pH (>8). Moreover, the higher solubility of AO with respect to amorphous $Al(OH)_3$ indicates that AO should be favoured thermodynamically upon precipitation (Carrier *et al*., 2007).

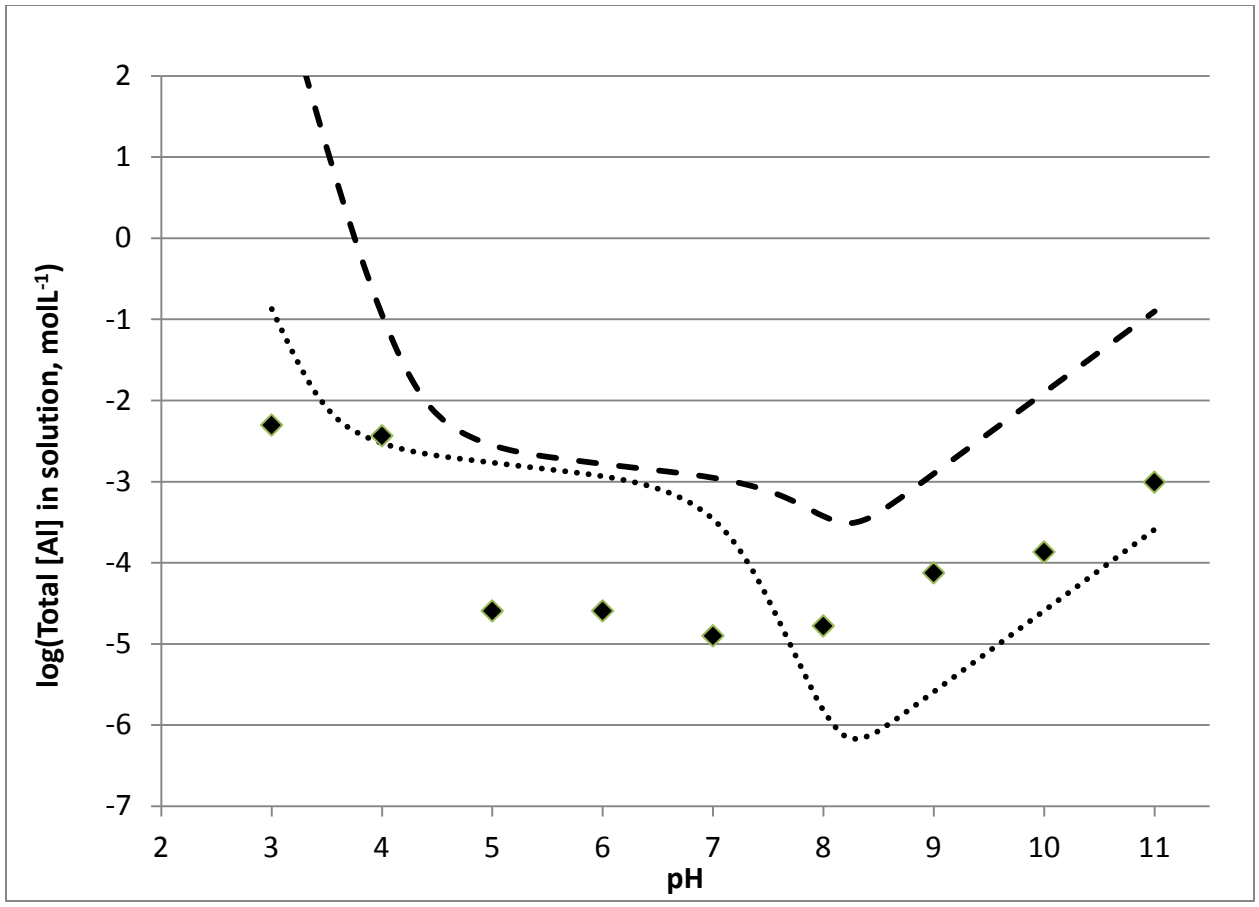


Figure 32. Solubility profiles. Concentration of [Al(III)] in solution (log scale) as a function of pH for AO (♦), crystalline $Al(OH)_3$ (dotted line), and amorphous $Al(OH)_3$ (dashed line).

### 4.4.3. Coordinate geometry of Al in aluminium hydroxide–based adsorbents

Aluminium NMR chemical shifts are directly related to the coordination number of the Al(III) ion (MacKenzie and Snith, 2002). Chemical shifts for octahedral Al(III) units appear between 10 and 20 ppm, while tetrahedral Al(III) centers exhibit peaks between 50 and 80 ppm. Resonances for five–coordinate Al(III) species, while less common, are typically observed in the range of 25–35 ppm.

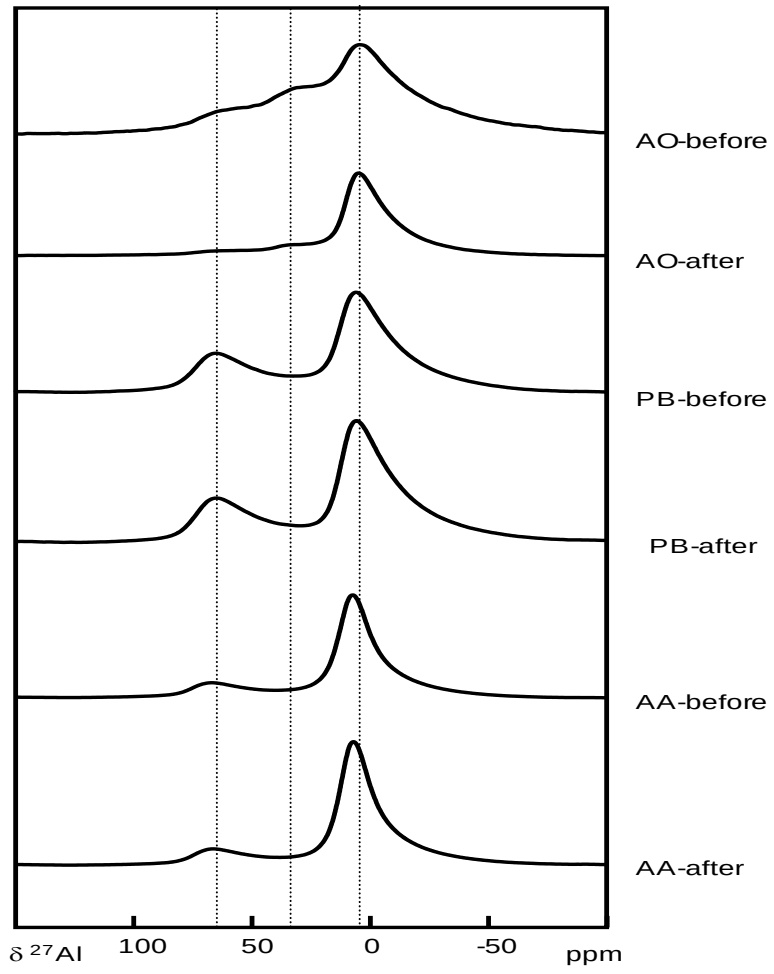


Figure 33. $^{27}$Al MAS NMR spectra recorded at room temperature for AO, psuedoboehmite (PB) and activated alumina (AA); before and after (10 mg/g) fluoride adsorption.

Figure 33 shows the $^{27}$Al NMR spectrum of AO, AA and PB before and after 10 mg/g fluoride adsorption. The spectrum for AO displayed one main signal at $\delta \sim 4.64$ and 5.01 ppm without and with fluoride, respectively. AO also showed two satellite signal peaks at $\delta \sim 31.5$ and 63.5 ppm (without F) and $\delta \sim 34.5$ and 67.0 ppm (with F). These three signals (for the two cases) were indicative of six–, five– and four–coordinate aluminium species, respectively (Akitt, 1992;

Bagshaw and Pinnaviaia, 1996; Urretavizcya *et al*., 1998). In the spectra of AA and PB, only two signals were observed. In the spectrum of AA, the signal at δ ~ 7.43 and 66.9 ppm (without F) and at δ ~ 7.31 and 66.6 ppm (with F), indicates that the six– and four–coordinated Al species were observed, respectively. In the spectrum of PB, a signal at δ ~ 6.11 and 65.4 ppm (without F) and PB at δ ~ 5.93 and 65.2 ppm (with F) also indicates that the six– and four–coordinated Al species were observed, respectively. The main signal assigned to six–coordinated Al species of AO after adsorption of fluoride shifted to δ = 5.01 ppm. Moreover, the resonance signal of AO exhibited a much broader distribution than that of AA and PB, implying that the low uniformity in chemical environment of Al species in the well–defined, regular shaped AA or PB adsorbents (Robert *et al*., 1991).

The features relevant to tetrahedral Al (~ 60 ppm), pentahedral Al (~ 30 ppm), and octahedral Al (~ 0 ppm) (Yarger *et al*., 1995; Stebbins *et al*., 2000) are revealed in the $^{27}$Al MAS NMR spectrum of AO and also amorphous $Al_2O_3$ thin film and are not consistent with the NMR patterns for crystalline alumina polymorphs (Wang *et al*., 1999; Kim *et al*., 2007). Thus, the five– and four– coordinations shown in AO are characteristic of amorphous aluminium (Sung *et al*., 2010).

### 4.4.4. Surface characterization of AO and AA based on FTIR spectroscopic technique

The FTIR spectra of the adsorbents (AO and AA) after the adsorption of 10 mg/g of fluoride are depicted in Figure 34. It shows the broad O–H stretching bands ranging from in the 3000 to 3700 $cm^{-1}$ and the absorption bands which peak at 1636 $cm^{-1}$ (Nakamoto, 1978), indicating that the solids were hydrated.

For the AO adsorbent, the broad band at 3417cm$^{-1}$ and the peak at 1636 cm$^{-1}$ could be assigned to the stretching and bending vibration of adsorbed water, and the peak at 1127 cm$^{-1}$ could be attributed to the bending vibration of hydroxyl group on metal oxides (Li *et al.*, 2010; Zhang *et al.*, 2005). After the sorption of 10 mg/g of fluoride, the bands at 3417 and 1127 cm$^{-1}$ were shifted to 3363 and 1636 cm$^{-1}$, respectively. Also, the intensity of peak at 1127cm$^{-1}$ decreased and diverged to two separate peaks at 1636 and 1450 cm$^{-1}$, which were still assigned for bending vibration of hydroxyl group of metal oxides (Zhang *et al.*, 2005). Therefore, the surface hydroxyl groups on the adsorbent were involved in the adsorption of fluoride.

It should be pointed out that the broad band at about 3417 cm$^{-1}$ was attributed to the stretching vibration of both the hydroxyl group on metal oxides and adsorbed water. Thus, the peak did not disappear after fluoride sorption, but its shape changed. This result further verified the involvement of surface hydroxyl group in the sorption of fluoride (Shubo *et al.*, 2011).

In addition, the small shoulder at 981 cm$^{-1}$ could be assigned to sulfate absorption (Serna *et al.*, 1977). The strong and broad absorption band centred at 560 cm$^{-1}$ probably resulted from the combined absorptions of sulfate, the Al–O stretching vibrations and the Al–OH wagging vibrational mode of molecular water. Therefore, the compound (AO) corresponded to a hydrated aluminum sulfate.

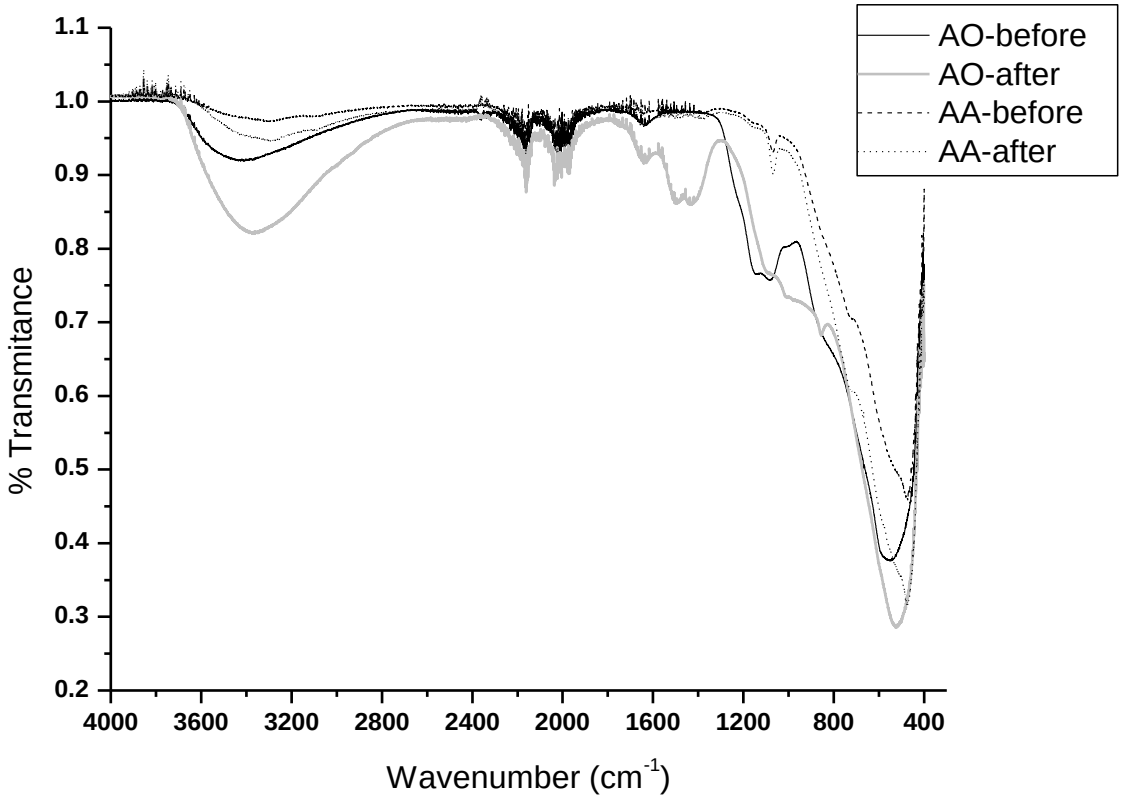


Figure 34. FTIR spectra of AO and AA before and after adsorption of 10 mg/g of fluoride.

### 4.4.5. Fluoride breakthrough in packed bed columns

The breakthrough curves for the column packed with AO, AA and PB were determined by plotting the effluent fluoride concentration against the effluent throughput volume (Figure 35). In all columns, fluoride removal was initially high, but decreases progressively over time. A pH variation of 7.0 ± 1.0 (AO), 8.0 ± 0.9 (AA) and 8.0 ± 1.0 (PB) were observed in the effluent solutions from all columns and for influent solution a pH of 8 ± 0.3 was recorded. The release of aluminium and sulfate from the aluminium hydroxide–based adsorbents is the issue concerning fluoride removal from water. The release of aluminium from AA and PB was higher than 0.2

mg/L, which is USEPA guideline for Al in drinking water. The amount of aluminium released from AA was observed to be in the range from 0.5–2.3 mg/L until fluoride breakthrough concentration (1.5 mg/L) and 0.5–1.2 mg/L for PB. However, the aluminium concentration in the effluent from AO was below 0.2 mg/L. The sulfate concentration in the effluent was also examined for AA and PB, which was found to be < 600 mg/L and < 350 mg/L, respectively, until fluoride breakthrough concentration. However, for AO the sulfate concentration was high (> 2000 mg/L), as compared with WHO test threshold level (WHO, 2011), during the first flash (< 10 eBV), but dropped immediately to a level below 550 mg/L. The adsorption capacities were calculated to be 10.6, 1.9 and 2.4 mg/g for AO, AA and PB, respectively. Thus, the adsorption capacity of AO is about 5 times higher than both AA and PB.

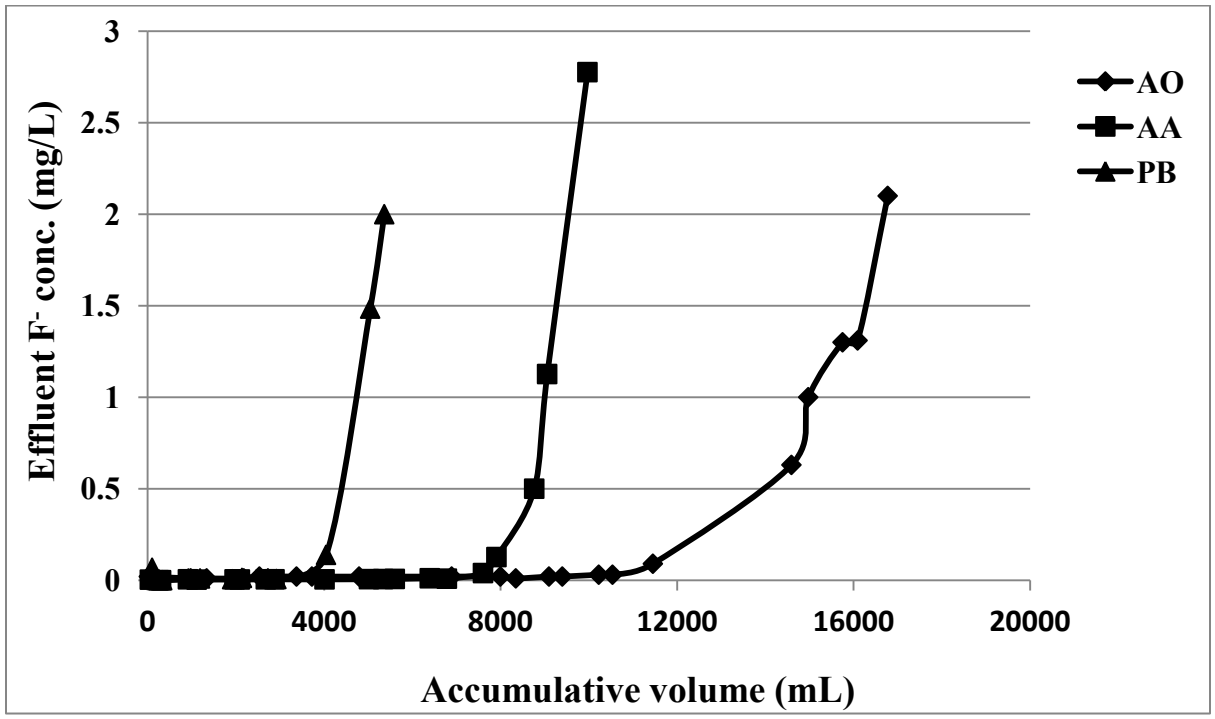


Figure 35. Fluoride breakthrough curves for AO (♦), AA (■) and PB (▲) at influent fluoride concentration (20 mg/L) and flow rate (10 eBV/day).

### 4.4.6. Regeneration potential of Al–hydroxide–based adsorbents

These columns were subjected to regeneration with sodium hydroxide, where 20% of AO was lost during the three regeneration cycles. The regenerated adsorbent, after being washed thoroughly until it is free from fluoride, were put to repeated use. It was found that there was a drastic change in capacity from 10.6 to 2.0 mg/g after the first cycle of operation. The AO adsorbent became unstable when regenerated with 0.01 M NaOH after three cycles. Further studies might need to select the best regenerant or working conditions for regenerating AO. On the other hand, the regeneration of AA and PB could not result in the loss of material and capacity for the three cycles of regeneration. However, the total fluoride capacity of AO even after three cycles was twice those of AA and PB as shown in Figure 36.

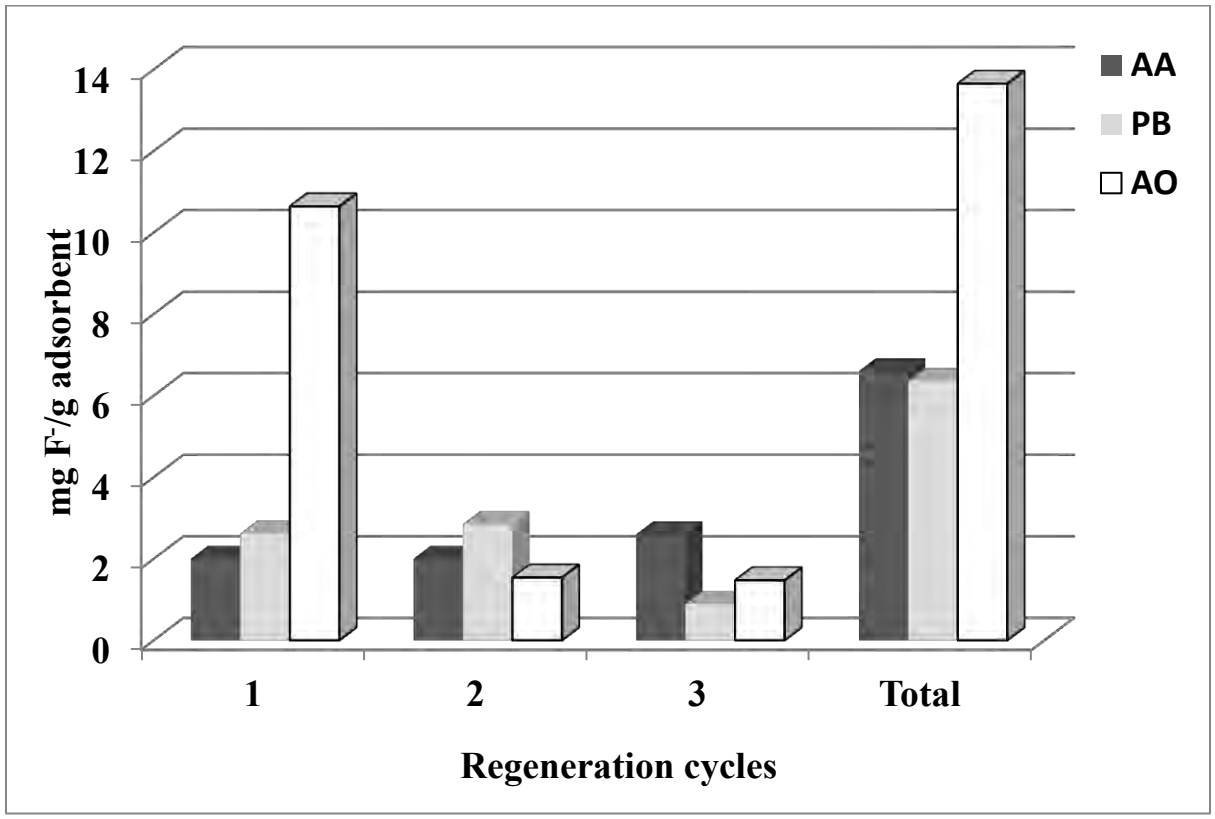


Figure 36. Repetitive performance of AO, AA and PB with regeneration between cycles.

## 4.5. Proposed structure of AO

### 4.5.1. Basaluminite

The characterization results for AO reported in section 4.1.1.; indicated that AO might be formulated as $Al(OH)_{2.7}(SO_4)_{0.1}$, which is similar to basaluminite in composition. The naturally occurring basic aluminium sulfate, basaluminite $Al_4(OH)_{10}SO_4 \cdot 5H_2O$ was first described by Hollingsworth and Bannister (1950) and more recently it was reported in sedimentary rocks in Kansas (Tien, 1967). The highly hydrated hydrobasaluminite $Al_4(OH)_{10}SO_4 \cdot 36H_2O$ which was found in moist samples reverted irreversibly to basaluminite on air–drying. Chemical analysis of basaluminite gives the composition $2Al_2O_3.SO_3.9H_2O$, which is equivalent to a formula of $Al_4SO_4(OH)_{10}.4H_2O$. It is suggested that the minerals possess a layered structure, probably containing gibbsite–like double–hydroxide layers with interlayers of sulfate ions and water molecules.

### 4.5.2. Occurrence of basaluminite

Hydrobasaluminite occurs as a reaction edge surrounding carbonate concretions, and is believed to have resulted from the neutralization of aluminium–bearing acidic sulfate solutions formed by oxidation of pyrite and subsequent leaching of clay. Basaluminite is formed as a dehydration product of hydrobasaluminite.

Amorphous basaluminite and Na-alunite were synthesized by adding 40 mL 1 M NaOH drop wise to 200 mL 0.05 M $Al_2(SO_4)_3 \cdot 16H_2O$ under constant stirring. Precipitates formed in the synthesis of amorphous basaluminite were washed immediately after precipitation.

### 4.5.3. Comparison of AO with basaluminite

The characterization results of basaluminite and AO is shown for comparison in Figure 37.

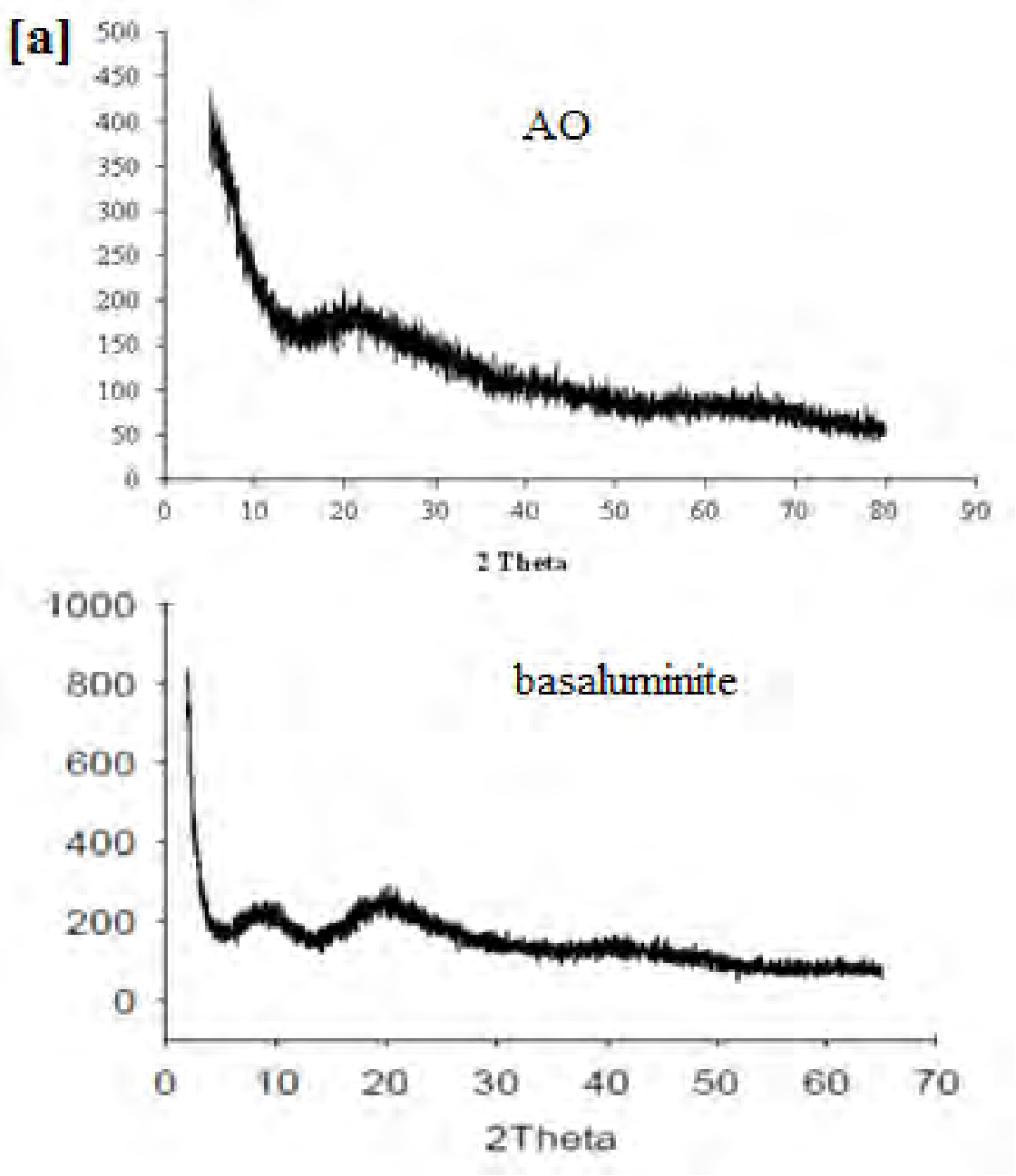

[b]

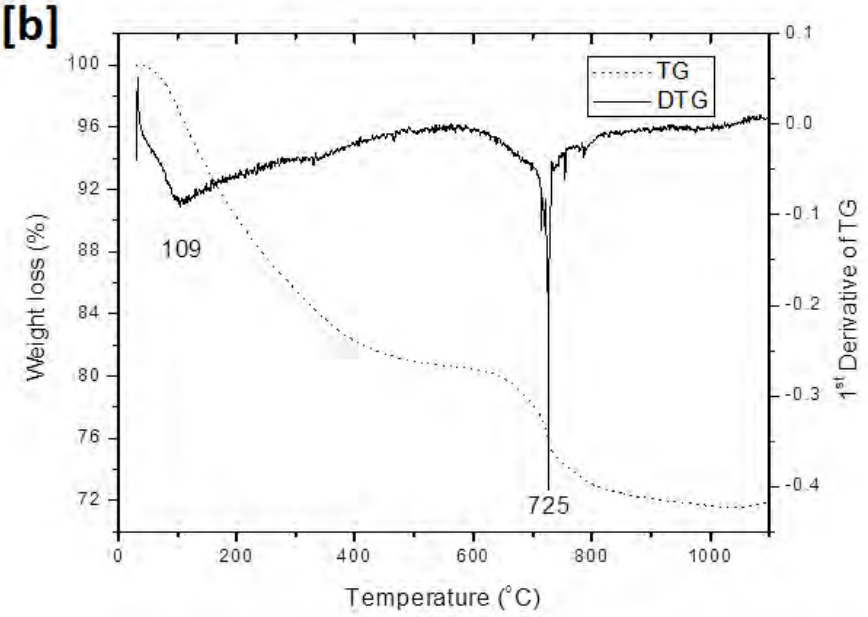
TG
DTG
Weight loss (%)
1st Derivative of TG
Temperature (°C)
109
725

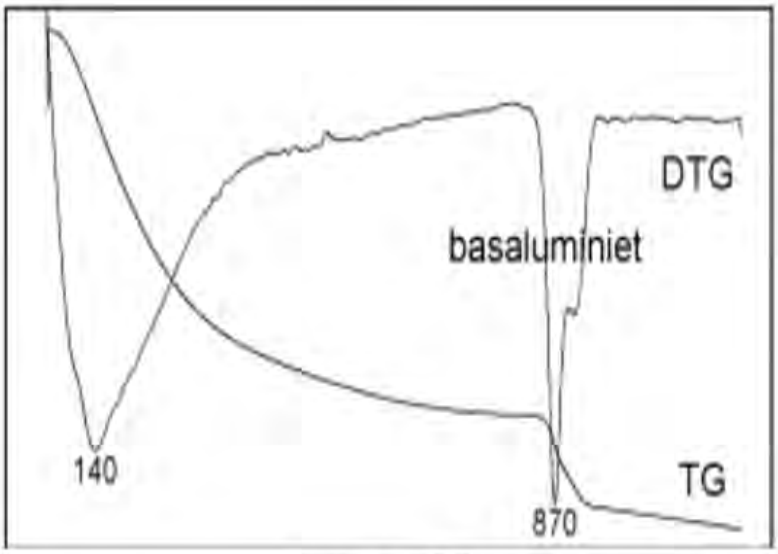
DTG
basaluminiet
TG
140
870
Temperature (°C)

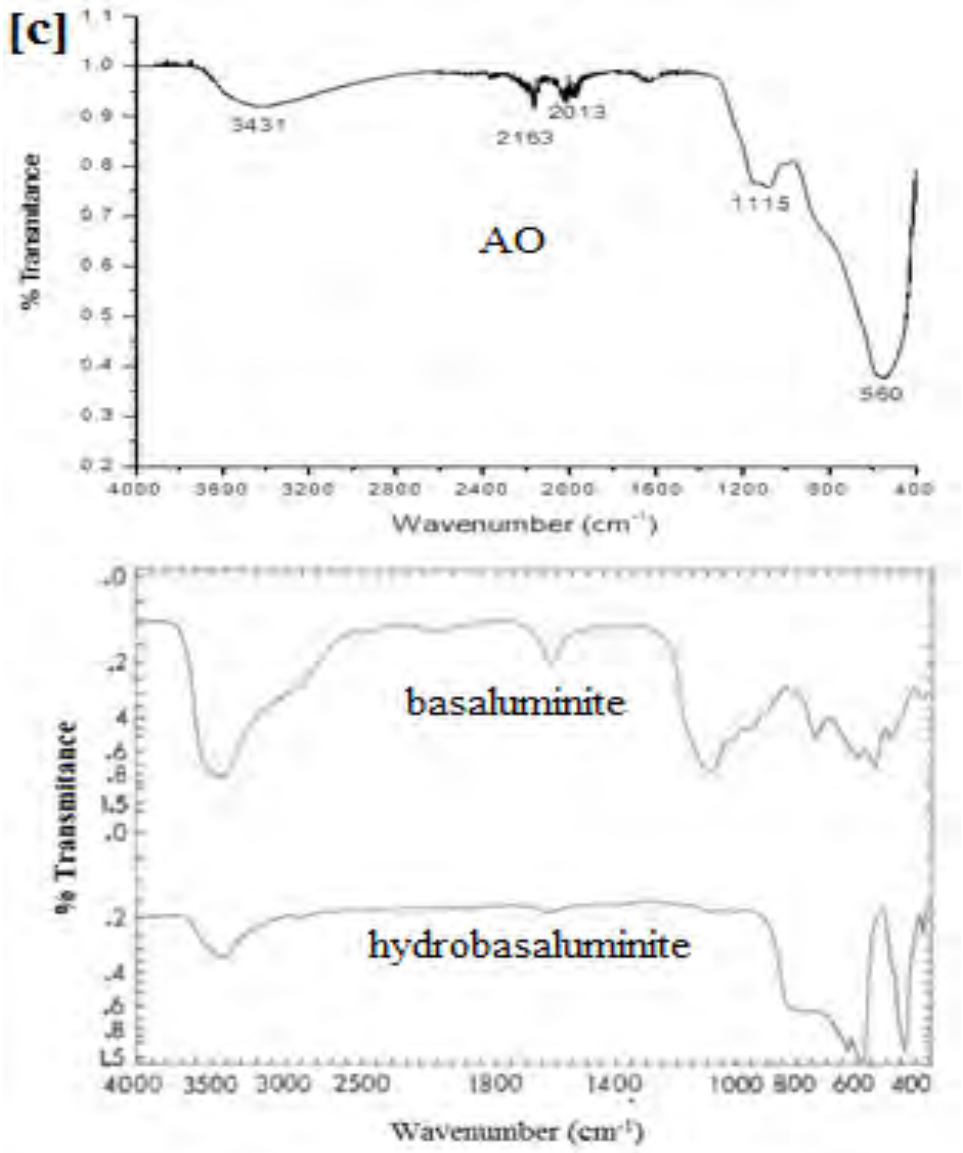


Figure 37. [a] XRD spectra of AO and basaluminite (Kim *et al.*, 2002), [b] TGA of AO and basaluminite (Kim, J.J., and Kim, S.J., 2003), and [c] FTIR spectra of AO, basaluminite and hydrobasaluminite (Tien, 1968).

X–ray diffraction analysis shows that the basaluminite consist mainly of an amorphous mineral having a broad peak (at around 9 and 20) 2Theta values (Figure 37a) with a small amount of quartz (Kim *et al.*, 2002).

From Figure 37b, AO adsorbent shows at 100–400 $^{o}$C a total weight loss of 14.87%, which corresponds to loss of water and at 725 $^{o}$C a total weight loss of 3.96%, which might be associated with the decomposition of sulfate to $SO_3$. The DTG curve of the basaluminite shows that dehydration is almost complete at about 400 °C connected with a weight loss of 25-38% (Figure 37b). The weight of basaluminite remains constant between 400 and 900 °C. The second weight loss begins approximately at 870 °C and is due to volatilization of $SO_3$ (Kim, J.J., and Kim, S.J., 2003).

From Figure 37c, basaluminite shows typical sulfate adsorption band in the regions from 580 to 670 $cm^{-1}$ and 1005 to 1200 $cm^{-1}$, which is also observed in the FTIR spectra of AO at 560 $cm^{-1}$ and 1115 $cm^{-1}$ (Tien, 1968).

### 4.5.4. Proposed chemical structure of AO adsorbent

The structural information of AO was deduced from characterization results and from spectral comparison of AO with basaluminite, which has very similar features with AO in many aspects.

The elemental composition analysis indicates that AO has $Al(OH)_{2.8}(SO_4)_{0.1}$ formula, and also characterization results (SEM, FTIR, and TGA) indicates that the AO adsorbent contain $SO_4$. $^{27}$Al NMR spectra also indicate the majority of Al is coordinated octahedrally to oxygen ($Al_6O$), and the rest involve pentahedral ($Al_5O$) and tetrahedral ($Al_4O$) coordinations.

The comparison of AO spectra with basaluminite (section 4.5.3.), clearly shows that AO is more or less similar with naturally existing basaluminite which is white in colour. Hence, the structure

of AO is most probably similar to the one shown in Figure 38. Yet, computational analysis and further characterization of AO adsorbent might be important to predict the exact structure of AO. The crystal structure of basaluminite was determined by Farkas and Pertlik, (1997) and is shown in Figure 38.

In addition, basaluminite might be used for fluoride removal as in its natural presence without any major modification or pre–treatment. Hopefully, it will have a positive impact on economics of defluoridation technologies if it maintains higher fluoride adsorption capacity as synthetic AO.

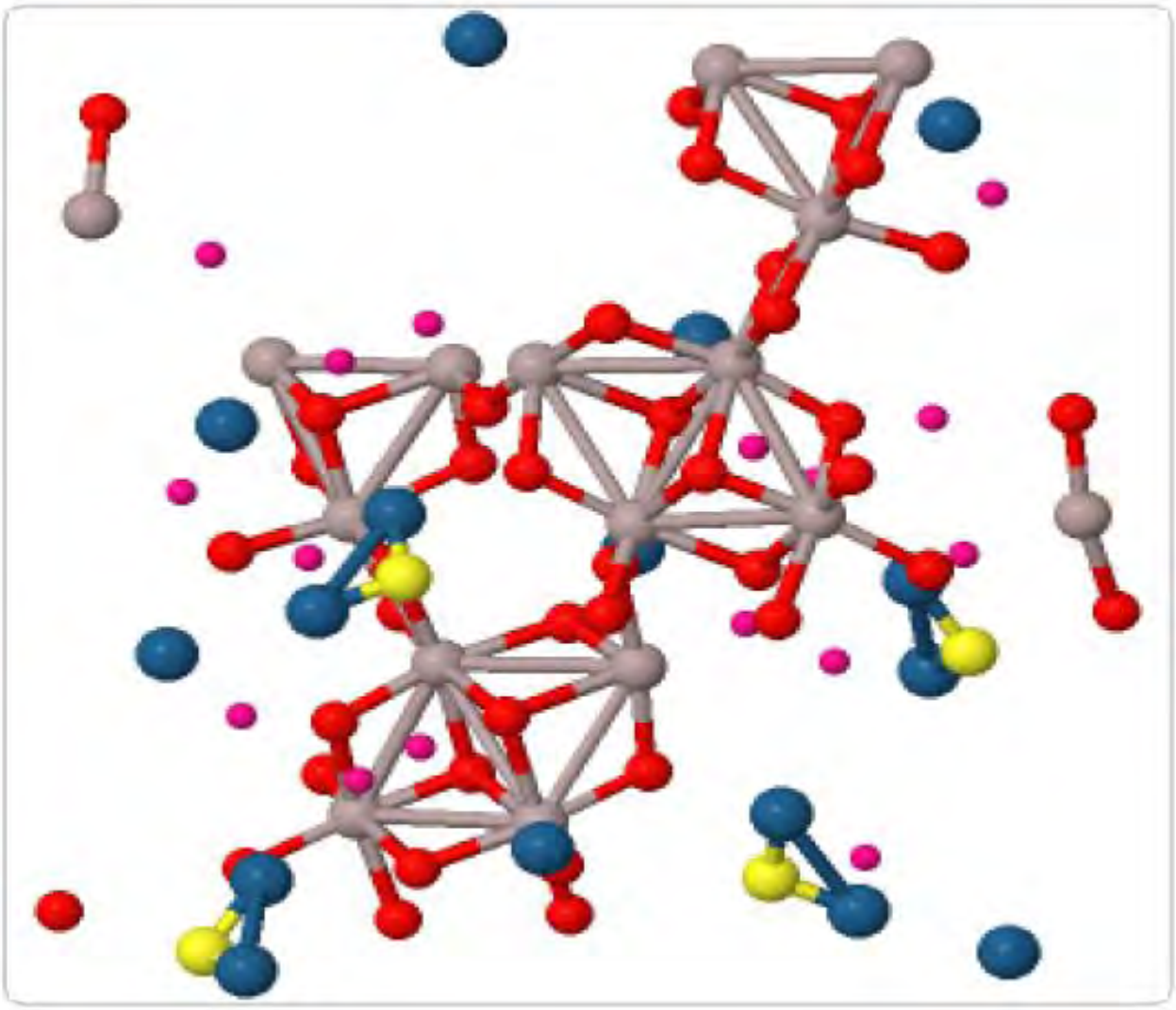

Figure 38. The crystal structure of basaluminite; grey (Al), red (O bonded with Al), yellow (S), blue (O bonded with S), pink ($H_2O$ molecule) (Farkas and Pertlik, 1997).

### 4.6. Pilot community defluoridation plant using AO in rural Ethiopia

#### 4.6.1. Performance evaluation of AO community scale defluoridation system

Fluoride in the feed water was removed from 8 to 10 mg/L to less than 0.1 mg/L. The fluoride adsorption capacities determined from the first and second field tests were 1.7 and 2.5 mg/g, respectively. The plant was functional for about three months until the fluoride content in the

treated water became 1.5 mg/L. Plant output varied between 81 and 160 $m^3$ to a fluoride breakthrough of approximately 1.5 mg/L for the two field tests, respectively.

The breakthrough curve for community pilot scale defluoridation plant is shown in Figure 39.

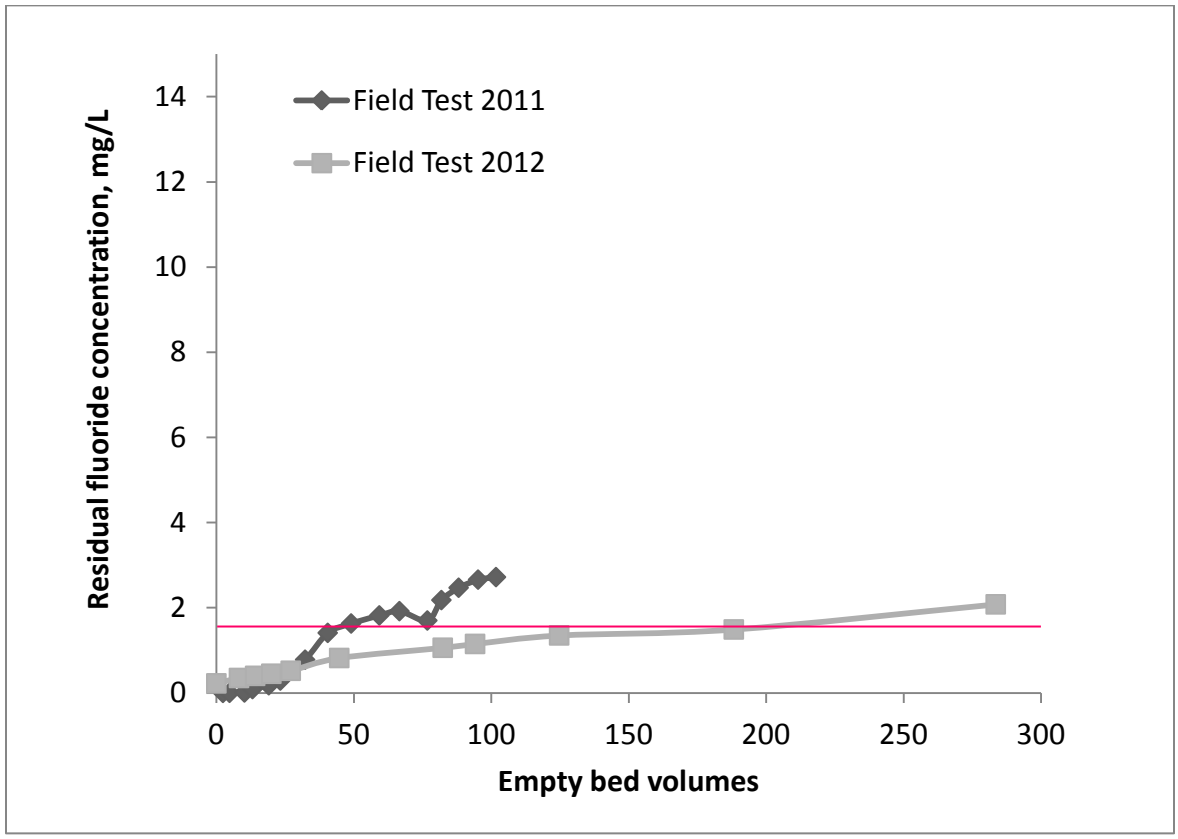


Figure 39. Breakthrough curve for field tests conducted in 2011 and 2012.

The system was considered to be simple for operation, acceptable by the society (Huber and Mosler, 2012) and less energy intensive process for fluoride removal in rural areas. No significant operational problems and complaints from the beneficiaries were experienced during operation. Spent AO media was disposed of into underground ponds away from the defluoridation plant.

The treated water quality is presented in Table 9 and it shows that the pH of raw water is on the average 8, which is mainly because of the presence of bicarbonate ions. The groundwaters in the Ethiopian Rift Valley are characterized by high amount of bicarbonate content (Tamiru, 1993). This accounts for the reduction of fluoride removal capacity of AO because of increasing pH as $HCO_3^-$ content increases. It is further interesting to note that the aluminium concentration in the treated water was higher than raw water because Al is leached from the adsorbent, but the concentration was by far less than 0.2 mg/L (USEPA, 2008). As it was observed from column experiments in the laboratory, the sulfate concentration during the first flush was about 1000 mg/L even after the washing procedure, however decreased below 600 mg/L soon after 10 eBV. The chloride concentration both in the feed and treated water was almost the same, which indicates that the presence of chloride ions does not affect the removal capacity of AO. However, the silicon concentrations from the raw to treated water diminished from ~ 30 to ~ 3 mg/L, indicating the adsorption of Si onto AO with a possible reduction in the fluoride adsorption capacity.

Table 9. Average water quality characteristics of groundwater and treated water before the fluoride concentration reaches 2.0 mg/L.

| Constituents | Raw water (mg/L) | Treated water (mg/L) |
|---|---|---|
| Fluoride | 8.1–10.1 | 0.01–2.18 |
| Sulfate | 7.1–9.5 | 69.1–1006 |
| Chloride | 63.4–67.7 | 61.9–68.2 |
| Aluminium | $(4.9–18.2) \times 10^{-3}$ | $(12.8–59.4) \times 10^{-3}$ |
| Sodium | 278–296 | 283–336 |
| Iron | 1.77–2.56 | 1.85–2.62 |
| Calcium | 29.5–33.1 | 22.3–71.5 |
| Silicon | 29.7–30.8 | 1.7–4.4 |
| Magnesium | 6.8–7.3 | 5.9–9.2 |
| Arsenic | $(1.3–5.1) \times 10^{-3}$ | $(0.2–0.4) \times 10^{-3}$ |
| Uranium | $(1.3–1.8) \times 10^{-3}$ | $(0.1–0.3) \times 10^{-3}$ |
| Selenium | $(2.9–5.1) \times 10^{-3}$ | $(0.1–0.8) \times 10^{-3}$ |
| pH | 7.84–8.23 | 6.68–8.30 |
| EC (µs/cm) | 1670–1850 | 1670–2680 |

### 4.6.2. Evaluation of the potential of AO for uptake of other contaminant ions

It was also observed that the AO has a potential to remove other contaminants such as arsenic, uranium, and selenium. Even though, the concentrations of these contaminants in the groundwater were below the WHO guideline values (WHO, 2011), the adsorbent reduced the concentrations far below their initial concentrations (Figure 40).

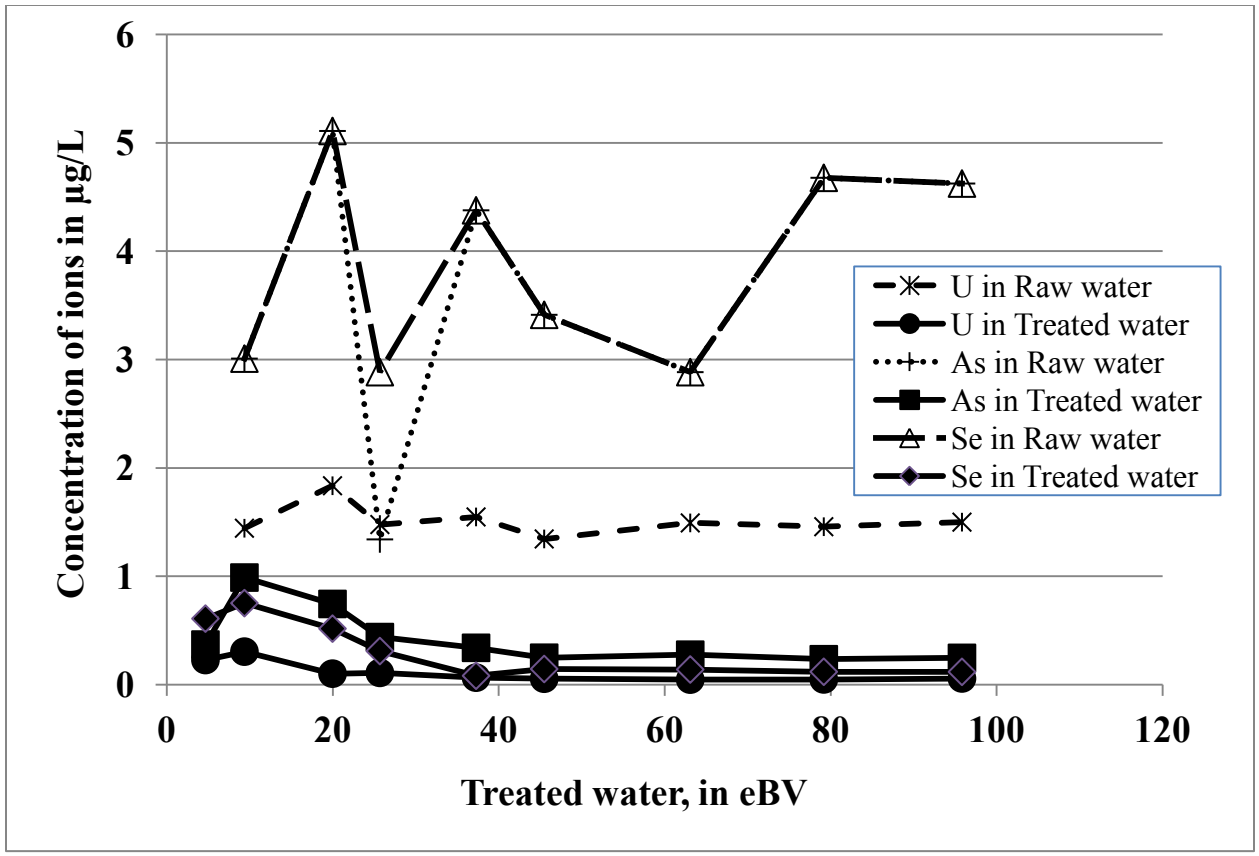


Figure 40. Potential of AO for uptake of other contaminants (As, U and Se).

### 4.6.3. Estimated capital and operational cost for AO community defluoridation pilot plant

The estimated capital and operational costs for one set of field tests are summarised in Table 10. The estimation for operational cost was based on the raw water fluoride concentration (9 mg/L), fluoride adsorption capacity of AO (2.5 mg/g) and consumption rate (1200 L/day). The AO community system utilized ~ 420 kg of AO and produced ~ 117 $m^3$ of treated water until effluent concentration was 1.5 mg/L. The system life span of the system was about three months. Therefore, the capital and operational costs of the 1200 L/day defluoridation plant is estimated at approximately Birr 161,987 (9700 USD) and Birr 220 (13 USD) per $m^3$ of treated water, respectively (2011 foreign exchange rate).

Table 10. Capital and operational costs for AO community defluoridation systems.

| Type of cost | | Ethiopian Birr | US Dollar |
|---|---|---|---|
| Capital | Construction | 96,787 | 5,796 |
| | Machineries and materials | 65,200 | 3,904 |
| Operational | For treatment of 117 $m^3$ of water | 13,944 | 835 |
| | Man power | 11,700 | 701 |
| | Total | 187,631 | 11,236 |

# Chapter 5

## 5. Conclusions

This work has shown the possible processes underlying the high fluoride uptake capacity of AO and has shown the potential and the limitations of AO for fluoride removal in the field. The AO adsorbent has the potential to be more effective for fluoride removal from groundwater than the widely used aluminium hydroxide–based adsorbents. The AO adsorbent, which was synthesized at an OH:Al ratio of 2.7 excelled in removing fluoride ions, as compared to other aluminium hydroxide–based adsorbents, as it possesses higher acidity and surface site concentrations. This is mainly because of optimum amount of sulfate associated with aluminium. Thus, high surface area and $Al_2O_3$ composition do not ensure better fluoride removal performance for aluminium hydroxide–based adsorbents. The chemical formula of AO could be formulated as $Al(OH)_{2.8}(SO_4)_{0.1}$, which is similar to naturally occurring mineral called basaluminite $[Al_4(OH)_{10}SO_4 \cdot xH_2O]$. Thus, the proposed structure for AO has much similarity with the crystal structure of basaluminite. XRD analysis of AO could not identify any crystalline structures and showed AO to be an amorphous compound. Representative low–magnification SEM images of AO indicate the presence of nanoparticles. The PZC of AO (9.57) is relatively high and hence facilitates fluoride adsorption through the electrostatic attraction between fluoride and adsorbent below its PZC.

The AOMO material appears dark brownish (brown–black) in colour since it consists of Mn and Fe as manganese and iron oxides. The TGA curve for AOMO indicates the formation and transformation of different forms of manganese and aluminium oxides; and later confirmed by the XRD investigation that AOMO constitutes poorly crystalline $MnO_2$ and $Al_2O_3$ phases. The

X–ray diffraction (XRD) pattern of nano–AlOOH showed high crystalline order of the synthesized compound, which is consistent and matched with XRD results of micro–sized AlOOH synthesized by other researches. The TGA also indicates the transformation of AlOOH into $Al_2O_3$. The characterization results for AA and PB were obtained from literature and showed that both constitute high proportion of $Al_2O_3$. It is also reported that these adsorbents had higher surface area (> 250 mg/g).

Batch studies for adsorption of fluoride onto those aluminium hydroxide–based adsorbents showed that AO possessed the upper hand in terms of fluoride removal efficiency. The presence of bicarbonate ion in the untreated water and the pH dependence of the process might be considered as limitation of this technology.

The AOMO was found to be very efficient in removing fluoride in a pH range of 5 to 7. Although all the studied isotherm and kinetics models showed fairly good fit to the experimental data, but the Freundlich isotherm and second order kinetics was found to be the best representative for fluoride adsorption on AOMO adsorbent. Besides, it was observed that the determination of the isotherm and kinetics parameters by non–linear methods was found to give more representative characteristics of adsorption than their linearized counter–parts. Nano–AlOOH has considerable potential for the removal of excess fluoride from aqueous solution. For a given initial fluoride concentration, the fluoride removal efficiency of the adsorbent increased with increasing adsorbent dose. Adsorption of fluoride is very rapid in the first 30 min and then increases slowly to reach pseudo–equilibrium. Initial concentrations of fluoride were found to affect the defluoridation efficiency of the adsorbent. High fluoride removal occurred between pH

6 to 8, and appreciable amount of fluoride was removed around pH 7.0. The Langmuir isotherm model was in good agreement with the experimental data, and the maximum adsorption capacities; $q_m$ of the adsorbent was 62.50 mg/g. The D–R model gave adsorption energy of 13.15 kJ/mol, which indicated the fluoride removal by nano–AlOOH involved a chemisorption process. The adsorption kinetics was well described by a pseudo–second order model.

The two adsorbents (AOMO and nano–AlOOH) have the potential to be implemented at a community scale in batch and continuous modes, respectively. Therefore, further studies are required to examine the performance of each adsorbent in their respective mode, either as prepared or after being coating onto a high surface area support media.

The solubility curve and $^{27}Al$ NMR spectrum for AO are indicative of the formation for amorphous aluminium hydroxide. In addition, the $^{27}Al$ NMR spectrum of AO showed the presence of six–, five– and four–coordinated aluminium species.

The continuous experiments indicate that it is necessary to control flow rate because of kinetic limitations. Moreover, the use of a post–treatment column containing calcite ($CaCO_3$) neutralizes pH and controls both aluminium and sulfate concentrations in the treated water. This approach enables us to use directly an acid adsorbent while maintaining the high fluoride adsorption capacity.

The release of aluminium from AA and PB and sulfate from AO adsorbents needs much more attention to ensure the quality of treated water. The adsorption capacity of AO is about 5 times

higher than those of AA and PB. The regeneration experiment with NaOH showed that AO exhibited a reduction in weight loss and adsorption capacity. Therefore, further studies might be needed to select the best regenerating agent or working conditions for regenerating AO.

The results have encouraged us to test the technology in small communities in the Ethiopian Rift Valley. Since the technology could be more economical for relatively low fluoride containing groundwater as the life time of the adsorption bed becomes longer. In addition, the local availability of the raw material might be an advantage to sustain the technology. The possibility to produce AO at a large scale also appears to be simple in terms of equipment, procedure and local availability of materials.

From the field tests that were conducted in rural Ethiopia, the fluoride level was reduced from 8 to 10 mg/L to less than 0.1 mg/L and this system was considered to be a simple operation, acceptable by the society and less energy intensive process. It was also observed that the AO has a potential to remove other contaminants such as arsenic, uranium, and selenium. The capital and operational costs of the 1200 L/day defluoridation plant was estimated at approximately Birr 161,987 (9700 USD) and Birr 220 (13 USD) per $m^3$ of treated water, respectively (2011 foreign exchange rate).

Although there are many materials tested for fluoride removal, their potential application at the grassroots level is very limited in areas where drinking water is heavily loaded with fluoride. Hence, this system might be an alternative defluoridation technology that would be implemented in rural communities, where the fluoride concentration is excessively high.

## References


Abe, I., Iwasaki, S., Tokimoto, T., Kawasaki, N., Nakamura, T., Tanada, S., 2004. Adsorption of fluoride ions onto carbonaceous materials. Journal of Colloid and Interface Science 275, 35–39.

Adhikary, S.K., Tipnis, U.K., Harkare, W.P., Govindan, K.P., 1989. Defluoridation during desalination of brackish water by electrodialysis. Desalination 71, 301–312.

Agarwal, M., Rai, K., Shrivastav, R., Dass, S., 2003. Defluoridation of water using amended clay. Journal of Cleaner Production 11, 439–444.

Akitt, J.W., 1992. NMR and chemistry: An introduction to modern NMR spectroscopy. 3rd ed., Chapman and Hall/Methuen, New York.

Alemu, S., Mulugeta, E., Zewge, F., Candravanshi, B.S., 2014. Water defluoridation by aluminium oxide–manganese oxide composite material. Journal of Environmental Technology 35, 1893–1903.

Amini, M., Mueller, K., Abbaspour, K.C., Rosenberg, T., Afyuni, M., Moller, K.N., Sarr, M., Johnson, A., 2008. Statistical modeling of global geogenic fluoride contamination in ground waters. Journal of Environmental Science and Technology 42, 3662–3668.

Ando, M., Tadano, M., Yamamoto, S., Tamura, K., Asanuma, S., Watanabe, T., Kondo, T., Sakurai, S., Ji, R.D., Liang, C., Chen, X.Q., Hong, Z., Cao, S., 2001. Health effects of fluoride pollution caused by coal burning. Science of the Total Environment 271, 107–116.

Ayoob, S., Gupta, A.K., 2006. Fluoride in drinking waters: a review on the status and stress effects. Critical Reviews in Environmental Science and Technology 36, 433–487.

Ayoob, S., Gupta, A.K., Bhat, V.T., 2008. A conceptual overview on sustainable technologies for defluoridation of drinking water and removal mechanisms. Critical Reviews in Environmental Science and Technology 38, 401–470.

Badillo–Almaraz, V.E., Flores, J.A., Arriola, H., Lopez, F.A., Ruiz–Ramirez, L., 2007. Elimination of fluoride ions in water for human consumption using hydroxyapatite as an adsorbent. Journal of Radioanalytical and Nuclear Chemistry 271, 741–744.

Bagshaw, S.A., Pinnaviaia, T.J., 1996. Mesoporous alumina molecular sieves. Angewandte Chemie International Edition in English 35, 1102–1105.

Bahena, J.L.R., Cabrera, A.R., Valdivieso, A.L., Urbina, R.H., 2002. Fluoride adsorption onto α–$Al_2O_3$ and its effect on the zeta potential at the alumina–aqueous electrolyte interface. Separation Science and Technology 37, 1973–1987.

Barbier, B., Mazounie, P., 1984. Flouride removal methods–filtration through activated alumina. Recommended technique, Water Supply 2, 5581–5582.

Beiding, W.A., Emerson, R.B., Williams, R.L., 1973. Agglomerating partially dehydrated gel–derived pseudoboehmitic alumina to form strong porous spheres. United State United States Kaiser Aluminium and Chemical Corporation (Oakland, CA), Patent No. 3714313. Available at http://www.freepatentsonline.com/3714313.html.

Bhargava, D.S., Killedar, D.J., 1992. Fluoride adsorption on fishbone charcoal through moving media adsorber. Water Research 26, 781–788.

Bhatnagar, A., Kumar, E., Sillanpaa, M., 2011. Fluoride removal from water by adsorption–A review. Chemical Engineering Journal 171, 811–840.

Bi, S., Wang, C., Cao, Q., Zhang, C., 2004. Studies on the mechanism of hydrolysis and polymerization of aluminium salts in aqueous solution: Correlations between the "Core–

links" model and "Cagelike" Keggin–$Al_{13}$ model. Coordination Chemistry Reviews 248, 441–445.

Biswas, K., Saha, S.K., Ghosh, U.C., 2007. Adsorption of fluoride from aqueous solution by a synthetic iron(III)–aluminium(III) mixed oxide. Industrial and Engineering Chemistry Research 46, 5346–5356.

Bjorvatn, K., Bardsen, A., Tekle–Haimanot, R., 1996. Defluoridation of drinking water by the use of clay/soil. In: Dahi, E., Bregnhoj, H., (eds). Proceedings of the 1st International Workshop on Fluorosis and Defluoridation of Water. International Society for Fluoride Research, Auckland, pp 40–45.

Bourikas, K., Vakros, J., Kordulis, Ch., Lycourghiotis, A., 2003. Potentiometric mass titrations: experimental and theoretical establishment of a new technique for determining the point of zero charge (PZC) of metal (hydr)oxides. Journal of Physical Chemistry 107, 9441–9451.

Brunson, L.R., Sabatini, D.A., 2009. An evaluation of fish bone char as an appropriate arsenic and fluoride removal technology for emerging regions. Environmental Engineering Science 26, 1777–1784.

Bulusu, K.R. Nawalakhe, W.G., 1990. Defluoridation of water with activated alumina in continuous contacting system. Indian Journal of Environmental Health 32, 197–218.

Bulusu, K.R., Sunderasan, B.B. Pathak, B.N., Nawlakhe, W.G., Kulkarni, D.N., Thergaonkar, V.P.J., 1979. Fluorides in water, defluoridation methods and their limitations. Journal of Institute Engineering (India)–Environmental Engineering Division, 60, 1–25.

Buxton, H.T., Shernoff, P.K., 1999. Groundwater resources of Kings and Queens counties, Long Island, New York United States America Geological Survey Water supply, Paper No. 2498, New York, USA.

Carrier, X., Marceau, E., Jean–François, L., Che, M., 2007. Transformations of γ–alumina in aqueous suspensions; alumina chemical weathering studied as a function of pH. Journal of Colloid and Interface Science 308, 429–437.

Cengeloglu Y., Kir, E., Ersoz, M., 2002. Removal of fluoride from aqueous solution by using red mud. Separation and Purification Technology 28, 81–86.

Chaturvedi, A.K., Yadava, K.P., Pathak, K.C., Singh, V.N., 1990. Defluoridation of water by adsorption on fly ash. Water Air and Soil Pollution 49, 51–61.

Chikuma, M., Nishimura, M., 1990. Selective sorption of fluoride ion by anion exchange resin modified with alizarin fluorine blue–praseodymium(III) complex. Reactive Polymers 13, 131–138.

Christoffersen, J., Christoffersen, M.R., Larsen, R., Moller, I.J., 1991. Regeneration by surface–coating of bone char used for defluoridation of water. Water Research 25, 227–229.

Chubar, N.I., Samanidou, V.F., Kouts, V.S., Gallios, G.G., Kanibolotsky, V.A., Strelko, V.V., Zhuravlev, I.Z., 2005. Adsorption of fluoride, chloride, bromide, and bromate ions on a novel ion exchanger. Journal of Colloid and Interface Science 291, 67–74.

Clifford, D.A., 1990. Ion exchange and inorganic adsorption in water quality and treatment. Water Quality and Treatment, 4th ed., Pontius, FW, McGraw–Hill Publication, pp 522.

Coetzee, P.P., Coetzee, L.L., Puka, R., Mubenga, S., 2003. Characterisation of selected South African clays for defluoridation of natural waters. Water South Africa 29, 331–338.

COWI, 1998. Review of practical experiences with defluoridation in rural water supply programmes Part II. Minsistry of Foreign Affairs, Danida: Copenhagen, pp 73.

Crapper, D.R., Krishnan, S.S., Dalton, A.J., 1973. Brain aluminium distribution in Alzheimer disease and experimental neurofibrillary degeneration. Science 180, 511–513.

Dahi, E., Mtalo, F., Njau, B., Bregnhoj, H., 1996. Defluoridation using the Nalgonda technique in Tanzania. Paper presented at 22nd WEDC conference, New Delhi, India.

Davison, A.M., Oli, H., Walker, G.S., Lewins, A.M., 1982. Water supply aluminium concentration, dialysis dementia, and effect of reverse–osmosis water treatment. Lancet 320, 785–787.

Dissanayake, C.B., 1991. The fluoride problem in the groundwater of Sri Lanka environmental management and health. International Journal of Environmental Studies 38, 137–155.

Edmunds, M., Smedley, P., 2005. Fluoride in natural waters. In: essentials of medical geology, impacts of natural environment on public health; Selinus, et al., Eds. Elsevier Academic Press: London, pp 301–329.

Fan, X., Parker, D.J., Smith, M.D., 2003. Adsorption kinetics of fluoride on low cost materials. Water Research 37, 4929–4937.

Farkas, L., Pertlik, F., 1997. Crystal structure determinations of felsobanyaite and basaluminite, $Al_4(SO_4)(OH)_{10}{\cdot}4H_2O$. Acta Mineralogica Petrographica 38, 5–15.

Farrah, H., Slavek, J., Pickering, W.F., 1987. Fluoride interactions with hydrous aluminium oxides and alumina. Australian Journal of Soil Research 25, 55–69.

Feleke, Z., Bekele, A., 2000. Alem Tena Catholic Church Defluoridation Pilot Study, Final Report, Ethiopia, pp 1–50.

Fink, G.J., Lindsay, F.K., 1936. Activated alumina for removing fluorides from drinking water. Industrial and Engineering Chemistry 28, 947–948.

Foo, K.Y., Hameed, B.H., 2010. Insights into the modeling of adsorption isotherm systems. Chemical Engineering Journal 156, 2–10.

Garmes, H., Persin, F., Sadeaur, J., Pourcelly, G., Mountadar, M., 2002. Defluoridation of growndwater by a hybrid process combining adsorption and Donnan dialysis. Desalination 145, 287–291.

Ghorai, S., Pant, K.K., 2004. Investigations on the column performance of fluoride adsorption by activated alumina in a fixed–bed. Chemical Engineering Journal 98, 165–173.

Ghorai, S., Pant, K.K., 2005. Equilibrium, kinetics and breakthrough studies for adsorption of fluoride on activated alumina. Separation and Purification Technology 42, 265–271.

Gogoi, P.K., Baruah, R., 2008. Fluoride removal from water by adsorption on acid activated kaolinite clay. Indian Journal of Chemical Technology 15, 500–503.

Gran, G., 1952. Determination of the equivalence point in potentiometric titrations Part II. Analyst 77, 661–671.

Gupta, A.K., Deva, D., Sharma, A., Verma, N., 2009. Adsorptive removal of fluoride by micro–nanohierarchal web of activated carbon fibers. Industrial and Engineering Chemistry Research 48, 9697–9707.

Hamilton, W.R., Wolley, A.R., Bishop, A.C., 1982. The country life guide to minerals, rocks and fossils. Country Life Books, tenth edition, Spain.

Handa, B.K., 1975. Geochemistry and genesis of fluoride–containing groundwaters in India. Ground Water 13, 275–281.

Hao, O.J., Huang, C.P., 1986. Adsorption characteristics of fluoride onto hydrous alumina. Journal of Environmental Engineering 112, 1054–1069.

Haron, M.J., Wan Yunus, W.M.Z., Wasay, S.A., 1995. Sorption of fluoride ions from aqueous solutions by a yttrium–loaded poly(hydroxamic acid) resin. International Journal of Environmental Studies 48, 245–255.

Hichour, M., Persin, F., Sandeaux, J., Gavach, C., 2000. Fluoride removal from waters by Donnan dialysis. Separation and Purification Technology 18, 1–11.

Ho, Y.S., Wang, C.C., 2004. Pseudo–isotherms for the sorption of cadmium ion onto tree fern. Proceedings of Biochemistry 39, 761–765.

Huang, C.J., Liu, J.C., 1999. Precipitate flotation of fluoride–containing wastewater from a semiconductor manufacturer. Water Research 33, 3403–3412.

Huber, A.C., Mosler, H., 2012. Determining behavioural factors for interventions to increase safe water consumption: A cross–sectional field study in rural Ethiopia. International Journal of Environmental Health Research 23, 1–12.

Hudak, P.F., 1999. Fluoride levels in Texas groundwater. Journal of Environmental Science and Health A34, 1659–1676.

Islam, M., Patel, R.K., 2007. Evaluation of fluoride removal efficiency of fluoride from aqueous solution using quick lime. Journal of Hazardous Material 143, 303–310.

Jacobsen, P., Dahi, E., 1997. Low cost domestic defluoridation of drinking water by means of locally charred bone. In: Dahi, E., and Neilsen, J.M. (eds). Proceedings of the 2nd international workshop on fluorosis and defluoridation of water, Addis Ababa, Ethiopia Novmber, 19–22.

Jaffery, F.N., Srivastava, A.K., Shaw, A., Viswanathan, P.N., Seth, P.K., 1998. Impact of nutrition on fluorosis. Industrial Toxicology Research Centre (ITRC): Lucknow, India, pp 86.

Jagtap, S., Yenkie, M.K., Labhsetwar, N., Rayalu, S., 2012. Fluoride in drinking water and defluoridation of water. Chemical Reviews 112, 2454–2466.

Jain, S., Jayaram, R.V., 2009. Removal of fluoride from contaminated drinking water using unmodified and aluminium hydroxide impregnated blue lime stone waste. Separation Science and Technology 44, 1436–1451.

Janardhana, C., Nageswara Rao, G., Sai Sathish, R., Sunil Kumar, P., Anil Kumar, V., Vijay Madhav, M., 2007. Study on defluoridation of drinking water using zirconium ion impregnated activated charcoals, Indian Journal of Chemical Technology 14, 350–354.

Johnson, A., Osterwalder, L., Zewge, F., Rohner, R., Mutheki, P.M., Samuel, E., 2011. Introducing fluoride removal filters to Ethiopia. Sandec News 12 / 2011. Available at http://www.eawag.ch/forschung/sandec/publikationen/ws/dl/SN12_Fluoride_Ethiopia.pdf.

Kamble, S.P., Deshpande, G., Barve, P.P., Rayalu, S., Labhsetwar, N.K., Malyshew, A., Kulkarni, B.D., 2010. Adsorption of fluoride from aqueous solution by alumina of alkoxide nature: Batch and continuous operation. Desalination 264, 15–23.

Kim, H.J., Lee, H.C., Lee, J.S., 2007. $^{27}$Al triple–quantum magic–angle spinning nuclear magnetic resonance characterization of nanostructured alumina materials. Journal of Physical Chemistry 111C, 1579–1583.

Kim, J.J., Kim, S.J., 2003. Environmental, mineralogical, and genetic characterization of ochreous and white precipitates from acid mine drainages in Taebaeg, Korea. Journal of Environmental Science and Technology 37, 2120–2126.

Kim, J.J., Kim, S.J., Tazaki, K., 2002. Mineralogical characterization of microbial ferrihydrite and schwertmannite, and non-biogenic Al-sulfate precipitates from acid mine drainage in the Donghae mine area, Korea. Journal of Environmental Geology 42, 19–31.

Kloos, H., Tekle–Haimanot, R., 1999. Distribution of fluoride and fluorosis in Ethiopia and prospects for control. Tropical Medicine and International Health 4, 355–364.

Koritnig, S., 1951. A Contribution of geochemistry of fluorine. Geochimica et Cosmochimica Acta 1, 89–116.

Ku, Y., Chiou, H.M., Wang, W., 2002. The removal of fluoride ion from aqueous solution by a cation synthetic resin. Separation Science and Technology 37, 89–103.

Kumar, E., Bhatnagar, A., Kumar, U., Sillanpaa, M., 2011. Defluoridation from aqueous solutions by nano–alumina: Characterization and sorption studies. Journal of Hazardous Material 186, 1042–1049.

Kummert, R., 1979. The surface complexation of organic acids with gamma–alumina and its importance for natural waters. Thesis ETH No. 6371, Swiss Federal Institute of Science and Technology, Zurich, Switzerland.

Larsen, M.J., Pearce, E.I.F., Ravnholt, G., 1994. The effectiveness of bone char in the defluoridation of water in relation to its crystallinity, carbon content and dissolution pattern. Arches Oral Biology 39, 807–816.

Letterman, R.D., Asolekar, S.R., 1990. Surface ionization of polynuclear species in Al(III) hydrolysis, I: titration results. Water Research 24, 931–939.

Lhassani, A., Rumeau, M., Benjelloun, D., Pontie, M., 2001. Selective demineralization of water by nanofilteration application to the defluoridation of brackish water. Water Research 35, 3260–3264.

Li, Y.H., Wang, S., Cao, A., Zhao, D., Zhang, X., Xu, C., Luan, Z., Ruan, D., Liang, J., Wu, D., Wei, B., 2001. Adsorption of fluoride from water by amorphous alumina supported on carbon nanotubes. Chemical Physics Letter 350, 412–416.

Lopez, M., Coca, J., Rosal, R., Garcia, R., Sastre, H., 1992. Modeling and experimental behavior of multicomponent anion–exchange with amberlite IRA–410. Hungarian Journal of Industrial Chemistry 20, 109–112.

Lounici, L., Adour, D., Belhocine, A., Elmidaoni, B., Barion, N.M., 2001. Novel technique to regenerate activated alumina bed saturated by fluoride ions. Chemical Engineering Journal 81, 153–160.

Luo F., Inoue K., 2004. The removal of fluoride ion by using metal(III)–loaded amberlite resins. Solvent Extraction and Ion Exchange 22, 305–322.

Lyengar, L., 1996. Technologies for fluoride removal. Available at http://www.samsamwater.com/library/TP40_22_Technologies_for_fluoride_removal.pdf.

Ma, Y., Wang, S.G., Fan, M., Gong, W.X., Gao, B.Y., 2009. Characteristics and defluoridation performance of granular activated carbons coated with manganese oxides. Journal of Hazardous Material 168, 1140–1146.

Ma, Y.X., Shi, F.M., Zheng, X.L., Ma, J., Yuan, J.M., 2005. Preparation of granular Zr–loaded bentonite and its defluoridation properties from aqueous solutions. Journal Harbin Institute of Technology (New Series) 12, 236–240.

MacKenzie, K.J.D., Snith, M.E., 2002. Multinuclear solid–state NMR of inorganic materials. Pergamon Press, New York.

Mahramanlioglu, M., Kizilcikli, I., Bicer, I.O., 2002. Adsorption of fluoride from aqueous solution by acid treated spent bleaching earth. Journal of Fluorine Chemistry 115, 41–47.

Maliyekkal, S.M., Sharma, A.K., Philipet, L., 2006. Manganese–oxide–coated alumina: A promising sorbent for defluoridation of water. Water Research 40, 3497–3506.

Maliyekkal, S.M., Shukla, S., Philip, L., Indumathi, M.N., 2008. Enhanced fluoride removal from drinking water by magnesia–amended activated alumina granules. Chemical Engineering Journal 140, 183–192.

Martyn, C.N., Barker, D.J.P., Osmond, C., Harris, E.C., Edwardson, J.A., Lacey, R.F., 1989. Geographical relation between Alzheimer's disease and aluminium in drinking water. Lancet 1, 59–62.

Meenakshi, Maheshwari, R.C., 2006. Fluoride in drinking water and its removal. Journal of Hazardous Material 137, 456–463.

Meenakshi, S., Viswanathan, N., 2007. Identification of selective ion–exchange resin for fluoride sorption. Journal of Colloid and Interface Science 308, 438–450.

Miller, R.G., Kopfler, F.C., Kelty, K.C., Stobler, J.A., Ulmer, N.S., 1984. The occurrence of aluminium in drinking water. Journal of American Water Works Association 76, 84–91.

Mjengera, H., Mkongo, G., 2003. Appropriate defluoridation technology for use in flourotic areas in Tanzania. Physics and Chemistry of the Earth, 28, 1097–1104.

Mjengera, H.J., Mtalo, F.W., Mashauri, D.A., Tjell, C.H., 1997. Fluoride removal using heat activated animal bone media. In: Dahi, E. and Nielsen, J.M. (eds). Proceedings of the 2nd international workshop on fluorosis and defluoridation of water, Addis Ababa, Ethiopia, November 19–22.

Moges, G., Zewge, F., Socher, M., 1996. Preliminary investigations on the defluoridation of water using fired clay chips. Journal of African Earth Sciences 22, 479–482.

Mohan Rao, N.V.R., Bhaskaran, C.S., 1988. Studies on defluoridation of water. Journal of Fluorine Chemistry 41, 17–24.

Müller, B., 1992. ChemEQL V2.0, Swiss Federal Institute of Environmental Science and Technology, Kastanienbaum, Switzerland.

Mulugeta, E., Zewge, F., Johnson, C.A., Chandravanshi, B.S., 2013. A high–capacity aluminium hydroxide–based adsorbent for water defluoridation. Desalination and Water Treatment. doi: 10.1080/19443994.2013.811108

Nair, K.R, Manji, F., Gitonga, J.N., 1984. The occurrence and distribution of fluoride in groundwaters of Kenya. In: Challenges in African hydrology and water resources, Proceedings of the Harare Symposium, IAHS Publications 144, 75–86.

Nakamoto, K., 1978. Infrared and Raman spectra of inorganic and coordination compounds. Wiley, New York, pp 103–110.

Nawlakhe, W.G., Kulkarni, D.N., Pathak, B.N., Bulusu, K.R., 1975. Defluoridation of water with alum. Indian Journal of Environmental Health 17, 26–65.

Nawlakhe, W.G., Rao, A.V.J., 1990. Evaluation of defluoridation plant at Tartatur. Journal of Indian Water Works Association 13, 287–290.

Ndiaye, P.I., Moulin, P., Dominguez, L., Millet, J.C., Charbit, F., 2005. Removal of fluoride from electronic industrial effluent by RO membrane separation. Desalination 173, 25–32.

Nielsen, J.M., Dahi, E., 2002. Fluoride exposure of East African consumers using alkaline salt deposits known as magadi (trona) as a food preparation aid. Food Additives and Contaminants 19, 709–714.

Nigussie, W., Zewge, F., Chandravanshi, B.S., 2007. Removal of excess fluoride from water using waste residue from alum manufacturing process. Journal of Hazardous Material 147, 954–963.

Onyango, M.S., Kojima, Y., Aoyi, O., Bernardo, E.C., Matsuda, H., 2004. Adsorption equilibrium modeling and solution chemistry dependence of fluoride removal from water by trivalent–cation–exchanged zeolite F–9. Journal of Colloid and Interface Science 279, 341–350.

Onyango, M.S., Kojima, Y., Kumar, A., Kuchar, D., Kubota, M., Matsuda, H., 2006. Uptake of fluoride by $Al^{3+}$ pretreated low–silica synthetic zeolites: Adsorption equilibrium and rate studies. Separation Science and Technology 41, 683–704.

Parida, K.M., Amaresh, C.P., Das, J., Naruparaj, S., 2009. Synthesis and characterization of nano–sized porous gamma–alumina by control precipitation method. Materials Chemistry and Physics 113, 244–248.

Patel, G., Pal, U., Menon, S., 2009. Removal of fluoride from aqueous solution by CaO nanoparticles. Separation Science and Technology 44, 2806–2826.

Pathak, A., Panda, A.B., Tarafdar, A., Pramanik, P., 2003. Synthesis of nano–sized metal oxide powders and their application in separation technology. Journal of the Indian Chemical Society 80, 289–296.

Phantumvanit, P., Songpaisan, Y., Moller, I.J., 1988. Defluoridator for individual households. World Health Forum 9, 555–556.

Popat, K.M., Anand, P.S., Dasare, B.D., 1994. Selective removal of fluoride ions from water by the aluminium form of the amino methyl phosphonic acid–type ion exchanger. Reactive Polymers 23, 23–32.

Priyantha, N., Padamasiri, J.P., 1996. Proceedings: prevention of fluorosis in Sri Lanka. Peradeniya, Sri Lanka, University of Peradeniya.

Rajchagool, S, Rajchagool, C., 1997. Solving the fluorosis problem in a developing country. In: Dahi, E. and Nielsen, J.M. (eds). Proceedings of the 2nd international workshop on fluorosis and defluoridation of water, Addis Ababa, Ethiopia, November 19–22. Dunedin, New Zealand, International Society for Fluoride Research.

Ramo, J.H., Sarpola, A.T., Hellman, A.H., Leiviska, T.A., Hietapelto, V.K., Jokela, J.T., Laitinen, R.S., 2008. Colloidal surfaces and oligomeric species generated by water treatment chemicals. Chemical Speciation and Bioavailability 20, 13–22.

Ramos, R.L., Ovalle–Turrubiartes, J., Sanchez–Castillo, M.A., 1999. Adsorption of fluoride from aqueous solution on aluminium–impregnated carbon. Carbon 37, 609–617.

Rao, V.K., Mahajan, C.L., 1988. Defluoridation of drinking water in developing countries alternative and innovative technologies. Proceedings of the 20th Mid Atlantic Industrial Waste Conference, pp 55.

Reimann, C., Banks, D., 2004. Setting action levels for drinking water: Are we protecting our health or our economy (or our backs!)? Science of the Total Environment 532, 13–21.

Reimann, C., Bjorvatn, K., Frengstad, B., Melaku, Z., Tekle–Haimanot, R., Siewers, U., 2003. Drinking water quality in the Ethiopian section of the East African rift valley I–data and health aspects. Science of the Total Environment 311, 65–80.

Robert, C.T.S., Jennifer, C.S., Ian, M.T., 1991. $^{27}$Al nuclear magnetic resonance spectroscopy investigation of thermal transformation sequences of alumina hydrates. Journal of Materials Chemistry 1, 875–879.

Rubel, F., Wooseley, R.D., 1979. The removal of excess fluoride from drinking water by activated alumina. Journal of the American Water Works Association 71, 45–49.

Sathish, S., Geetha, M., Udayakumar, A., Senthil, K.S., Asokamani, R., 2012. Granulation of nano alumina powder for improved flowability by spray drying. Trans Indian Institute of Metal 65, 485–490.

Saxena, V.K., Ahmed, S., 2003. Inferring the chemical parameters for the dissolution of fluoride in groundwater. Environmental Geology 43, 731–736.

Scherrer, P., 1918. Determining the size and internal structure of colloidal particles by means of X–ray. News from the Society of Sciences and Humanities, Mathematics and Physical Class 26, 98–100.

Schoeman, J.J., 2009. Performance of a water defluoridation plant in a rural area in South Africa. Water South Africa 35, 97–101.

Schoeman, J.J., MacLeod, H., 1987. The effect of particle size and interfering ions on fluoride removal by activated alumina. Water South Africa 13, 229–234.

Schoeman, J.J., Steyn, A., 2000. Defluoridation, denitrification and desalination of water using ion–exchange and reverse osmosis technology, WRC Report TT 124/00, Water Research Commission: South Africa.

Sehn, P., 2008. Fluoride removal with extra low energy reverse osmosis membranes: three years of large scale field experience in Finland. Desalination 223, 73–84.

Serna, C.J., White, J.L., Hem, S.L., 1977. Anion–aluminum hydroxide interactions. Journal of American Soil Science Society 42, 1009–1013.

Shaheen, W.M., Hong, K.S., 2002. Thermal characterization and physicochemical properties of $Fe_2O_3$–$Mn_2O_3$/$Al_2O_3$ system. Thermochimica Acta 381, 153–164.

Shaheen, W.M., Selie, M.M., 2000. Thermal decompositions of pure and mixed manganese carbonate and ammonium molybdate tetrahydrate. Journal of Thermal Analysis and Colorimetry 59, 961–970.

Shimelis, B., Zewge, F., Chandravanshi, B.S., 2006. Removal of excess fluoride from water by aluminium hydroxide. Bulletin of Chemical Society of Ethiopia 20, 17–34.

Shubo, D., Han, L., Wei, Z., Jun, H., Gang, Y., 2011. Mn–Ce oxide as a high-capacity adsorbent for fluoride removal from water. Journal of Hazardous Materials 186, 1360–1366.

Simons, R., 1993. Trace element removal from ash dam waters by nanofiltration and diffusion dialysis. Desalination 89, 325–341.

Solangi, I.B., Memon, S., Bhanger, M.I., 2009. Removal of fluoride from aqueous environment by modified Amberlite resin. Journal of Hazardous Material 171, 815–819.

Stebbins, J.F., Kroeker, S., Lee, S.K., Kiczenski, T.J.J., 2000. Quantification of five– and six–coordinated aluminium in aluminosilicate and fluoride–containing glasses by high–field, high–resolution $^{27}$Al NMR. Journal of Non–crystalline Solids 275, 1–6.

Sujana, M.G., Thakur, R.S., Rao, S.B., 1998. Removal of fluoride from aqueous solution by using alum sludge. Journal of Colloid and Interface Science 206, 94–101.

Sung, K.L., Sun, Y.P., Yoo, S.Y., Jaehyun, M., 2010. Structure and disorder in amorphous alumina thin films: Insights from high–resolution solid–state NMR. Journal of Physical Chemistry C114, 13890–13894.

Tamiru, A., 1993. Preliminary analysis of the availability of groundwater in Ethiopia. SINET: Ethiopian Journal of Science 16, 43–59.

Tekle–Haimanot, R., 2005. Study of fluoride and fluorosis in Ethiopia with recommendations on appropriate defluoridation technologies, Consultancy Report, UNICEF–Ethiopia, pp 1–55.

Tekle–Haimanot, R., Fekadu, A., Bushura, B., 1987. Endemic fluorosis in the Ethiopian Rift Valley. Journal of Tropical and Geographical Medicine 39, 209–217.

Tekle–Haimanot, R., Melaku, Z., Kloos, H., Reimann, C., Fantaye, W., Zerihun, L., Bjorvatn, K., 2006. The geographic distribution of fluoride in surface and groundwater in Ethiopia with an emphasis on the Rift Valley. Science of the Total Environment 367, 182–190.

Temuujin, J., Jadambaa, T.S., Mackenzie, K.J.D., Angerer, P., Portef, F., Riley, F., 2000. Thermal formation of corundum from aluminium hydroxides prepared from various aluminium salts. Bulletin of Materials Science 23, 301–304.

Teng, S.X., Wang, S.G., Gong, W.X., Liu, X.W., Gao, B.Y., 2009. Removal of fluoride by hydrous manganese oxide–coated alumina: performance and mechanism. Journal of Hazardous Material 168, 1004–1011.

Tien, P.L., 1968. Hydrobasaluminite and basaluminite in cabaniss formation (middle Pennsylvanian), southeastern Kansas. The American Mineralogist 53, 722–732.

Tressaud, A., 2006. Advances in fluorine science, fluorine and the environment, agrochemicals, archaeology, green chemistry and water. Volume 2, Elsevier Science Limited.

Tripathy, S.S., Raichur, A.M., 2008. Abatement of fluoride from water using manganese dioxide coated activated alumina. Journal Hazardous Material 153, 1043–1051.

Turner, B.D., Binning, P., Stipp, S.L.S., 2005. Fluoride removal by calcite: evidence for fluorite precipitation and surface adsorption. Environmental Science and Technology 39, 9561–9568.

Urretavizcaya, G., Cavalieri, A.L., Porto–Lopez, J.M., Sobrados, I., Sanz, J., 1998. Thermal evolution of alumina prepared by the sol–gel technique. Journal of Materials Synthesis and Processing 6, 1–7.

UNESCO. Trace elements in groundwater and public health. Available at http://www.iah.org/briefings/Trace/trace.pdf.

USEPA, 2007. Method 3051A, Microwave assisted acid digestion of sediments, sludges, soils, and oils. U.S. Environmental Protection Agency, Washington, DC. pp1–30.

USEPA, 2008. United States national secondary drinking water regulations. United States Environmental Protection Agency, Washington, D.C.

Valenzuela–Vasquez, L., Ramirez–Henandez, J., Reyes–Lopez, J., Sol–Uribe, A., Lazaro–Mancilla, O., 2006. The origin of fluoride in groundwater supply to Hermosillo city, Sonora, Mexico. Environmental Geology 51, 17–27.

Viswanathan, N., Meenakshi, S., 2009. Role of metal ion incorporation in ion exchange resin on the selectivity of fluoride. Journal of Hazardous Material 162, 920–930.

Wang, J.A., Bokhimi, X., Morales, A., Novaro, O., Lopez, T., Gomez, R., 1999. Aluminium local environment and defects in the crystalline structure of sol–gel alumina catalyst. Journal of Physical Chemistry 103B, 299–303.

Wang, S.G., Ma, Y., Shi, Y.J., Gong, W.X., 2009. Defluoridation performance and mechanism of nano–scale aluminium oxide hydroxide in aqueous solution. Journal of Chemical Technology and Biotechnology 84, 1043–1050.

Wefers, K., Misra, C., 1987. Oxides and hydroxides of aluminium. Alcoa Technical Paper No.19, Alcoa Research Laboratories, Pittsburgh, PA.

Weingartner, F., Liebertz, J., 1978. Granular active alumina with high apparent density and high mechanical durability. United State Swiss Aluminium Limited (Chippis, CH), Patent No. 4083911. Available at http://www.freepatentsonline.com/4083911.html.

WHO, 1994. Fluorides and oral health, (Technical Report Series No. 846). World Health Organisation, Geneva, Switzerland.

WHO, 1996. Guidelines for drinking water quality. Volume 2. Health Criteria and Other Supporting Information. 2nd ed. World Health Organization, Geneva, Switzerland.

WHO, 2004. Guidelines for drinking water quality, 3rd ed., World Health Organization: Geneva, Switzerland, pp 375–378, 301–303.

WHO, 2011. Guidelines for drinking water quality. 4th ed., World Health Organization, Geneva, Switzerland.

Yang, X., Sun, Z., Wang, D., Forsling, W., 2007. Surface acid–base properties and hydration/dehydration mechanisms of aluminium (hydr)oxides. Journal of Colloid and Interface Science 308, 395–404.

Yarger, J.L., Smith, K.H., Nieman, R.A., Diefenbacher, J., Wolf, G.H., McMillan, P.F., Poe, B.T., 1995. Al coordination changes in high–pressure aluminosilicate liquids. Science 270, 1964–1967.

Zeng, B., Hong, Y., 1988. Geochemical environment related to human endemic fluorosis in China. In: Geochemistry and Health, Science Reviews, London.

Zerabruk, S., Chandravanshi B.S., Zewge, F., 2010. Fluoride in black and green tea (*Camellia Sinensis*) infusions in Ethiopia: measurement and safety evaluation. Bulletin of the Chemical Society of Ethiopia 24, 327–338.

Zevenbergen, C., Van Reeuwijk, L.P., Frapporti, G., Louws, R.J., Schuiling, R.D., 1996. A simple method for defluoridation of drinking water at village level by adsorption on Ando soil in Kenya. Science of the Total Environment 188, 225–232.

Zewge, F., 2005. Solution to the fluoride problem in the rift valley region of Ethiopia. A Biannual News Letter, Chemical Society of Ethiopia 14, 15–22.

Zhang, Y., Yang, M., Dou, X., He, H., Wang, D., 2005. Arsenate adsorption on an Fe–Ce bimetal oxide adsorbent: role of surface properties. Journal of Environmental Science and Technology 39, 7246–7253.

Zhao, X., Wang, J., Wu, F., Wang, T., Cai, Y., Shi, Y., Jiang, G., 2010. Removal of fluoride from aqueous media by $Fe_3O_4$@$Al(OH)_3$ magnetic nanoparticles. Journal of Hazardous Material 173, 102–109.

Zhuang, J.I.E., Yu, G.R., 2002. Effect of surface coatings on electrochemical properties and contaminant sorption of clay minerals. Chemosphere 49, 619–628.

# Appendices

## A. List of publications

**Annex 1.** Eyobel Mulugeta, Feleke Zewge, C. Annette Johnson, and Bhagwan Singh Chandravanshi, A high–capacity aluminium hydroxide–based adsorbent for water defluoridation, Desalination and Water Treatment. doi: 10.1080/19443994.2013.811108

**Annex 2.** Sheta Alemu, Eyobel Mulugeta, Feleke Zewge and Bhagwan Singh Candravanshi, Water defluoridation by aluminium oxide–manganese oxide composite material, Journal of Environmental Technology. 2014, Vol. 35, No. 15, 1893–1903, http://dx.doi.org/10.1080/09593330.2014.885584

**Annex 3.** Fentahun Adeno, Eyobel Mulugeta, Feleke Zewge and Yonas Chebude, Adsorptive removal of fluoride from water using nanoscale aluminium oxide hydroxide (AlOOH), Bulletin of the Chemical Society of Ethiopia. 2014, Vol. 28, No. 2, 215-227, DOI: http://dx.doi.org/10.4314/bcse.v28i2.6

**Annex 4.** Eyobel Mulugeta, Feleke Zewge and Bhagwan Singh Chandravanshi, Development of household water defluoridation process using aluminium hydroxide–based adsorbent, Water Environment Research. Manuscript is accepted on June 08, 2014.

**Annex 5.** Eyobel Mulugeta, Feleke Zewge, C. Annette Johnson, and Bhagwan Singh Chandravanshi, Aluminium hydro (oxide)–based (AO) adsorbent for defluoridation of drinking water: Optimization, performance comparison, and field testing, Original manuscript is ready for submition.

**B. Oral presentations**

1. Eyobel Mulugeta, Development and field implementation of a novel AO–based community defluoridation system at Tsutchigragona village, Oromia Regional State, Integrated Fluorosis Mitigation Approaches, Ministry of Water and Energy, Adama, Ethiopia, **2011**.
2. Eyobel Mulugeta, Optimization and acceptance of fluoride removal options for drinking water in rural Ethiopia, the Eawag/AAU Collaborative Project (IZ 70Z0–124000/1), Addis Ababa, Ethiopia, **2012**.
3. Eyobel Mulugeta, Development and field implementation of a novel aluminium hydro(oxide)-based technique for fluoride removal in rural Ethiopia, GeoGen 2013 International conference, Addis Ababa, Ethiopia, **2013**.
4. Eyobel Mulugeta, Development of a high capacity aluminium hydroxide-based adsorbents for defluoridation of drinking water, $7^{th}$ International conference of the Africa MRS, Dec 8-13, Addis Ababa, Ethiopia, **2013**.